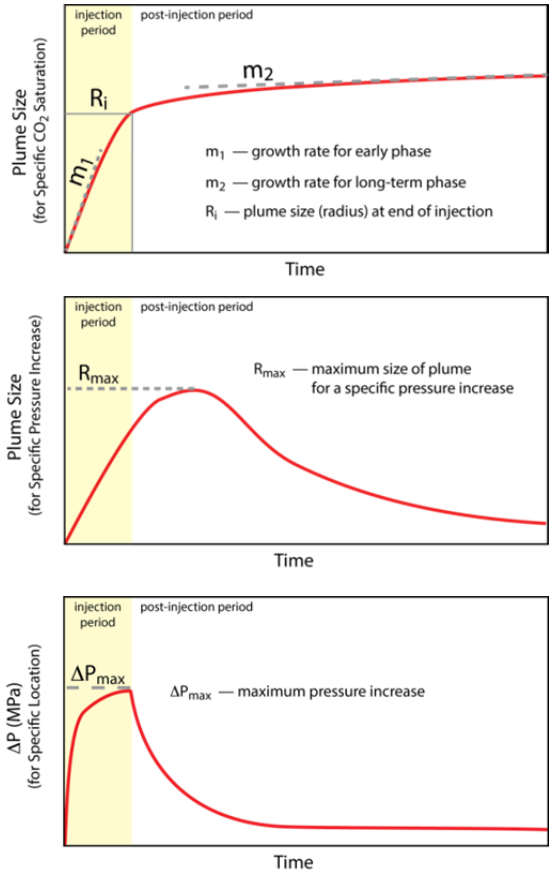

Use of Science-Based Prediction to Characterize Reservoir Behavior as a Function of Injection Characteristics, Geological Variables, and Time

12 November 2014

Office of Fossil Energy

NRAP-TRS-I-005-2014

Disclaimer

This report was prepared as an account of work sponsored by an agency of the United States Government. Neither the United States Government nor any agency thereof, nor any of their employees, makes any warranty, express or implied, or assumes any legal liability or responsibility for the accuracy, completeness, or usefulness of any information, apparatus, product, or process disclosed, or represents that its use would not infringe privately owned rights. Reference therein to any specific commercial product, process, or service by trade name, trademark, manufacturer, or otherwise does not necessarily constitute or imply its endorsement, recommendation, or favoring by the United States Government or any agency thereof. The views and opinions of authors expressed therein do not necessarily state or reflect those of the United States Government or any agency thereof.

This report has been reviewed by National Energy Technology Laboratory (NETL), Lawrence Berkeley National Laboratory (LBNL), Lawrence Livermore National Laboratory (LLNL), Los Alamos National Laboratory (LANL), Pacific Northwest National Laboratory (PNNL), and the NRAP Executive Committee and approved for public release.

Cover Illustration: (Top) CO_2 Plume Profile—Schematic of the time evolution of a plume of CO_2 exceeding a given threshold saturation. (Middle) Pressure Plume Profile—Schematic of the time evolution of a pressure plume defined for a specific threshold. (Bottom) Pressure Differential Profile—Schematic of the time evolution of a pressure differential predicted at a particular point in reservoir.

Suggested Citation: Bromhal, G.; Arcentales Bastidas, D.; Birkholzer, J.; Cihan, A.; Dempsey, D.; Fathi, E.; King, S.; Pawar, R.; Richard, T.; Wainwright, H.; Zhang, Y.; Guthrie, G. *Use of Science-Based Prediction to Characterize Reservoir Behavior as a Function of Injection Characteristics, Geological Variables, and Time*; NRAP-TRS-I-005-2014; NRAP Technical Report Series; U.S. Department of Energy, National Energy Technology Laboratory: Morgantown, WV, 2014; p 76.

An electronic version of this report can be found at:
http://www.netl.doe.gov/research/on-site-research/publications/featured-technical-reports

https://edx.netl.doe.gov/nrap

Use of Science-Based Prediction to Characterize Reservoir Behavior as a Function of Injection Characteristics, Geological Variables, and Time

Grant Bromhal[1], Danilo Arcentales Bastidas[1,2], Jens Birkholzer[3], Abdullah Cihan[3], David Dempsey[4], Ebrahim Fathi[1,2], Seth King[5], Rajesh Pawar[4], Tom Richard[6,7], Haruko Wainwright[3], Yingqi Zhang[3], George Guthrie[4]

[1]U.S. Department of Energy, Office of Research and Development, National Energy Technology Laboratory, 3610 Collins Ferry Road, Morgantown, WV 256507

[2]Benjamin M. Statler College of Engineering and Mineral Resources, West Virginia University, Morgantown, WV 26506

[3]Earth Sciences Division, Lawrence Berkeley National Laboratory, 1 Cyclotron Road Berkeley, CA 94720

[4]Earth and Environmental Sciences Division, Los Alamos National Laboratory, 4200 W Jemez Road #300, Los Alamos, NM 87545

[5]U.S. Department of Energy, Office of Research and Development, National Energy Technology Laboratory, URS, 3610 Collins Ferry Road, Morgantown, WV 256507

[6]The Pennsylvania State University, Department of Agricultural and Biological Engineering, 244 Agricultural Engineering Building, University Park, PA 16802

[7]U.S. Department of Energy, Office of Research and Development, National Energy Technology Laboratory, 626 Cochrans Mill Road, Pittsburgh, PA 15236

NRAP-TRS-I-005-2014

Level I Technical Report Series

12 November 2014

This page intentionally left blank.

Table of Contents

EXECUTIVE SUMMARY **1**

1. FOCUS AND GENERAL APPROACH **4**
1.1 RISK METRICS 4
1.2 RESERVOIRS CONSIDERED 8
1.3 INJECTION AND POST-INJECTION SCENARIOS 9
1.4 COMPUTATIONAL APPROACH 9

2. KEY FINDINGS **10**
2.1 GENERAL AND TEMPORAL BEHAVIOR OF RISK METRICS 10
2.2 SPECIFIC BEHAVIOR OF RISK METRICS 10
2.3 RELATIVE IMPACT OF OPERATIONAL AND GEOLOGICAL VARIABLES 14
2.4 STOCHASTIC AND SENSITIVITY ANALYSIS OF RISK METRICS 16

3. DETAILED ANALYSIS OF RESERVOIR BEHAVIOR **18**

4. RELEVANCE TO REGIONAL PARTNERSHIPS LARGE SCALE PROJECTS **21**

5. REFERENCES **23**

APPENDIX A: DETAILS OF SIMULATIONS OF UNSTRUCTURED SANDSTONE LAYERED FIELD **A-1**

APPENDIX B: DETAILS OF SIMULATIONS OF CITRONELLE-LIKE FIELD **B-1**

APPENDIX C: DETAILS OF SIMULATIONS OF ROCK SPRINGS UPLIFT (RSU) AND RELATED FIELDS **C-1**

List of Figures

Figure 1: CO_2 Plume Profile—Schematic of the time evolution of a plume of CO_2 exceeding a given threshold saturation. 6

Figure 2: Pressure Plume Profile—Schematic of the time evolution of a pressure plume defined for a specific threshold. 7

Figure 3: Pressure Differential Profile—Schematic of the time evolution of a pressure differential predicted at a particular point in reservoir. 7

Figure 4: Radius of saturation plume during injection for single layer sandstone case with 30 years of injection. 11

Figure 5: Injection and post-injection CO_2 plume growth rates. Examples drawn from simulations of the single-layer sandstone case; graph of mass of CO_2 is for a horizontal reservoir, whereas graph of porosity is for reservoir tiled by 1°. 11

Figure 6: Pressure plume radii. for a) different threshold values with 100 mD reservoir permeability and b) different permeability values with a 0.5 MPa threshold. Examples drawn from simulations of the single-layer sandstone case with a horizontal reservoir. 12

Figure 7: Pressure plume radii for different threshold values for a) 10 mD permeability and b) 1,000 mD permeability reservoir. Examples drawn from simulations of the single-layer sandstone case with a horizontal reservoir. 13

Figure 8: Pressure magnitude at three locations in reservoir. Example drawn from simulations of the single-layer sandstone case with a horizontal reservoir. 13

Figure 9: Pressure magnitude as a function of reservoir permeability at 1 and 5 km from the injection point. Example drawn from simulations of the single-layer sandstone case with the reservoir tilted by 1°. 14

Figure 10: Size of CO_2 plume at the end of injection (Ri) as a function of mass of CO_2 injected for three different values of reservoir permeability. Example drawn from simulations of the single-layer sandstone case with the reservoir tilted by 1°. 15

Figure 11: Summary of behavior of pressure and CO_2 plumes in the RSU reservoir for 10-year injection simulations at three different injection rates: 0.1 Mt yr^{-1}, 1 Mt yr^{-1}, and 5 Mt yr^{-1}. 17

List of Tables

Table 1: Parameters and ranges used in reservoir simulations 19

Table 2: Reservoir properties and relative impacts based on sensitivity and stochastic analysis of parameters 20

Table 3: RCSP Phase III characteristics 22

Acronyms, Abbreviations, and Symbols

Term	Description
AoR	Area of review
Big Sky	Big Sky Regional Carbon Sequestration Partnership
CO_2	Carbon dioxide
CMG	Computer Modeling Group (commercial reservoir simulator)
ΔP	Difference in pressure (relative to pre-injection pressure)
ΔP_{max}	Maximum difference in pressure (relative to pre-injection pressure)
ΔP_{thr}	Threshold value used to define pressure plume
D	Darcy
DOE	Department of Energy
EPA	Environmental Protection Agency
FEHM	Finite Element Heat and Mass (LANL reservoir simulator)
ft	Feet
IAM	Integrated assessment model
GEOST	Geostatistical code used to generate spatial distributions of parameters
kt	Thousand metric tons (i.e., 10^6 kg)
LANL	Los Alamos National Laboratory
LBNL	Lawrence Berkeley National Laboratory
m_1	Growth rate of CO_2 plume during early phase of injection
m_2	Long term growth rate of CO_2 plume
mD	milliDarcy (10^{-3} Darcy)
MGSC	Midwest Geological Sequestration Partnership
MPa	MegaPascal (10^6 Pa)
MRCSP	Midwest Regional Carbon Sequestration Partnership
Mt	Million metric tons (i.e., 10^9 kg)
nD	nano Darcy (10^{-9} Darcy)
NETL	National Energy Technology Laboratory
NRAP	National Risk Assessment Partnership
Pa	Pascal
PCOR	Plains CO_2 Reduction Partnership
PDF	Probability Distribution Function
PISC	Post-injection site care
psi	Pounds per square inch
R_i	Effective radius of plume at the end of injection (assumes a circular plume)
R_{max}	Maximum effective radius of pressure plume (assumes a circular plume)
RCSP	Regional Carbon Sequestration Partnership

Term	Description
S_{thr}	Threshold value used to define saturation plume
SECARB	Southeast Regional Carbon Sequestration Partnership
SWP	Southwest Regional Partnership
TOUGH2	Transport of Unsaturated Groundwater and Heat, version 2 (LBNL simulation model)
TP2D	Reduced physics reservoir simulator from LBNL
yr	Year

Acknowledgments

This work was completed as part of the National Risk Assessment Partnership (NRAP) project. Support for this project came from the Department of Energy's (DOE) Office of Fossil Energy's Crosscutting Research program. The authors wish to acknowledge Robert Romanosky (NETL Strategic Center for Coal) and Regis Conrad (DOE Office of Fossil Energy) for programmatic guidance, direction, and support.

The authors also wish to acknowledge Mark Ackiewicz, Regis Conrad, Susan Maley, Traci Rodosta, and Steven Seachman for their guidance, comments, and support.

This page intentionally left blank.

EXECUTIVE SUMMARY

This report summarizes a detailed study designed to generate a baseline understanding of how pressure plumes and carbon dioxide (CO_2) plumes behave in CO_2 storage reservoirs as a function of storage-site properties, injection conditions, and time. The goal of the study was to provide quantitative insight into how operational and geologic factors can impact risk at storage sites both during injection and post injection.

The study focused on reservoir performance. Thus, this study does not explore risk directly; calculation of risk requires coupling reservoir behavior to other features and processes at the storage site (such as flow along legacy wells). Nevertheless, the focus on reservoir behavior provides critical insight into how the storage system is expected to evolve relative to risk. Specifically, the evolution of differential pressure and CO_2 plumes in the reservoir are central to two categories of potential impacts of concern: fluid release from the reservoir (which could pose a risk to groundwater resources), and slippage along a critically stressed fault (which could produce a felt seismic event). Hence, this aspect of reservoir behavior is central to assessment of risk at a storage site. Future work will utilize the National Risk Assessment Partnership's (NRAP) integrated assessment models (IAMs) to link reservoir behavior with direct technical risk metrics, such as leakage of CO_2 back to the atmosphere or the nature of potential groundwater impacts.

We identified several simple metrics that facilitate the quantification of reservoir behavior for different injection conditions (e.g., rates or durations) and for various reservoir properties. These metrics were applied to results from detailed simulations of >2,300 different scenarios. The resulting analysis helps to elucidate the expected risk-related behavior for scenarios ranging from small pilot tests to large-scale storage operations, demonstrating how this behavior varies over both space and time. Hence, this analysis can help to inform consideration of questions such as: How large of an area might be impacted for a given size of injection? How much of a pressure increase might a reservoir experience for a given size of injection? How will sites evolve post injection for a given size of injection?

Three distinct types of reservoirs were selected to help understand the behavior of a diverse range of potential storage formations. The simulated reservoirs possessed characteristics that are consistent with aspects of several depositional environments: clastic deltaic, strandplain, shelf, fluvial deltaic, turbidite, and carbonate reef. These cover several of the high and medium potential types of depositional systems found to be important for geologic carbon storage in the U.S. (DOE-NETL, 2010). Models for each of these reservoirs probed a common set of variables: reservoir permeability, porosity, compressibility, permeability anisotropy, salinity, size, and thickness and the permeability of the formations overlying and underlying the reservoir. In addition, each of the models explored some reservoir-specific variables (e.g., reservoir heterogeneity, tilt, etc.). Reservoir simulations were conducted at various injection rates and durations to probe the relationship between project size or reservoir conditions and risk.

Three main metrics were identified to help characterize the reservoir behavior over time: *the CO_2 plume area, the pressure differential plume area, and the pressure differential at a location in the reservoir*. These metrics were quantified in each of the simulation runs for the reservoirs simulated. The leakage and induced seismicity risks associated with a CO_2 sequestration site are directly dependent on these three metrics. By aggregating the results from these simulations, characteristic time-dependent profiles were identified for each of these metrics.

Several key findings emerged from the general behavior of the three risk metrics investigated. These findings can help to reframe the discussion about the anticipated behavior of storage sites in the context of potential risks over time (i.e., risk profiles).

These key findings include:

- *The growth of a CO_2 plume exhibits a characteristic evolution over time, growing during the injection phase and transitioning to stabilization or a slower growth rate post injection.*
- *The growth of a pressure plume exhibits a characteristic evolution over time, growing during injection until it ultimately reaches a maximum area before it begins to decay.*
- *The pressure differential at most locations within the reservoir exhibits a characteristic evolution over time, growing rapidly during the initial phases of injection and decaying once it reaches a maximum.*

Focusing on the risk metrics, a few key parameters have been identified that help to characterize important behaviors of a storage formation that are necessary factors in estimating risk over time. The variables identified are: *slope of CO_2 plume growth during and after injection, size of CO_2 plume at end of injection, maximum pressure plume size, and maximum differential pressure at a point*. Simulations can be used to estimate the values of these parameters to help characterize any storage formation with respect to potential leakage or induced seismic risks.

Based on these metrics and the simulations performed in this study, we have identified a fourth key finding:

- *The impact of reservoir properties on CO_2 and pressure plume size can be on the same order as the impact of the rate and mass of CO_2 injected.*

In other words, injecting the same mass or rate of CO_2 at different sites with different reservoir properties can result in significantly different behavior with respect to the risk metrics above. For example, some behaviors (e.g., pressure increase required to induce a fault-slip event) may be observed with only 1 Mt of CO_2 injected at one site, whereas 100 Mt of injected CO_2 may not be enough CO_2 to cause the same behavior at another site. This is a strong argument for implementing a portfolio of research-demonstration sites capable of injecting a wide range of rates and masses of CO_2, with injection into multiple distinct storage formations from different depositional environments.

The relative size of the differential pressure and CO_2 plumes can vary significantly. For example, in the cases studied the ratio of maximum differential pressure plume size to CO_2 plume size ranged from 0.2:1 to 12:1. Multiple thresholds were evaluated to determine the differential pressure plume size, as elevated pressure can impact a number of risk factors including induced seismicity and leakage through wellbores and faults. At present there is no risk-based standard basis for identifying an appropriate pressure threshold at a site. Since the size of the pressure plume is an important component in both risk and cost (e.g., area required for monitoring), further research into determining appropriate site-specific risk-based pressure threshold values is warranted, as well is developing efficient techniques to identify actual pressures at distances away from the injector to help validate model predictions and reduce uncertainty.

Finally, a qualitative assessment was done on the geologic variables probed in this study (e.g., permeability, porosity, etc.) with respect to their relative importance on impacting the sizes of

pressure and CO_2 plumes in the reservoir. In several cases, the variables had the same level of impact, regardless of the formation type. In other cases, the depositional environment, size, or boundary conditions did have an impact. These impacts are laid out in more detail in Section 3 and Table 2 in the text.

1. FOCUS AND GENERAL APPROACH

Safe and effective long-term storage of carbon dioxide (CO_2) requires that the behavior of geologic storage sites can be predicted and that the geologic storage systems perform within an acceptable range. Ultimately, the performance of each site is unique, and any prediction of performance must be based on site-specific detail. However, many decisions must be made (*e.g.*, by policy makers, regulators, operators) before comprehensive site-specific detail is available. This practical reality necessitates the development of tools and methodologies for predicting the range of potential behavior that is expected for a site, where uncertainties in key site characteristics are expected to be large during initial site evaluation, but diminish over time. The National Risk Assessment Partnership (NRAP) is developing toolsets and methodologies to better understand system behaviors under these conditions.

There are two early questions that must be answered in the evaluation of a potential CO_2 storage site: What is the likely size to expect for areas of potential impact? And, how long after injection is stopped should the site be monitored to have confidence that it is performing as expected and does not pose significant risk?[1] Underlying both of these questions is the need for a more fundamental understanding of how CO_2 storage reservoirs behave relative to performance and risk as a function of storage-site properties, injection conditions, and time.

Although answers to these questions will be unique for specific sites, a general understanding of expected behavior for typical sites is important in early decisions, including those decisions that can guide field tests.

The primary goal of this investigation was to leverage NRAP toolsets and methodologies to probe the behavior of three prototypical reservoir types under a variety of injection conditions relative to pressure and CO_2 saturation, both of which are important factors in assessing potential impacts of concern. The reservoir site geologies included single layer sandstone, multi-layer sandstone interbedded with shale, and multi-layer limestone-dolostone. For each of these the specific properties were varied over a large number of simulation runs to represent a range of different depositional environments. Examining the behavior of these prototypical sites serves to elucidate the potential behavior of many of the anticipated real CO_2 storage sites anticipated, providing a general description of this behavior as a function of site properties and the amount of CO_2 injected.

1.1 RISK METRICS

The risk metrics that were identified and analyzed in this study include the CO_2 plume area, the pressure differential plume area, and the pressure differential at a point.

The CO_2 plume area was used because it ties to potential impacts of concern, primarily the potential for CO_2 to be transported beyond the primary storage reservoir (or compartment) to groundwater aquifers and/or other subsurface resources of economic value. Because the risks

[1] We intentionally avoid the use of regulatory-specific terms such as “area of review” (AOR) and “post-injection site care” (PISC). However, the technical results in this report can help to inform considerations of these terms.

associated with a CO_2 plume are dependent on saturation of CO_2 (e.g., mobile vs. immobile CO_2), multiple threshold saturations were considered. ("Saturation" refers to the volume fraction of a discrete CO_2 fluid phase in pores relative to other fluids in the pore, such as brine. It is not used to describe chemical thermodynamic conditions in the system.)

The differential pressure plume area was used because it ties to several potential impacts of concern. Pressure differential is a primary driver for CO_2 and/or brine movement out of a storage reservoir, which could result in impacts to groundwater aquifers and/or other subsurface resources (*e.g.*, hydrocarbon deposits). Pressure also ties to change in effective stress near the storage site, which is a primary driver in the potential to induce seismic events. Because pressure changes relative to initial reservoir pressure are the driving force for both of these impacts, the change in pressure (ΔP) was the focus of this effort. For each site and scenario, ΔP was determined relative to the original pressure prior to initiation of CO_2 injection (considered to be hydrostatic for this study).

In the context of predicting the probability of a specific impact (i.e., for assessment of risk), both the magnitude of pressure change and the area over which that pressure change occurs are primary factors. Hence, two specific metrics were explored relative to pressure: 1) the area of the differential pressure plume and 2) the pressure differential at a location in the reservoir. Because the risks associated with a differential pressure plume vary with the magnitude of ΔP (e.g., brine leakage or induced seismicity), different ΔP thresholds were considered in definition of plume area. Also, it should be noted that these metrics are only reservoir-related, whereas ultimate quantification of risk additionally involves taking into consideration other parts of the storage-site system.

1.1.1 CO_2 Saturation Plume

The probability that a potentially vulnerable feature in the storage system (e.g., a leaky well or leaky fault) is exposed to CO_2 is directly related to the *area of the CO_2 plume*. The evolution of this area over time during and after injection, termed the CO_2 plume profile, serves as a measure of how site storage risks evolve over time. For each site and scenario, the size of the CO_2 plume area was determined relative to specific saturation thresholds. The common thresholds that were used across all three prototypical sites were residual saturation (which is a measure of the CO_2 saturation that must be exceeded in a reservoir before the CO_2 phase is mobile), and zero saturation (which defines the plume area where even the slightest presence of a discrete CO_2 phase is predicted).

As shown in the detailed simulation results in Section 2, the area of the CO_2 plume evolves over time with a characteristic shape (Figure 1). In each of the reservoir types investigated, the plume area increased rapidly during injection, followed by a slower rate of increase in the post injection period. This metric (size of CO_2 plume) was monitored using three simple parameters. The slopes of the early growth during injection (m_1) and later growth post injection (m_2) were calculated and used to evaluate the spread of the CO_2 plume over time. The third variable monitored was the size of the CO_2 plume at the end of injection (R_i), where R_i is the effective radius of the plume as derived from the calculated plume area by assuming a circular plume. Although plumes did not always have a circular footprint, reporting the plume size as an effective radius facilitates an intuitive comparison among different sites and scenarios. Although our current analysis tracked only the above three parameters for CO_2 plume, future studies may

consider additional parameters to track plume asymmetry and migration of the plume center of mass.

Post-injection behavior was simulated for a period of approximately 10 times the length of injection to inform decision-making in the post injection period at the time scale of decades to centuries. Over thousands of years, the size and shape of the CO_2 plume may change in other ways not considered in this analysis.

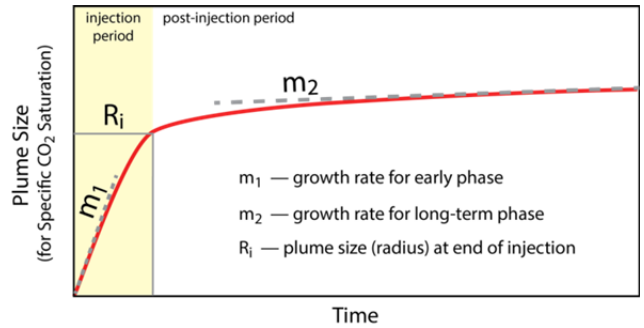

Figure 1: CO_2 Plume Profile—Schematic of the time evolution of a plume of CO_2 exceeding a given threshold saturation.

1.1.2 Area of Differential Pressure Plume

The probability that a given pressure increase is experienced by a potentially vulnerable feature in the storage system (e.g., a leaky well or a stressed fault) is directly related to the *area of the differential pressure plume*. The evolution of this area over time during and after injection, termed the differential pressure plume profile, serves as one measure of how site storage risks evolve over time. In this investigation, the area of the increase in pressure was determined relative to specific thresholds, ranging from 0.1 MPa (a small but measurable pressure increase) to 0.5 or 1.0 MPa (thresholds that are roughly sufficient to drive fluids from a reservoir to an overlying aquifer for many scenarios) to 5 MPa (a threshold that could cause some existing faults to exceed critical stress).

Figure 2 illustrates how the area of the differential pressure plume evolves over time, with a characteristic shape abstracted from detailed simulations from each of the prototypical reservoir types. The area increased during injection to a maximum point (which typically occurred after injection ceased) before decaying. The timing of the maximum pressure differential area is dependent on several factors, and no clear trends were identified except that it seems to occur later with larger injection volumes, other things being equal. Note that the characteristic shape of the pressure plume profile is significantly different from the CO_2 saturation plume profile. Unlike the CO_2 saturation plume, the differential pressure plume size increases to a maximum value and decays significantly over the post-injection time period simulated. The maximum size of the pressure plume (R_{max}) was used to track the behavior of this metric, where R_{max} is the effective radius of the plume at its maximum value as derived from the calculated plume area by assuming a circular plume, for reasons previously discussed.

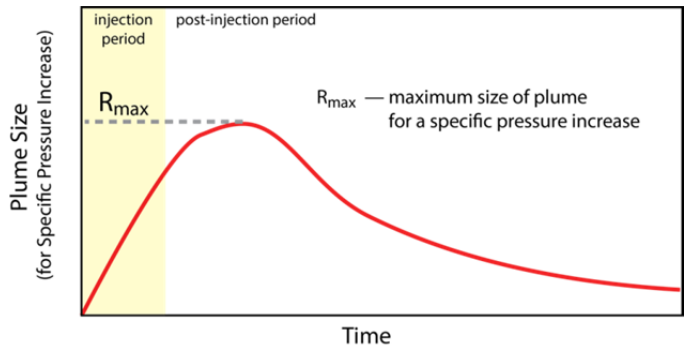

Figure 2: Pressure Plume Profile—Schematic of the time evolution of a pressure plume defined for a specific threshold.

1.1.3 Differential Pressure at a Location in the Reservoir

The evolution of the pressure increase at a specific location in the reservoir, termed the pressure differential profile, ties to the magnitude of risk both spatially and temporally, as the pressure decays post injection. In this effort, pressure evolution was tracked at various distances from the injection point (specifically at 1, 5, and 10 km).

As shown in the detailed simulation results in Section 2, the pressure differential evolution at a specific location evolves characteristically over time in the reservoirs explored (Figure 3), growing rapidly during the injection phase and decaying rapidly post injection. It should be noted that there can be variability in the time-dependent differential pressure profile at a location based on reservoir heterogeneity or the arrival of carbon dioxide at the location before injection ends. Figure 3 is just a schematic of a typical differential pressure profile; the maximum pressure value can occur at the end of injection or at some time pre- or post-injection. The maximum increase in the pressure (ΔP_{max}) was used to track the behavior of this metric, where ΔP_{max} was determined relative to the pressure before injection.

It is important to note that in the reservoirs studied here, the pressure differential was calculated for a reservoir that was assumed to be in hydrostatic equilibrium before injection started. If a reservoir is initially at pressures either above or below the hydrostatic equilibrium, a different baseline pressure may be more relevant to consider in assessing the pressure differential most relevant to risk evaluation.

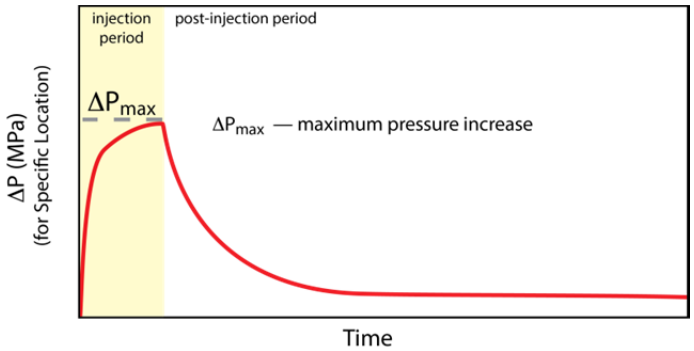

Figure 3: Pressure Differential Profile—Schematic of the time evolution of a pressure differential predicted at a particular point in reservoir.

1.2 RESERVOIRS CONSIDERED

Three types of reservoirs were considered: an unbound, flat, single-layer sandstone; a domal, multi-layer sandstone with interbedded shale; and a domal, multi-layer limestone-dolostone. Models for each of these reservoirs probed a common set of variables in addition to the reservoir-specific variations noted below. This common set of variables was: permeability, porosity, compressibility, permeability ratio, salinity, model domain, thickness, and permeability of the surrounding formations.

The single-layer sandstone reservoir allowed characterization of reservoir behavior as a function of permeability, tilt of the reservoir–seal interface, and injection dynamics. It was a completely unstructured and homogeneous reservoir. Base case permeabilities, porosities, and initial conditions were based on the Kimberlina site in California (Wainwright et al., 2012); however, bounding faults at the margins of the real site were removed from the model and boundary conditions were varied to simulate relatively open and closed environments. The storage unit was modeled using a single layer with homogeneous permeability that was changed (10–1000 mD) from realization to realization; the tilt of the reservoir was also varied (0–3°). This model could be representative of a variety of key depositional environments, such as a clastic deltaic, strandplain, or shelf. This model was originally built on the TOUGH2 platform, and the bulk of the simulations were performed with the reduced-order model TP3D after comparison with TOUGH2 output; details of this model and the accompanying calculations are provided in Appendix A.

The multi-layer sandstone reservoir allowed characterization of reservoir behavior as a function of vertical layering and a domed top surface. This prototypical site was based on a history-matched model of the Citronelle reservoir, which has multiple, laterally discontinuous low-permeability units distributed vertically within the reservoir unit and spatially-variable porosity and permeability in each reservoir layer, varying between 3–33% and 1–2,100 mD, respectively, and encompasses an area 5x5 km^2. The formation was modeled as both an open and closed system. This reservoir is representative of a fluvial deltaic or turbidite environment. This model was built on the CMG platform; details of this model and the accompanying calculations are provided in Appendix B. An upscaled model of the Citronelle reservoir was also built based on Cartesian grids and covered a 10x10 km^2 area. In the upscaled model structure, the isopach, porosity and permeability maps were also upscaled. The porosity range remained the same as the smaller model, but the permeability was varied between 1–1,000 mD.

The multi-layer limestone-dolostone reservoir allowed characterization of reservoir behavior as a function of heterogeneous hydrologic properties within the reservoir—both lateral and vertical heterogeneity. There were two storage units, one sandstone and another limestone, each with spatially heterogeneous permeability (1–210 mD) and porosity (5–15%). It was based on a numerical model developed for the Rock Springs Uplift site (Deng et al., 2012) in Wyoming that is being considered by the State of Wyoming as a potential future CO_2 sequestration site. The numerical model was developed using the FEHM simulator coupled with GEOST (to generate spatial distributions of heterogeneous parameters). Details of this model and the accompanying calculations are provided in Appendix C.

1.3 INJECTION AND POST-INJECTION SCENARIOS

All injection scenarios assumed a single injection well in the reservoir, centered in most cases but in the actual location for the history-matched Citronelle case. In addition, simulations for each of the three reservoirs explored reservoir behavior assuming a constant rate over the course of the injection. It should be noted that most of the constant rate simulations did not limit the maximum reservoir pressure at or below the lithostatic pressure so that they would not be constrained by the wellbore geometry.

The injection scenarios explored a range of injection rates (from 10 kt/yr to 5Mt/yr) and two injection durations (3 and 30 years), resulting in a wide range of total mass of injected CO_2 (30 kt–150 Mt).

Reservoir behavior was simulated post injection for between ~30 and ~300 years—depending on the size of the injection—with pressures and saturations in each simulation grid block being recorded at various time points.

1.4 COMPUTATIONAL APPROACH

Three teams were assembled to model the different reservoirs described above, from LBNL (Appendix A), NETL (Appendix B), and LANL (Appendix C). A detailed description of the results from each of these teams can be found in the appendices. Each of the reservoir simulations considered multiphase flow and thermodynamic effects at the continuum scale using finite-volume or finite-difference methods. In general, these simulations were run on physics-based models using commercial and non-commercial but publically available reservoir simulators; in some cases reduced physics models were used once agreement with the full-physics based model was confirmed. Computational times to complete simulation runs ranged from 1 to 24 hours, and between 35 and 800 simulations were performed for each reservoir. More than 2,300 scenarios were investigated in total.

For the single-layer sandstone reservoir, over 800 simulations were run between TOUGH2 (for validation) and the reduced-order model TP3D. The domain size was 100x100 km^2, all parameters were identified in a sensitivity analysis, and the runs took between 1 and 10 hours.

An additional 800 simulations were conducted for a single-layer sandstone using a Latin hypercube sampling (LHS) approach to determine values for variable parameters. The domain size in these simulations differed from those described above for TOUGH2 and TP3D, but the parameter space sampled was similar. Simulations were run using the FEHM code.

For the multi-layer domal sandstone, approximately 35 simulations were conducted on a detailed reservoir based on a 5x5 km^2 domain size and using the commercially-available CMG finite difference code. These simulations took approximately 4 hours each.

An additional 200 simulations were conducted for an upscaled model of the multi-layer domal sandstone based on a 10x10 km^2 domain size. These simulations also utilized CMG, but parameters were varied based on an LHS technique. These simulations took between 2 and 9 hours each.

For the multi-layer domal, limestone-dolostone reservoir, approximately 500 simulations were performed, using the FEHM code. The domain varied between 16x16 km^2 and 100x100 km^2, and simulations took between 8 and 24 hours each.

2. KEY FINDINGS

2.1 GENERAL AND TEMPORAL BEHAVIOR OF RISK METRICS

Several key findings emerged from the general behavior of the three risk metrics investigated. These findings can help to reframe the discussion about the anticipated behavior of storage sites in the context of potential risks over time (i.e., risk profiles). Although these metrics do not include all components of risk, as proxies for risk they provide a critical insight into the behavior of the reservoir, which is a fundamental component of any carbon storage risk assessment.

- *The growth of a CO_2 plume exhibits a characteristic evolution over time, growing during the injection phase but stabilizing to a slower growth rate post injection.*
- *The growth of the differential pressure plume exhibits a characteristic evolution over time, growing during injection until it ultimately reaches a maximum area before it begins to decay.*
- *The pressure increase at locations within the reservoir exhibits a characteristic evolution over time, growing rapidly during the initial phases of injection and decaying rapidly post injection. The magnitude of the pressure increase is higher closer to the injection point.*

As noted, the current focus has been on three prototypical non-closed reservoirs, but it is anticipated that these general behaviors are likely to be common for most reservoir conditions considered for CO_2 storage. Nevertheless, extension of this work to other types of reservoirs will serve to bolster the understanding of anticipated behavior of reservoirs (which can facilitate early evaluations of specific sites in the future by both regulators and operators).

2.2 SPECIFIC BEHAVIOR OF RISK METRICS

The analysis of the specific behavior of the risk metrics was made using three reservoir types that were explored as a function of injection scenarios and potential geologic variability. We have studied the behavior of both large and moderately sized open and closed systems. While the conclusions generally hold true for all of these conditions, we have focused our base analysis on the large open systems, as they are most likely to be selected at CO_2 storage sites, and we have pointed out different behaviors for smaller closed systems when they occur and when our analysis warranted it.

- *Sizes of CO_2-saturation plumes (as well as the plume rate of growth post-injection) increase with the total amount of injected CO_2 (Figure 4).* The saturation plume size at the end of injection (R_i) is primarily a function of the total injected mass and is less affected by the actual rate of injection. During injection, the saturation plume grows at a rate (m_1) that is followed by a slower rate (m_2) after injection ceases. Eventually, the plume should stop completely, though it did not always stop within the time frame of the simulations run in this study. The post-injection growth rate depends mainly on the injected mass of CO_2, the reservoir porosity, reservoir thickness, and the dip angle, but can be impacted modestly by other parameters, such as reservoir compressibility. For favorable reservoir conditions and small injection amounts, the size of the CO_2 plume may remain nearly constant soon after injection (e.g., no dip, <1 Mt CO_2 injected). For higher injection rates and dip angles (e.g., >30 Mt CO_2 and 3° dip), the CO_2 plume size

may continue to grow after injection ceases, although relatively slowly compared to the rate during injection. This behavior varies only slightly for the different reservoir conditions explored. For the various types of reservoirs investigated, injection masses of 100 kt, 1 Mt, and 10 Mt resulted in plume radii of 0.1–0.5 km, 0.5–1.8 km, and 1.5–3 km at the end of injection, respectively.

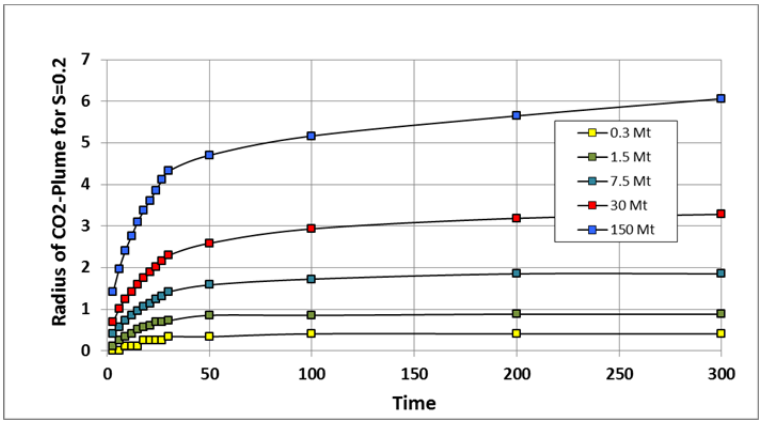

Figure 4: Radius of saturation plume during injection for single layer sandstone case with 30 years of injection.

- *Sizes of CO_2 plumes (as well as their rate of growth) are inversely tied to reservoir porosity (Figure 5).* For porosities that varied from 5–35%, the growth rate during the injection phase (m_1) varied by about a factor of 5, and by an order of magnitude for the growth rate after injection ceased (m_2). Permeability generally did not have as large of an impact on the CO_2 plume size as porosity, though it did have a moderate effect. This relationship relative to geologic parameters (e.g., porosity) is comparable to the magnitude of the impact exhibited for injection masses or volumes.

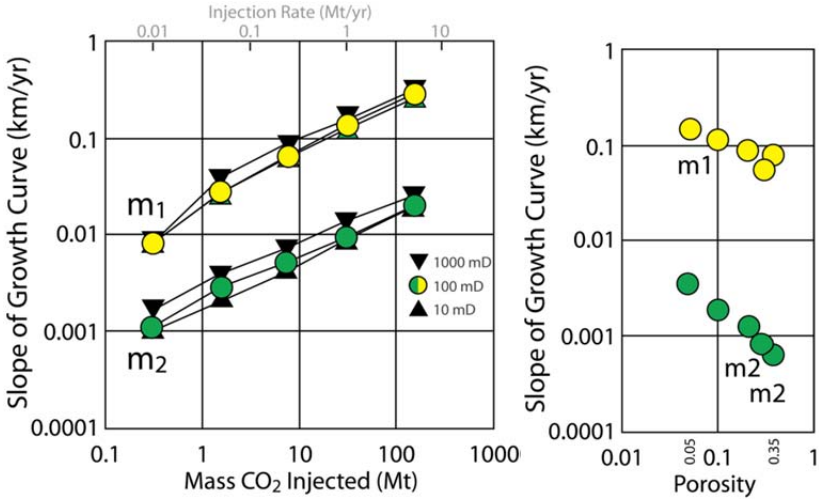

Figure 5: Injection and post-injection CO_2 plume growth rates. Examples drawn from simulations of the single-layer sandstone case; graph of mass of CO_2 is for a horizontal reservoir, whereas graph of porosity is for reservoir tiled by 1°.

- *The size of differential pressure plumes (defined for specific differential pressure thresholds) increases with total amount and rate of injected CO_2 (Figure 6).* In other words, the size of differential pressure plumes ties to the amount injected, in addition to

the rate of injection. During injection, the plume characteristically grows at an approximately constant rate that depends on the injection rate (only constant injection rates simulated), the reservoir permeability, and the reservoir volume (thickness and domain size); this growth continues for ~1–30 years post injection (for the scenarios studied), with the pressure plume reaching a maximum size followed by a period of shrinkage that can last years to centuries, depending on the total mass of CO_2 injected and the permeability of the reservoir. The length of the relaxation period can vary significantly, but the time to peak was primarily related to the total mass injected and reservoir permeability. Otherwise, the general shape of the differential pressure plume profile was fairly consistent (similar to a lognormal PDF curve) for the various reservoir conditions explored. For the various types of reservoirs investigated and a 0.5MPa threshold, injection masses of 100 kt, 1 Mt, and 100 Mt result in maximum pressure plume radii of <0.1 km, 0.1–1 km, and 1–30 km, respectively. Note that the plume size increased non-linearly as the threshold pressure differential decreased, i.e., going from 0.5 MPa to 0.1 MPa results in a 10–20x increase in plume size for some injected masses.

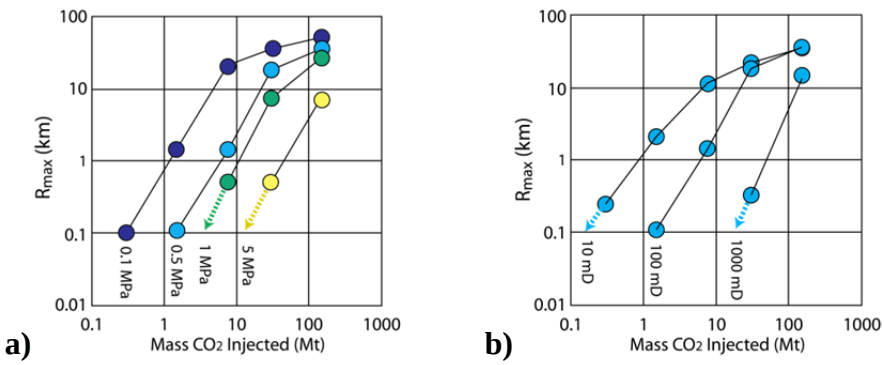

Figure 6: Pressure plume radii. for a) different threshold values with 100 mD reservoir permeability and b) different permeability values with a 0.5 MPa threshold. Examples drawn from simulations of the single-layer sandstone case with a horizontal reservoir.

- *Size of differential pressure plumes (defined for specific pressure thresholds) is highly impacted by reservoir permeability (Figures 7a and 7b).* For open systems and larger injection volumes and durations (>1Mt and 10-30 years), this was an inverse relationship, where the higher reservoir permeability caused smaller plume sizes. For the domal closed system, this was a positive correlation, where higher reservoir permeability caused larger plume sizes. This relationship relative to geologic parameters (e.g., permeability) is comparable to the relationship exhibited for injection amounts. In other words, the amount of CO_2 needed to achieve a specific increase in pressure will depend on the permeability at the site.

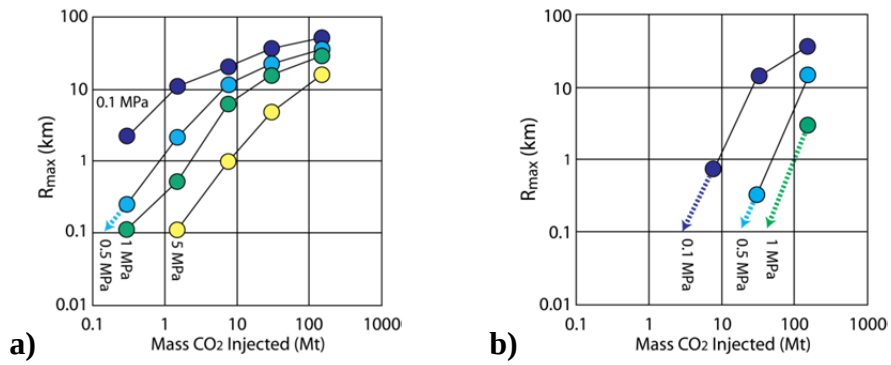

Figure 7: Pressure plume radii for different threshold values for a) 10 mD permeability and b) 1,000 mD permeability reservoir. Examples drawn from simulations of the single-layer sandstone case with a horizontal reservoir.

- *Key pressure thresholds may not be reached for some injection and reservoir conditions (Figure 7).* For higher reservoir permeability and lower injection rates, the maximum pressure in the reservoir will be limited. For example, a pressure increase of 1–5 MPa, was not reached in the example shown in Figure 7b for injection masses under 1 Mt of CO_2.
- *Magnitude of pressure increase above the initial (e.g., hydrostatic) pressure (at different reservoir locations) increases with the total amount and rate of injected CO_2 and with the location in the reservoir (Figure 8).* During injection, the maximum pressure increase at a location in the reservoir demonstrates a power law relationship to the total amount of CO_2 injected at the point when injection ceases.

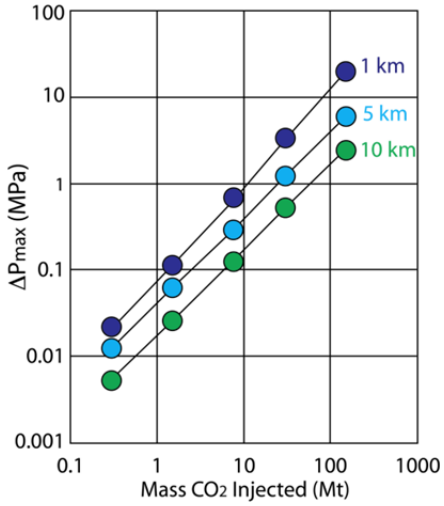

Figure 8: Pressure magnitude at three locations in reservoir. Example drawn from simulations of the single-layer sandstone case with a horizontal reservoir.

- *The magnitude of the pressure increase above initial (or hydrostatic) pressure (at different reservoir locations) decreases with an increase in horizontal permeability (Figure 9).* This relationship relative to geologic parameters (e.g., permeability) is comparable to the relationship exhibited for the injected mass of CO_2. Other geologic parameters have an impact on the pressure increase, but they are less significant than the permeability relationship.

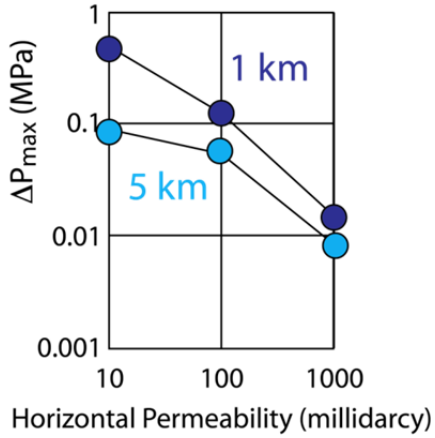

Figure 9: Pressure magnitude as a function of reservoir permeability at 1 and 5 km from the injection point. Example drawn from simulations of the single-layer sandstone case with the reservoir tilted by 1°.

- *The ratio of maximum pressure plume size to CO_2 plume size varies between 0.2:1 and 12:1 for the scenarios studied*. As a general rule, for larger injection volumes, the pressure plume is larger than the CO_2 plume, and in some cases much larger. However, when the total injected mass is small (e.g., <500 kt) and the permeability is large (e.g., >500 mD), the CO_2 plume can be larger than the pressure plume.

2.3 RELATIVE IMPACT OF OPERATIONAL AND GEOLOGICAL VARIABLES

Both operational and geological parameters impact the behavior of the reservoir. The relative (qualitative) impact of key reservoir parameters was assessed qualitatively for each of the three reservoir types investigated, and that assessment is presented in Section 3 below. In this section, we provide a general (semi-quantitative) assessment of the relative impact of operational and geological parameters, drawing on relationships demonstrated in earlier figures.

Three operational parameters were considered, each of which had a high impact on the behavior of the reservoir: injection rate, injection time, and total mass injected. The first two are independent, but the third parameter is, of course, a function of the first two. Several geological variables were also considered, including porosity, permeability, compressibility, permeability ratio (k_h:k_v), salinity, model domain, thickness, permeability of the surrounding formations, reservoir tilt, and reservoir heterogeneity. Each of these can impact the behavior of CO_2 and pressure plumes, to various degrees, as reflected in the results of the simulation. In this section, however, we focus on two of these parameters for the purpose of illustration: porosity and permeability. These parameters vary between reservoirs, and they can vary within reservoirs. Their impact serves to illustrate the relative magnitude that geological parameters can have on reservoir behavior.

Injected mass of CO_2 correlates with the observed behavior for both pressure and CO_2 plume areas. Figure 5 illustrates that increasing the mass of CO_2 by an order of magnitude can change the growth rate of the CO_2 plume both during and post injection by slightly less than an order of magnitude. Figure 10 shows a similar behavior for the size of CO_2 plume at the end of injection. Hence, scaling operational parameters up from 1 Mt CO_2 injected to 10 Mt CO_2 might be expected to impact the nature of the CO_2 plume by a factor of slightly less than ~10.

The differential pressure plume area exhibits a similar behavior. Figure 6a illustrates that increasing the mass of CO_2 by an order of magnitude can change the size of a differential pressure plume by slightly more than an order of magnitude. Hence, scaling operational parameters up from 1 Mt CO_2 injected to 10 Mt CO_2 might be expected to impact the nature of the differential pressure plume by a factor of slightly more than ~10.

Geologic variability can have a similar order of magnitude impact on pressure- and CO_2-plume behavior. Figure 5 illustrates that a variation in porosity that might be expected in a reservoir (5–35%) can change the growth rate in CO_2 plume by slightly less than an order of magnitude. Figure 6b illustrates that variation in the permeability by a factor of 10 can change the size of the differential pressure plume by slightly more than a factor of 10. Figure 9 illustrates a similar response for magnitude of the differential pressure plume (where a factor of 10 change in permeability has an impact on magnitude of slightly less than a factor of 10).

This analysis is not intended to reflect the exact details of how operational and geologic parameters impact reservoir behavior. Rather, by focusing on order-of-magnitude effects, the general trends become apparent. Namely, operational and geological parameters both impact the behavior of the reservoir relative to risk, and confirmation of their impacts at a field scale is an important element of verifying the ability of simulation tools to predict risk-related behavior over a range of scenarios.

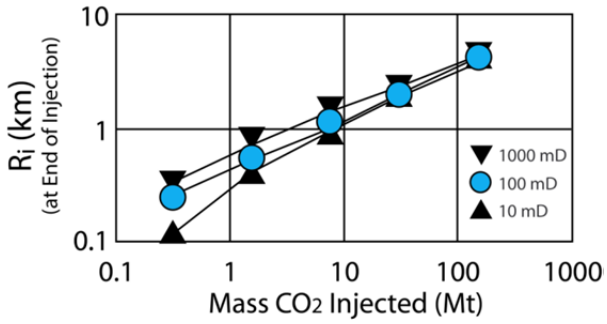

Figure 10: Size of CO_2 plume at the end of injection (Ri) as a function of mass of CO_2 injected for three different values of reservoir permeability. Example drawn from simulations of the single-layer sandstone case with the reservoir tilted by 1°.

2.4 STOCHASTIC AND SENSITIVITY ANALYSIS OF RISK METRICS

Two main approaches were taken to address the influence of different reservoir and operational parameters on the risk metrics described in Section 1. The first was a sensitivity analysis, where a base set of parameters was defined, and then each parameter was varied individually to determine the impact that parameter has on the injection mass relationships. This approach has the benefit that the relationship between the input variables and the parameter of interest can be simply identified and plotted on a single curve (such as several of those shown in Section 2.2). One of the issues with this approach, however, is that the impact can only be studied around the base case, unless a prohibitively large number of simulations are performed (e.g., for 10 parameters and only 3 values each, the number of combinations would be 3^{10}). Thus, it is hard to tell from a sensitivity analysis how varying one parameter influences the impact of another (e.g., how compressibility impacts the CO_2 plume size when the permeability is high vs. low). Nonetheless, it is a very useful technique, and it was performed for the single-layer sandstone reservoir and the history-matched Citronelle-based reservoir.

The second approach is to use an LHS technique to choose the input parameters for each realization. The weakness of this approach is that it is difficult to represent the impact of a single variable in a simple plot, such as those shown in Section 1. The strength of this approach is that with a relatively few simulation runs, the relative impact of multiple variables can be examined. Two reservoirs were explored using LHS in order to probe statistically how the behavior of the risk metrics ties to key geologic variables, the larger non-history-matched multi-layer domal sandstone and the multi-layer limestone-dolostone. The models for these reservoirs were developed assuming homogeneous properties within each reservoir layer, and all geologic structure was taken out of the second model. The geologic variables such as porosity, permeability, etc. (described more fully in Section 3) were assumed to be constant for a simulation run, but varied from one run to another by sampling from statistical distributions for individual variable. The injection rate was varied between 10 kt/yr–5 Mt/yr. Three separate injection durations were used including 3, 10, and 30 years, followed by 27, 90, and 270 years post-injection durations, respectively. For each of the injection duration scenarios, 100 simulation runs were performed. Simulation results were used to perform multi-variate stochastic analysis of pressure and saturation plume size dependence on uncertain geologic parameters. Correlation coefficients for pressure and saturation plume sizes were calculated for different uncertain parameters. Both the CO_2 saturation and pressure plume sizes are most sensitive to total mass of CO_2 injected. Other parameters that affect the two plume size metrics in decreasing order include reservoir permeability, porosity, thickness, compressibility, and permeability anisotropy, though the sensitivities with respect to these parameters are different for the two cases.

Another piece of the stochastic study involved performing multiple realizations (~30) of porosity and permeability for the same injection mass cases for the multilayer limestone-dolostone case. Figure 11 shows the impact of the reservoir heterogeneity on the sizes of both CO_2 and pressure plumes. The thinner lines show the behavior of each realization, while the solid line shows the average behavior across all realizations. The heterogeneity can impact the plume size by a factor of two, for the level of variability considered in this example, which is appropriate for a carbonate structure such as the one modeled. Other depositional environments, such as highly complex fluvial or alluvial systems, could have a greater impact caused by reservoir heterogeneity.

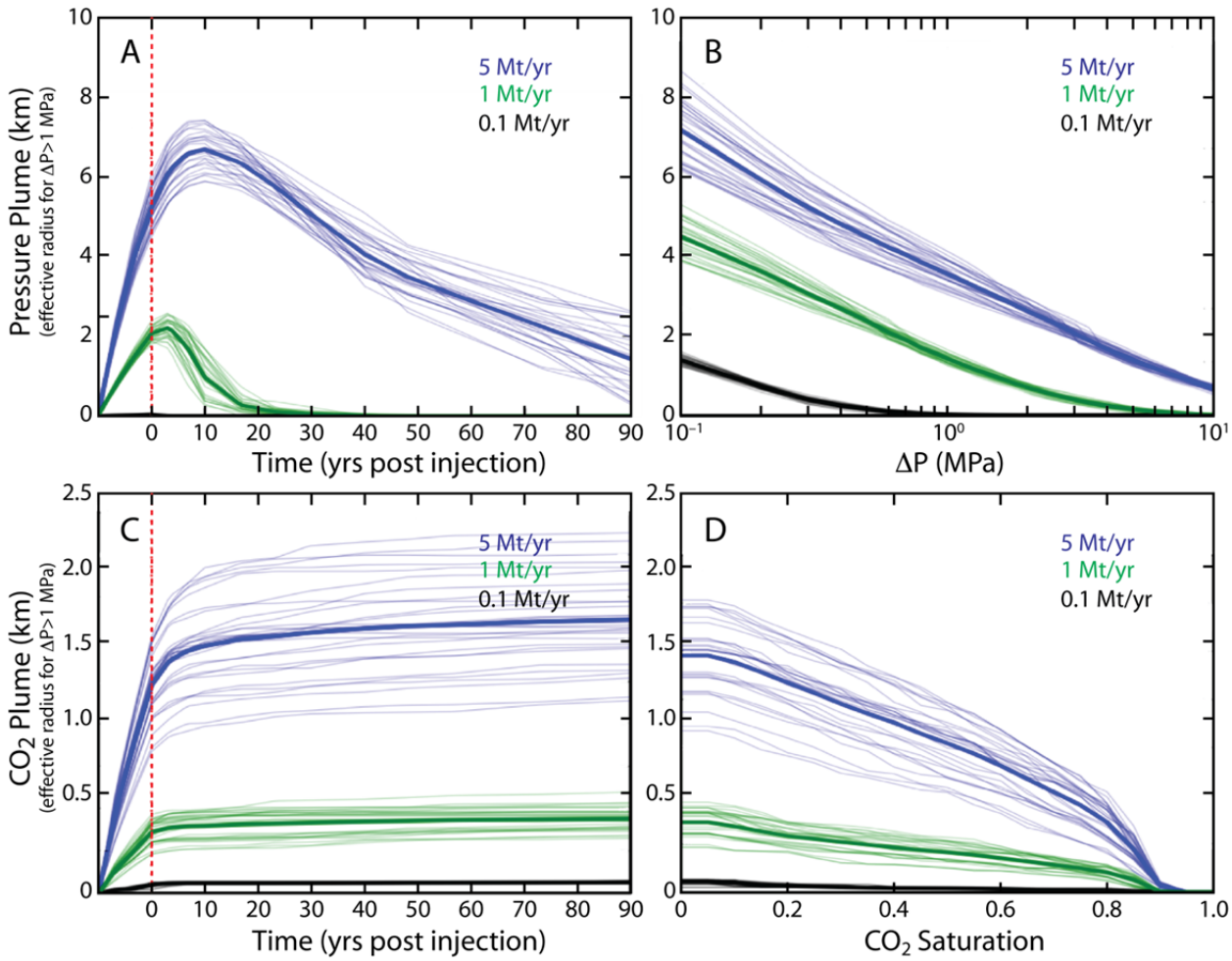

Figure 11: Summary of behavior of pressure and CO_2 plumes in the RSU reservoir for 10-year injection simulations at three different injection rates: 0.1 Mt yr^{-1} (black), 1 Mt yr^{-1} (green), and 5 Mt yr^{-1} (blue). Individual realizations are lightly colored, whereas the ensemble average is bolded. (A) Area of pressure as a function of time plume for a threshold value of ΔP=1 MPa. The end of injection is indicated by a red dotted line. (B) Area of pressure plume at the end of injection for different threshold values of ΔP. C) Area of CO_2 plume as a function of time for a saturation threshold of S=0. (D) Area of CO_2 plume the end of injection for different saturation thresholds.

3. DETAILED ANALYSIS OF RESERVOIR BEHAVIOR

A recent U.S. Department of Energy (DOE) report (DOE-NETL, 2010) outlines the different types of reservoirs that are suitable for carbon storage. Among the more important types, in terms of their known capacity for storage in the U.S., are deltaic, shelf clastic, shelf carbonate, strandplain, reef, fluvial deltaic, eolian, fluvial and alluvial, and turbidite. The reservoirs we have simulated here were meant to help investigate the behavior of many of these types of formations. As described in Section 1.2, the reservoirs simulated could represent deltaic, strandplain, shelf clastic, fluvial deltaic, turbidite, shelf carbonate, and carbonate reef depositional environments. These cover a majority of the types of depositional systems found to be important for geologic carbon storage in the U.S.

Each individual reservoir and each storage site will be different and must be simulated in a site-specific way. However, the simulations performed for this analysis were made to help represent general reservoir behavior and the overall results can be useful in high-level reservoir characterization. From site to site, reservoirs may differ in many ways, both in terms of the geologic structure and the reservoir properties within that structure. The two main types of structure for geologic storage sites are domal systems (e.g., anticline) and unstructured systems (e.g., flat or dipping layer-cake). Another major category of reservoir would also be a compartmentalized formation, which would behave much as an unstructured system with closed boundaries.

Many reservoir properties are known to have an impact on the reservoir behavior, and several of those have been investigated here, in both a homogeneous and heterogeneous (i.e., porosity and permeability) fashion. In addition to reservoir porosity and permeability, which have been mentioned above many times, several other reservoir and subsurface properties were considered in this analysis to see what impact they would have on the three metrics discussed in Sections 1 and 2. Table 1 shows a list of the parameters used and the ranges for each of them in the majority of the simulations.

After analyzing the results using sensitivity analysis or LHS, each of the three modeling teams categorized the impacts of the different operational and reservoir parameters into a high, medium, or low category. These categorizations were based on the stochastic or sensitivity analyses performed and are described more fully in the appendices of this document. Table 2 summarizes the impacts of several different reservoir properties studied, with a general consensus of the three teams around the impacts of different parameters and notes when there was variability on the impacts from different reservoir types or conditions.

There were some differences in impacts of parameters between the domal structure vs. the larger, more open, systems. First, as the larger systems were modeled as open systems, the primary mechanism for storage is displacement of brine by the CO_2. For the domal reservoir, when it was modeled as a closed system, the dominant mechanism for storage is compression, particularly for the larger injection masses. These two characteristics caused there to be a number of differences in the impacts of reservoir characteristics on plume sizes. For the unstructured open systems and larger injection volumes (i.e., 10-100Mt total), the impact of increased reservoir permeability was to decrease the size of the differential pressure plume. For the domal closed systems, the impact of increased reservoir permeability was to increase the size of the differential pressure plume. For the domal, closed system, the salinity also had a slightly higher impact on the

differential pressure and saturation plumes than the open unstructured systems, as the salinity impacts the solubility of CO_2 in the brine. Finally, the thickness and the permeability anisotropy had a lesser impact on the CO_2 saturation plume for the domal system because the migration of the CO_2 plume (particularly post injection) is dominated more by the structure of the reservoir than those other factors.

Finally, the relative size of the pressure and CO_2 plumes can vary significantly, ranging from 0.2:1 to 12:1 ratio of pressure plume size to CO_2 plume size in the cases studied. The size of the differential pressure plume is inversely and non-linearly dependent on the critical pressure threshold used, such that a 5 times increase in the pressure threshold can decrease the differential pressure plume size by much more than 5 times. Additionally, it was seen that even modest reservoir heterogeneity can have a significant impact on the size of differential pressure and CO_2 plumes.

In this study, several different pressure thresholds were used, as there is no standard basis for identifying an appropriate pressure threshold at a site, other than the amount required to move a column of brine against a freshwater gradient to a groundwater aquifer. Since the size of the pressure plume is an important component in both risk and cost (e.g., area required for monitoring), further research into determining an appropriate risk-based pressure threshold value is warranted, as well as developing efficient techniques to identify actual pressures at distances far from the injector to help validate model predictions and reduce uncertainty.

Table 1: Parameters and ranges used in reservoir simulations

Parameter	Min	Max	Notes
Porosity	5%	30%	Max value higher in heterogeneous history-matched model
Permeability	1 mD	1,000 mD	Max value higher in heterogeneous history-matched model
Permeability ratio	0.01	1	
Thickness	50 m	200 m	Actual value used for history-matched reservoir
Compressibility	$6x10^{-6}$	$6x10^{-5}$	
Salinity	30,000 ppm	300,000 ppm	
Caprock Permeability	100 nD	0.01 mD	
Dipping angle of reservoir	0°	3°	Only for unstructured sandstone reservoir

Table 2: Reservoir properties and relative impacts based on sensitivity and stochastic analysis of parameters

Parameter	Impact on Pressure	Impact on Saturation	Notes
Porosity	Medium	High	For closed systems, the impact of porosity can be higher, depending on pressure threshold and injection rate.
Permeability (k)	High	High	For closed systems, the impact of permeability can be lower, depending on pressure threshold and injection rate.
Compressibility	Low-Medium	Low	Compressibility will have a higher impact on pressure for a closed system where the pore volume is within an order of magnitude of the injected volume.
Thickness	Low-Medium	Low-Medium	There is some variability between reservoirs on whether thickness impacts pressure or saturation plume size more.
k_h:k_v	Low	Low-Medium	
Salinity	Low	Low	
Caprock Permeability	Low-Medium	Low	Caprock permeability has more impact when injection rate or mass is not too high and caprock permeability is low.
Boundary Conditions	Medium-High	Low	Boundary conditions are important for higher injection volumes or smaller reservoirs.
Dip angle	Low	Low	Dip angles were only considered up to 3 degrees.
Residual Water Saturation	Low	Low	
Residual Gas Saturation	Low	Medium	

4. RELEVANCE TO REGIONAL PARTNERSHIPS LARGE SCALE PROJECTS

The Regional Carbon Storage Partnerships (RCSPs) are organizations funded through DOE's Carbon Storage Program that perform small- to large-scale carbon storage field projects throughout the U.S. and Canada. Phase I and II projects of the RCSPs involved regional characterization and nineteen small-scale injection projects. Phase III (Deployment Phase) field projects (~1 Mt total CO_2 injected per project except for SECARB's Citronelle Project) are meant to address technical challenges and demonstrate the capability for safe and permanent injection of CO_2 into the subsurface.. This section is meant as a discussion about how the results in the previous sections can inform current and future large-scale field project.

Phase II projects injected CO_2 masses ranging from ~50 t to ~620 kt. Currently, Phase III projects all plan to inject at least ~1 Mt of total CO_2 into the formations that are being studied, with the exception of SECARB's second injection project, which is expected to inject approximately 150 kt. Table 3 lists and describes the current and planned Phase III sites.

Current injections probe a range of key geologic factors (permeability, reservoir lithology, caprock lithology, caprock geometry), allowing testing/validation of predictive models for pressure and CO_2 plumes over a range of conditions. Current injections also consider a narrow range of operational conditions (nominally ~1 Mt of total injection mass). Additional field tests at higher injection rates and volumes would significantly expand testing/validation of predictive models for pressure and CO_2 plumes over a larger range of mass stored and at scales closer to commercial.

Predictions on the behavior of storage reservoirs as a function of injected mass suggest a roughly 1:1 relationship between injected mass and both increase in size of plume (CO_2 or pressure) as well as increase in pressure at a given location in the reservoir. Hence, additional field sites injecting ~2 Mt of CO_2 over a similar duration would roughly double the testing/validation envelope for operational conditions.

Two important observations in the context of the RCSPs emerged from the simulations described herein relative to the description of plume behavior both pre- and post-injection. First, as noted, plume behavior during injection is predicted to be strongly tied to geological properties such as porosity, permeability and reservoir lithology. Each of the Phase III 1 Mt CO_2 injections into saline formations provides an opportunity to verify predictions of reservoir behavior that are instrumental to quantifying potential risks. As implied by the analysis of these simulations, good observations on the change in plume area over time and, in the case of pressure, the change in pressure over time (ΔP) will significantly help to verify predictions of reservoir behavior as needed for risk assessment (both during injection and post injection).

Second, a related observation ties to the predicted behavior of reservoirs post injection. Growth rate in the CO_2 and pressure plumes is expected to change following injection, and it may be possible to verify this through post injection monitoring that occurs in the years following injection. For example, the growth rate in the CO_2 plume is expected to slow by a factor of 10 or more post injection (e.g., Figure 5), and documenting this change in growth rate in field demonstrations would help to verify the predictions on reservoir behavior. The magnitude of the differential pressure at different locations in the reservoir is predicted to decay rapidly (relative to the growth rate) in the time period following injection and the time scale for this decay is

related to the amount of CO_2 injected. This behavior will be particularly important to verify with post injection monitoring of pressure evolution at different points in the reservoir.

Table 3: RCSP Phase III characteristics

Partnership (Project)	Reservoir Formation (Lithology)	Reservoir Properties	Caprock Formation (Lithology)	Caprock Geometry
Big Sky (Kevin Dome Project)	Duperow (dolostone)	ϕ = 10–15% k = 20-100 mD depth = ~4,000 ft	Upper Duperow and Potlatch (anhydrite)	domal
MGSP (Illinois Basin Decatur Project)	Mt. Simon (arkosic sandstone)	ϕ= 18-25% k = 40-380 mD depth = ~7,000 ft	Eau Claire (shale)	flat
MRSCP (Michigan Basin Project)	Niagaran Reef (carbonate reef)	ϕ = 3–11% k = 1 mD; 50 mD depth = ~5,500ft	Salina (evaporates & shale)	domal
PCOR (Bell Creek Field Project)	Muddy (sandstone)	ϕ = 25–35% k = 150-1175 mD depth = 4,500 ft	Mowry (shale)	flat; dipping
SECARB (Cranfield Project)	Lower Tuscaloosa (conglomerates and sandstones)	ϕ = 25% k = 50-1000 mD depth = ~10,500 ft	Middle Tuscaloosa (mudstone)	dipping leg of domal structure
SECARB (Citronelle Project)	Paluxy (sandstone)	ϕ = 22% k = 12-3,950 mD (284 mD ave.) depth = ~9,400 ft	Washita-Fredericksburg (shale)	domal
SWP (Farnsworth Unit, Ochiltree Project)	Morrow (sandstone)	ϕ = 15% k = 10-500 mD (54 mD ave.) depth = ~7,800 ft	Morrow (shale)	flat; dipping

5. REFERENCES

Bandilla, K.W.; Kraemer, S. R.; Birkholzer, J. T. Using semi-analytic solutions to approximate the area of potential impact for carbon dioxide injection. *International Journal of Greenhouse Gas Control* **2012,** *8*, 196–204. DOI: 10.1016/j.ijggc.2012.02.009

Deng, H.; Stauffer, P. H.; Dai, Z.; Jiao, Z; Surdam, R. Simulation of industrial-scale CO_2 storage: Multi-scale heterogeneity and its impacts on storage capacity, injectivity and leakage. *IJCCG* **2012,** *10*, 397–418.

Wainwright, H.; Finsterle, S.; Zhou, Q.; Birkholzer, J. *Modeling the Performance of Large-Scale CO_2 Storage Systems: A Comparison of Different Sensitivity Analysis Methods*; NRAP-TRS-III-002-2012; NRAP Technical Report Series; U.S. Department of Energy, National Energy Technology Laboratory: Morgantown, WV, 2012; p 24.

NETL. *Geologic Storage Formation Classification*; DOE/NETL-2010/1420; U.S. Department of Energy, National Energy Technology Laboratory, 2010.

This page intentionally left blank.

APPENDICES

This page intentionally left blank.

APPENDIX A: DETAILS OF SIMULATIONS OF UNSTRUCTURED SANDSTONE LAYERED FIELD

Executive Summary

Lawrence Berkeley National Laboratory (LBNL) performed a series of reservoir simulations to provide scientific support on understanding of plume sizes (both pressure and CO_2 saturation) for geological CO_2 storage projects as part of the National Risk Assessment Partnership (NRAP) project. Two types of reservoirs have been investigated: and a generic model to systematically simulate CO_2 and pressure behavior over a range of representative site conditions, evaluate the plume sizes for CO_2 saturation extent and pressure buildup, and to derive conclusions on how a variety of factors could influence plume sizes; and a site specific model (Kimberlina model) to focus on how injection volume could affect plume sizes for a realistic site. The factors studied in the generic model simulation include: geologic structure (formation dipping); geologic closure (open, close vs semi-open reservoir); injection volume (injection rate and injection length), brine salinity, formation and caprock properties (including depth and geological properties), and threshold value for defining plume sizes. Results are summarized over a series of 800 simulations. A global sensitivity analysis was performed to study the relative importance of geological properties. The conclusions from the global sensitivity analysis are consistent with the ones from the series of simulations.

Introduction

The delineation of the Area of Review (AoR) is based on the *Maximum Extent of the Separate-phase Plume or Pressure-front* methodology (U.S. EPA, 2011). The overarching purpose of the AoR is to protect drinking water resources due to CO_2 presence and pressure buildup in the injection zone (Nicot, 2006). Understanding how reservoir properties and operational factors influence CO_2 migration and pressure behavior over a range of site conditions provides support for site characterization and risk assessment of CO_2 storage projects. In terms of risk metrics, we use the pressure plume size, defined as the area with a pressure buildup higher a threshold pressure increase (P_{thr}); and the CO_2 (saturation) plume size, defined as the area with a CO_2 saturation higher a threshold pressure increase (S_{thr}).

What affects plume sizes? Geological properties, e.g., rock permeability and porosity, may play an important role in determining the plume size. Figure A1 shows the pressure increase for a constant rate injection scenario at the end of 30 year injection, with two reservoirs having different permeabilities. In the higher permeability case, the pressure propagates faster, while the pressure increase around the injection location is not as high as in the low permeability case. But the reservoir has a larger area with low to moderate pressure increase. For example, if the pressure plume size is delineated based on a relatively small threshold pressure of P_{thr}= 0.2 MPa, and the reservoir has high permeability, the pressure plume will be larger compared to that in a low-permeability reservoir at the end of injection. The pressure plume for the reservoir with high permeability may start to dissipate after the injection stops, so the maximum value is reached at the end of injection. Note that the pressure plume may become zero after CO_2 injection stops, depending on the model boundary conditions. How fast it becomes zero depends on other factors like permeability and compressibility. For the reservoir with low permeability, the pressure plume will be smaller at the end of injection, but will continue to grow, until it reaches its maximum value after which the pressure plume may gradually diminish. If the pressure plume has already reached the system boundary during its increasing phase, then the maximum pressure

plume is as large as the size of the reservoir. However, if the P_{thr} is larger than the maximum pressure buildup in the reservoir with high permeability at the end of injection, the corresponding pressure plume is zero.

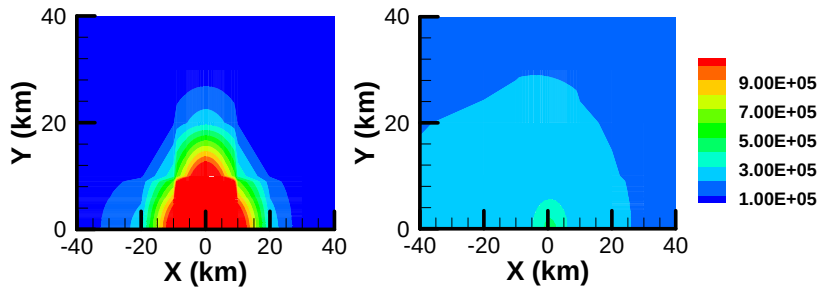

(a) (b)

Figure A1: Illustration of the pressure plume dependence on the P_{thr} for a closed system, showing pressure increase ΔP (Pa) after 30 years of CO_2 injection at a rate of 1Mt/yr for a reservoir with permeability of (a) 0.01 D; (b) 1 D. Formation has a 1 degree dipping in X direction.

As a result, how various geological properties affect plume sizes also depends on many factors other than hydrological properties, specifically the threshold value used for the calculation, the total injected mass, the size of the reservoir, and boundary conditions. Notice the choice of a P_{thr} is not random. In the EPA Area of Review guidance for Class VI wells, P_{thr} is defined as the pressure needed to lift formation brine up the length of an unplugged well to an underground source of drinking water (Bandila et al., 2012). Therefore, the value of P_{thr} can vary strongly for different reservoir conditions.

To study how various factors affect pressure/CO_2 plume sizes, we used two models and performed about 800 numerical simulations. The first model is a generic model used to systematically simulate CO_2 and pressure behavior over a range of site conditions, evaluate the plume sizes for pressure plume and CO_2 saturation plume, and to derive conclusions about the factors influencing plume sizes under representative reservoir conditions. Many number of scenarios were considered in the generic model to study various factors including: geologic structure (formation dipping); geologic closure (open, close vs semi-open reservoir); injection volume (injection rate and injection length), brine salinity, formation and caprock properties (including depth and geological properties), and threshold value for defining plume sizes. All these scenarios are rate-controlled CO_2 injection. The first part for the generic model focuses on how injection rate, threshold, and boundary conditions affect plume sizes with selected results. The second part focuses on how geological properties affect plume sizes. Finally a global sensitivity analysis is performed using the generic model to understand parameter importance on plume sizes. The second model is a site specific model (Kimberlina model) to study how injected volume affects plume sizes for a specific site. It will be discussed in the last section.

Notice it is much harder to quantify maximum CO_2 plume sizes than maximum pressure plume sizes, as CO_2 plume may continue to grow for a long period of time, until it is entirely trapped by residual trapping or dissolution trapping, which will take a long time. In fact, it is almost impossible to run the simulation long enough to the point it is entirely trapped and obtain the maximum CO_2 plume sizes. As a result, for CO_2 plume, we focus on how various factors influencing the size at the end of CO_2 injection, and how they influence its growth after the injection stops.

The Generic Model

1. Model and Scenario Description

A generic model is defined (a schematic of the model is shown in Figure A2) to understand how various factors affect the plume sizes. The horizontal extent of the model is:–40-km≤x≤60-km (dipping in X direction), –50-km≤y≤50-km (symmetric in Y direction). The vertical extent varies, depending on the reservoir thickness and if caprock and baserock are included in the scenario. A single injection well is located at X = 0 m, Y = 0 m. Injection is over the entire vertical thickness. The model grid has a finer discretization within the 6-km radius surrounding the wellbore. The simulations were conducted considering different (1) boundary conditions (Table A1), (2) geological properties (Table A2), (3) operational factors (Table A3), and (4) plume size threshold values (Table A4). In these simulations, one parameter/factor is varied at a time using the conditions/values defined in Tables A1–A3, potential correlations among parameters were not considered.

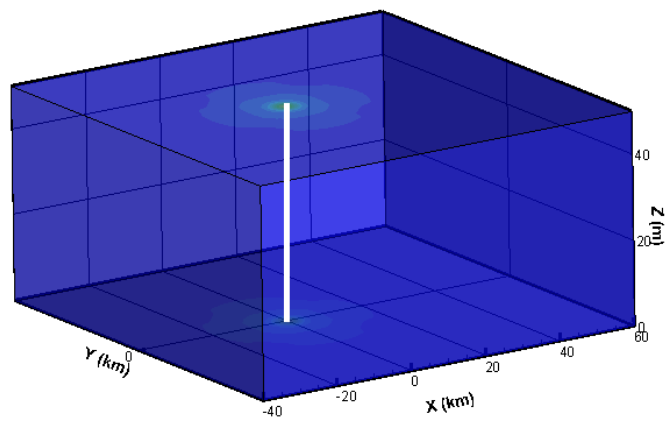

Figure A2. Schematic of the generic model. The model extends to 100 km in both X and Y directions; the formation dips in X direction. The reservoir thickness Z varies.

Table A1. Boundary conditions considered for representative reservoir conditions. The caprock is 80-m thick, and the baserock is 40-m thick in S3 and S4.

Boundary Condition (BC)	Definition
Closed system (S1)	No flow BC at all sides. No caprock and baserock
Open system (S2)	No flow BC for top and bottom, constant pressure at side boundaries, no caprock and baserock
Semi-open system (S3)	No flow BC for the side, low permeability caprock and baserock are connected to constant pressure boundaries
Open system with permeable caprock and baserock (S4)	A combination of open system and semi-open system: constant pressure at side boundaries, low permeability caprock and baserock are connected to constant pressure boundaries.

Table A2: Reservoir properties considered for representative reservoir conditions. The first value of each line is considered as the base case scenario.

Reservoir Properties	Values Used
(horizontal) Permeability (m^2)	10^{-13}, 10^{-12}, 10^{-14}
Porosity	0.2, 0.1, 0.3
(Pore) Compressibility (Pa^{-1})	1.5×10^{-9}, 3×10^{-10}, 3×10^{-9}
Anisotropy ratio (k_v/k_h)	0.1, 0.01, 1
Residual gas saturation (S_{gr})	0.2, 0.1, 0.3
Residual liquid saturation (S_{lr})	0.3, 0.1, 0.2
Salinity (g/L)	100, 10, 230
Cap-/baserock permeability (m^2)	10^{-18}, 10^{-19}, 10^{-17}
Formation dip (degree)	1, 0, 3
Reservoir thickness (m)	50, 100, 200

Table A3: Operational factors considered for representative scenarios.

Operational Factors	Values Used
Injection duration (yr)	3, 30
Post-injection period simulated (yr)	47 (for 3-yr injection), 270 (for 30-yr injection)
Injection rate (yr^{-1})	10 kt, 50 kt, 250 kt, 1 Mt, 5 Mt

Table A4: Threshold values used for the generic model.

P_{thr} (MPa)	0.1, 0.5, 1
S_{thr}	S_{gr}, 0.01, 1.e-4

2. Simulation Tool

Due to the large size of the system considered and the computational cost associated with such a big model, a two-phase flow code based on the Finite Volume method, developed at LBNL, (TP3D) was chosen to make a large number of simulations possible. The Jacobian matrix is solved analytically instead of numerically in the TP3D. A few assumptions made in the TP3D

include: (1) CO_2 dissolution is ignored; (2) density effects due to pressure changes are ignored; (3) viscosity changes due to pressure changes are ignored. The TP3D code was verified with both analytical solutions for single-phase simple problems and the TOUGH2 numerical simulator (Pruess et al., 1999) for more complex problems with two-phase flow. Testing the TP3D with the TOUGH2 simulator for a number of simulation cases shows that the pressure distributions and the CO_2 plume sizes calculated by the two codes for 300-yr simulation times are very similar. Some differences in the model results were observed in CO_2 saturation distributions inside the CO_2 plume, especially near the edges of the plume. This difference is mainly due to CO_2 dissolution, which is accounted for in TOUGH2/ECO2N, but ignored in TP3D. However, CO_2 dissolution can have significant effects on evolution of CO_2 at longer time-scales or at shorter time-scales when the GCS includes brine injection/extraction schemes. Based on our analyses, the area of the CO_2 plume calculated from TP3D is considered to be a good approximation for pure CO_2 injection scenarios without any alternating brine injection/extraction schemes.

3. Selected Results and Key Findings

The discussion here focuses on the influence on plume sizes from factors listed in Tables A1, A3 and A4. The influence from different geological properties is discussed in the next section.

A base case scenario for the generic model is defined as: open system, 50-m thickness reservoir, dipping angle 1 degree, injection rate=1 Mt/yr, injection duration=30 yr, post-injection = 270 yr (total simulation time is 300 yr), $k_h=1\times10^{-13}$ m^2, $k_v/k_h=0.1$, porosity = 0.2, $S_{gr}=0.2$, $S_{lr}=0.3$, pore compressibility=1.5×10^{-9} Pa^{-1}, salinity = 100 g/L. The selected results are based on this base case scenario.

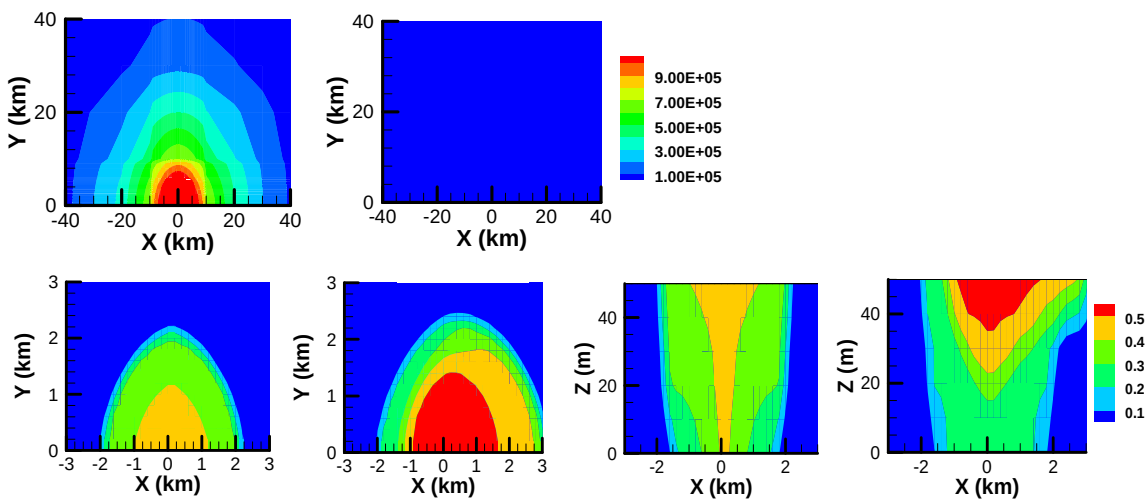

Figure A3: The two upper figures show ΔP distribution at the end of the injection (30 yr, left) and at 300 yr (right). The left two lower figures show the model top layer CO_2 saturations (S_g) at 30 yr and 300 yr, and the right two lower figures show vertical S_g profiles at 30 yr and 300 yr for base case scenario.

Figure A3 shows the base case scenario the pressure increase and plume distribution at the end of injection and at the end of simulation for the base case scenario. The pressure buildup dissipated at 300 yr entirely because of the open boundary. Compared to Figure A1(a) – pressure increase distribution at 30 yr for a closed system, the pressure front extends further, but the largest pressure buildup is less. In terms of CO_2 plume movement, one can see not only the CO_2 plume

size is larger at 300 yr (compared to it at the end of injection 30 yr), but also the CO_2 saturation (S_g) is much higher at the top layer of the model. This is because CO_2 moved upwards during post injection period due to the buoyancy effect, as can be seen from the vertical S_g profiles shown in Figure A3.

Based on the base case scenario, one factor is varied at a time to study the influence on pressure plume sizes and CO_2 plume growth from each individual factor.

- *Injection rate vs. pressure plume size*

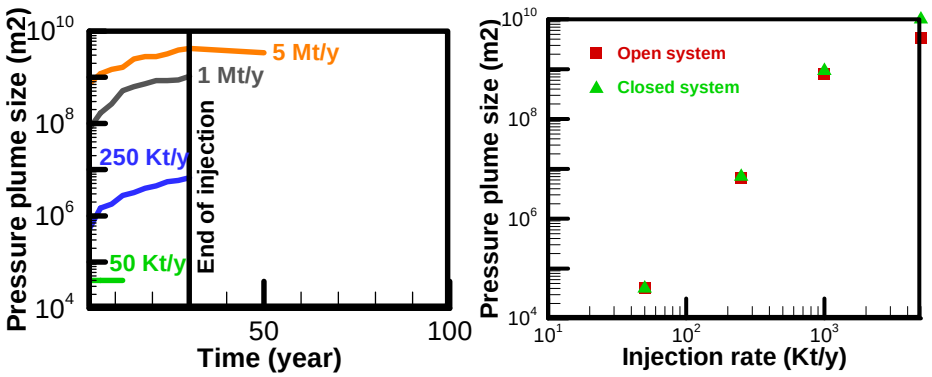

(a) (b)

Figure A4. (a) Pressure plume size over time for various injection rates – the base case open system. The simulations were performed to 300 years. The sudden stopped lines mean the pressure plume size value drops to zero (same for the rest of the figures); (b) Maximum pressure plume size for various injection rates – for both open and closed system. P_{thr}=5 bar.

Figure A4 shows the pressure plume sizes over time for different injection rates. For most cases, the pressure plume stops to grow after injection stops. Notice pressure plume size is zero for the 10 kt/yr injection rate, therefore it is not shown on the figure. For higher injection rate cases (e.g., 1 Mt/yr, 5 Mt/yr), the pressure plumes continue to grow for a while before reaching their maximum value. Note that the pressure plume sizes become zero at some point after injection stops. This happens when the maximum pressure drops below the threshold pressure (in which case the pressure lines in the figures stop). We also plot the maximum pressure plume size vs. injection rate, for both open system and closed system. The maximum pressure plume size is the same for smaller injection rate for both systems; but for higher injection rates (e.g., 1 Mt/yr, 5 Mt/yr), when pressure buildup gets close to the system boundary, it gets dissipated in the open system, but not in the closed system. Therefore, the maximum pressure plume size is larger in the closed system than in the open system.

- *Injection rate vs. CO_2 plume size*

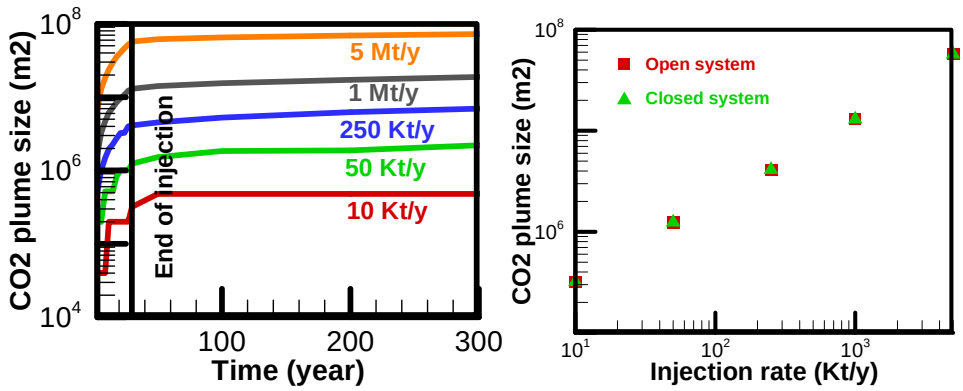

(a) (b)

Figure A5: (a) CO_2 plume size over time for various injection rates – the base case open system; (b) the CO_2 plume size at the end of the injection for various injection rates – for both open and closed system, the CO_2 plume size is identical for both cases. S_{thr}=0.01.

Figure A5 shows the CO_2 plume size over time as a function of injection rate. The CO_2 plume growth slows down after the injection stops compared to it during injection phase. The CO_2 plume continues to grow even at 300 years in most cases. For the case with 10 kt/yr injection rate, the CO_2 saturation at the center of the plume is still a little above residual gas saturation, which means not all the CO_2 is residually trapped. There is a possibility that it will continue to grow. Since dissolution is not included in the code, the dissolution trapping effect is ignored in these results. The CO_2 plume size is the same for both open and closed systems.

- *Threshold vs. pressure/CO_2 plume size*

Figure A6 shows both pressure plume size and CO_2 plume size as a function of different threshold values. When a large P_{thr} is used, the pressure plume size is not much affected by the boundary condition. The pressure plume size is more affected by boundary condition if a smaller value is used. This difference starts to appear when the pressure front ($\Delta P=P_{thr}$) reaches the boundary. For CO_2 plume size, there is a small difference between a threshold value of 0.2 and $1.\times10^{-2}$; the difference does not change much over time. There is not much difference between a threshold value of $1.\times10^{-2}$ or $1.\times10^{-4}$. As a result, the conclusions on plume extent will not be sensitive to the threshold value used.

Notice for a closed system, the injection rate and pressure threshold have an opposite effect on the maximum pressure plume size. For example, the maximum pressure plume size is the same if (a) the injection rate is 5 Mt/yr and the pressure threshold is 5 bar; and (b) the injection rate is 1 Mt/yr and pressure threshold is 1 bar. The relationship also applies to an open system if the injected volume is small enough that the pressure front does not reach the boundary.

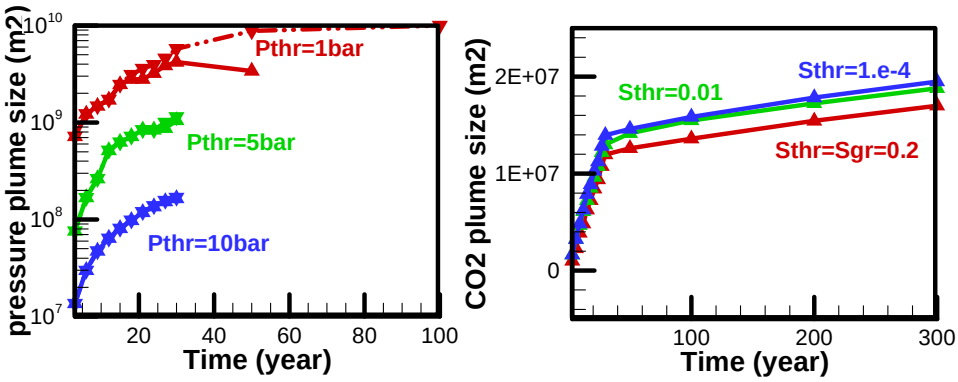

(a) (b)

Figure A6: (a) Pressure plume size and (b) CO_2 plume size as a function of different threshold values for both closed (dashed lines) and open (solid lines) system. The dashed and solid lines collapse into one for the CO_2 plume size plot because CO_2 plume sizes are not affected by boundary conditions in such a large system.

- *Boundary condition (BC) vs. pressure/CO_2 plume size*

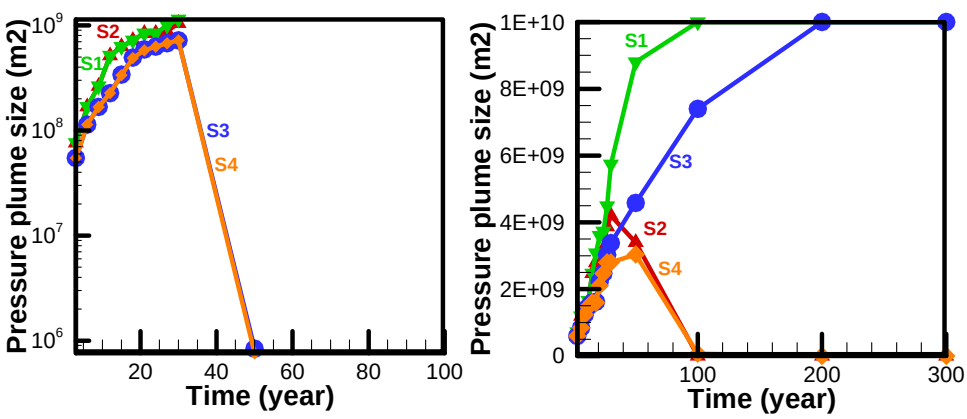

(a) (b)

Figure A7: Pressure plume size for different boundary conditions (listed in Table 3) for (a) injection rate = 1 Mt/yr and (b) injection rate = 5 Mt/yr.

Figure A7 shows how boundary conditions (listed in Table A1) affect pressure plume size. In S3 and S4 systems, pressure buildup gets attenuated by the cap- and base-rock immediately when injection starts. In fact, in the case of injection rate = 1 Mt/yr, this attenuation helps pressure dissipate enough so the open side boundary does not help reduce the pressure plume size. However, for the case of injection rate = 5 Mt/yr, even though the cap- and base-rock provide some permeability to reduce pressure buildup, the injection rate is so high that the open boundary helps pressure dissipate immediately from the beginning of the injection. Eventually, the pressure plume size is the same as the model domain size for both S1 and S3, but the pressure plume never reaches the boundary for S2 and S4 due to open BC at the sides.

Boundary conditions have very little effect on the CO_2 plume size. The largest difference (e.g., at 5 Mt/yr injection rate, between S1 and S4 at 300 years) in the CO_2 plume size is on the order of 2%.

Summary Results Regarding the Influence of Geological Factors on Plume Sizes

Pressure plume size

The following conclusions can be drawn for a closed system based on the simulation results:

- Both reservoir size and injection volume are important factors influencing the maximum pressure plume size;
- If there are no boundary effects, i.e., the model is large enough for the injected volume, the maximum pressure plume size is sensitive to permeability (larger permeability→ smaller pressure plume size, Figure 8a), porosity (larger porosity → smaller pressure plume size, Figure 8b), and compressibility (larger compressibility→ smaller pressure plume size, Figure 8c). The sensitivity to permeability becomes very high, especially for highly permeable formations.
- The maximum pressure plume size is also sensitive to the anisotropy ratio (larger $r = k_v/k_h$ → smaller pressure plume size) and residual gas saturation S_{gr} (smaller S_{gr} → smaller pressure plume size)
- For a given pressure threshold, formation dip and brine salinity, residual water saturation had hardly any effect on pressure plume size.

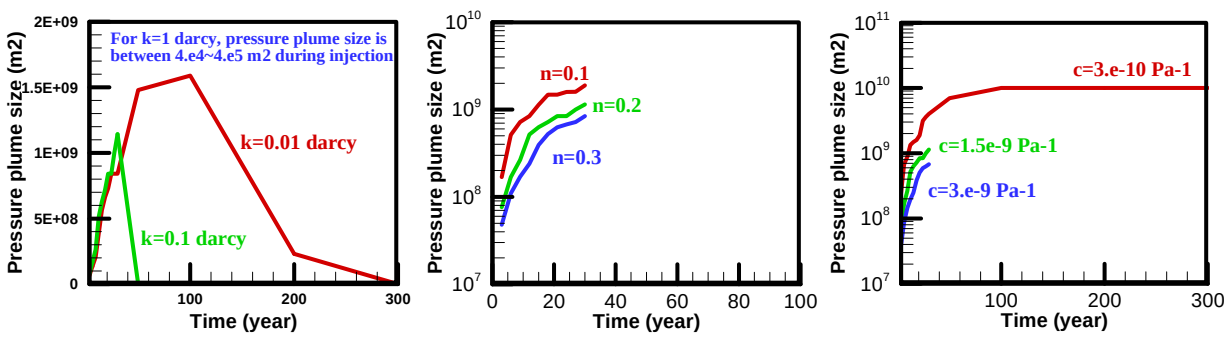

(a) (b) (c)

Figure A8. (a) permeability effect; (b) porosity effect; (c) compressibility effect on the pressure plume size for an injection rate of 1 M ton/y, P_{thr} = 5 bar, for a closed system

The following conclusions can be drawn for a semi-open system based on the simulation results:

- The conclusions on the maximum pressure plume size sensitivity to the geological parameters are similar to those for a closed system.
- The pressure plume size in a semi-open system is smaller than the pressure plume size in a closed system, if all other geological conditions are the same.

For an open system, the pressures at the boundary are held constant at the initial-condition values; therefore, the pressure plume size will never be able to reach the boundary. The simulations indicate the following:

- The conclusions regarding the pressure plume size sensitivity to the geological parameters are similar to those for a closed system, except that permeability has a greater effect on pressure plume size for an open system than for a closed system.
- The pressure plume size in an open system is smaller than the pressure plume size in a closed system, if all other geological conditions are the same.

CO_2 plume growth

For CO_2 plume growth, we summarize some of the general observations on the transient CO_2 plume size during and post- injection.

- CO_2 plume size is very sensitive to the formation porosity, both during injection and post-injection (smaller porosity → larger plume size), as shown in Figure A9.
- During the injection phase, the CO_2 plume size is also sensitive to permeability (higher permeability → larger plume size); the sensitivity becomes stronger at smaller injection rates (i.e., less viscous force), as shown in Figure A10.
- During the post-injection phase, the CO_2 plume size is sensitive to:
  - permeability (higher permeability → larger plume size);
  - residual gas saturation S_{gr} (smaller S_{gr} → larger plume size, because smaller S_{gr} means more CO_2 is mobile);
  - residual liquid saturation S_{lr} (larger S_{lr} → larger plume size, because larger S_{lr} means less space to accommodate injected CO_2);
  - salinity (higher salinity → larger plume size, i.e., more buoyancy effect);
  - anisotropy ratio r (larger r → larger plume size). More pronounced for smaller injection rate, i.e., a weaker viscous force in horizontal direction increases buoyancy effects.
  - formation dip (larger dip angle → larger plume size, i.e., more buoyancy effect).
- Boundary conditions do not affect CO_2 plume size much because a relatively large model domain is considered in these simulations.

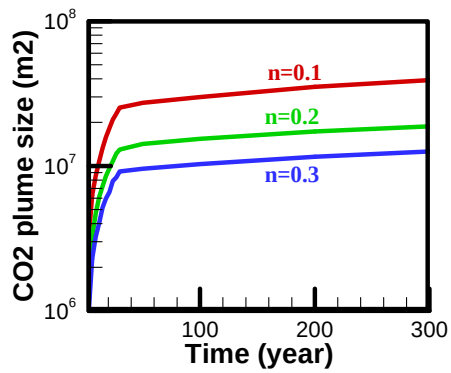

Figure A9: Porosity effect on the CO_2 plume size, injection rate=1 Mt/yr, S_{thr} = 0.01, a closed system.

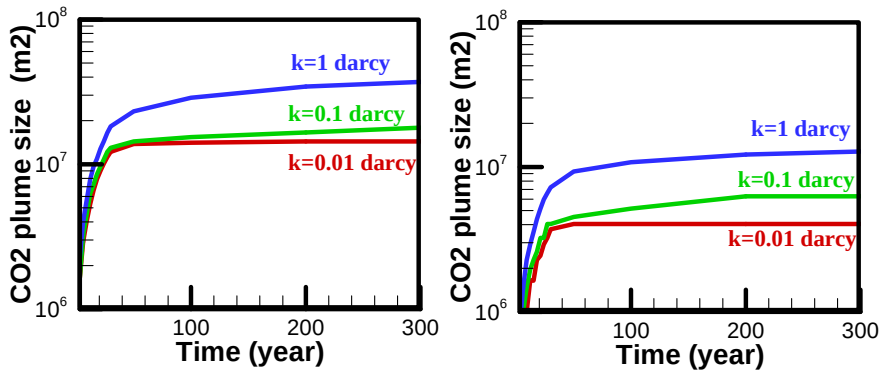

(a) (b)

Figure A10: Permeability effect on the CO_2 plume size for an injection rate of (a) 1 Mt/yr; and (b) 250 kt/yr, S_{thr} = 0.01, a closed system.

Global Sensitivity

A global sensitivity analysis was performed to understand how each parameter influences the plume size, considering the following discrete operational (injection rate) and geological conditions (formation dipping and boundary condition), and continuous parameter distributions:

- 30-year injection with 3 injection rates (kt/yr): 10, 250, 1000
- Two reservoir formation dipping: 0, 3
- Boundary condition (BC): constant pressure (open) and no flow (closed)
- Reservoir horizontal permeability, Kh (mD): 10–1000 (loguniform)
- kv/kh: 0.01–0.1 (loguniform)
- Porosity: 0.05–0.35 (uniform)
- Rock compressibility (1/Pa): 1.5×10-10–1.5×10-9 (loguniform)
- Three residual liquid saturations (Slr): 0.1, 0.2, 0.3
- Three residual gas saturation (Sgr): 0.1, 0.2, 0.3

300 MC simulations were performed for each of scenario combinations (injection rate, formation dipping and boundary conditions). The total number of scenario combinations is twelve. Selected results for the injection scenario 250 kt/yr are presented in Figures A11~A14.

Figures A11 and A12 show pressure plume size and CO_2 plume size over time using various threshold values for an open and closed system, respectively. The pressure plume sizes are generally smaller for an open system than a closed system. There are cases where the pressure plume size keeps increasing after the injection stops, when the threshold pressure is low. This is because the extent of lower pressure expands as the over-pressure dissipates. CO_2 plume sizes in both systems are similar, as we discussed in the previous section, the boundary conditions do not affect the plume. These results are consistent with results in the previous section.

Sobol' index is used to quantify the parameter importance in this analysis. It is defined as variance of conditional expectation when the parameter is fixed, over the total variance of the system response. Sobol' index is a measure of the amount of variability in the response due to each individual parameter, and it is considered to be a quantitative sensitivity index to measure the effect of each parameter without interaction effects with other parameters. In this study, Sobol' index is computed using the MC simulation results, based on the approximation method developed by Wainwright et al. (2014).

Figures A13 and A14 are the Sobol' indices over time for an open and a closed system, respectively. For pressure extent, the formation permeability is the most sensitive parameters over time in an open system. In a closed system, when P_{thr}=1bar, the pressure plume sizes in many simulations, are the same as the system size, in which case, porosity becomes the most important factor; and compressibility becomes more important; permeability does not play a role anymore. This conclusion is consistent with the Equation 1 in the previous section. For CO_2 plume size, the porosity is the most sensitive parameter. Different threshold values have little impact. Residual gas and liquid saturation have less impact on pressure/CO_2 plume size compared to other factors. When P_{thr}=10 bar, the conclusions on the importance of factors are the same for closed and open system, as the corresponding pressure ($\Delta P \geq 10$ bar) front have not reached the boundaries. This conclusion is also consistent with previous results.

Figure A15 and A16 show the Sobol' indices at the end of simulation including all three injection rates. For an open system, the parameter importance ranking on the pressure plume size and CO_2 plume size does not change significantly for different injection rates, dip angles and different threshold values. The horizontal and vertical permeabilities are the most important parameters for the pressure plume size, while the porosity is a dominant parameter for the CO_2 plume size. For a closed system, large injection rates or small P_{thr} leads to the maximum pressure plume size the same as the system size, changing the most important parameter from permeability (small injection rate, large P_{thr}) to porosity. In fact, because the maximum pressure plume size is always the same as the system size, the maximum pressure plume size is deterministic and the corresponding parameter Sobol' index is zero (as shown in Figure A16, P_{thr}= 1 bar, and injection rate = 1 Mt/yr).

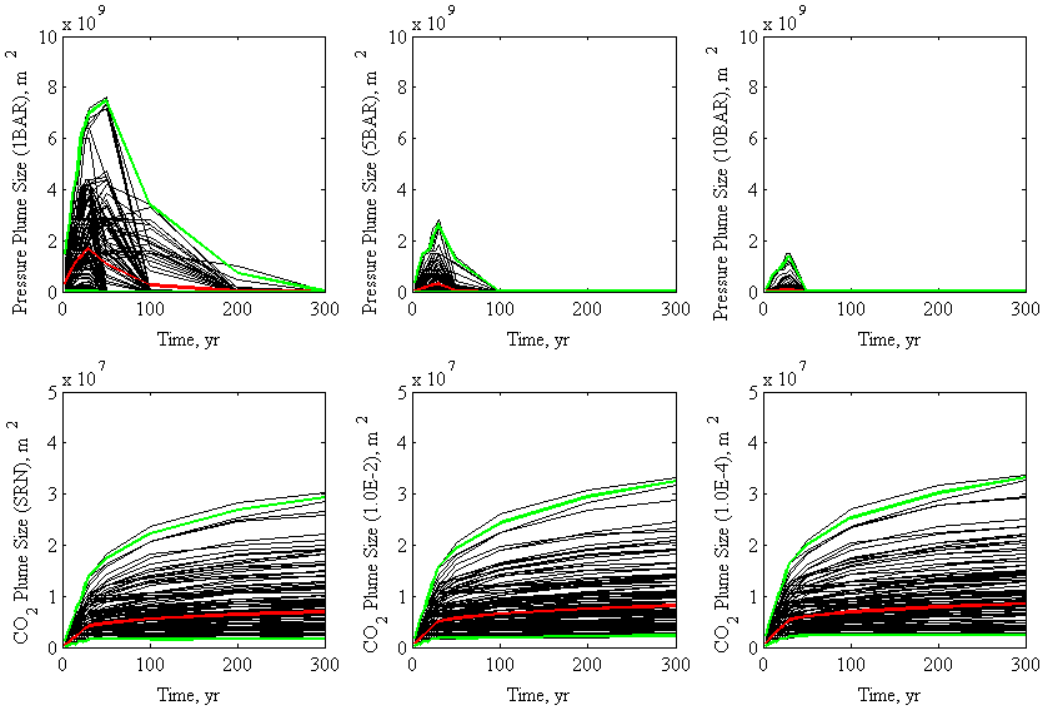

Figure A11: Monte Carlo simulations for an open BC, injection rate = 250 kt/yr, dip=0.

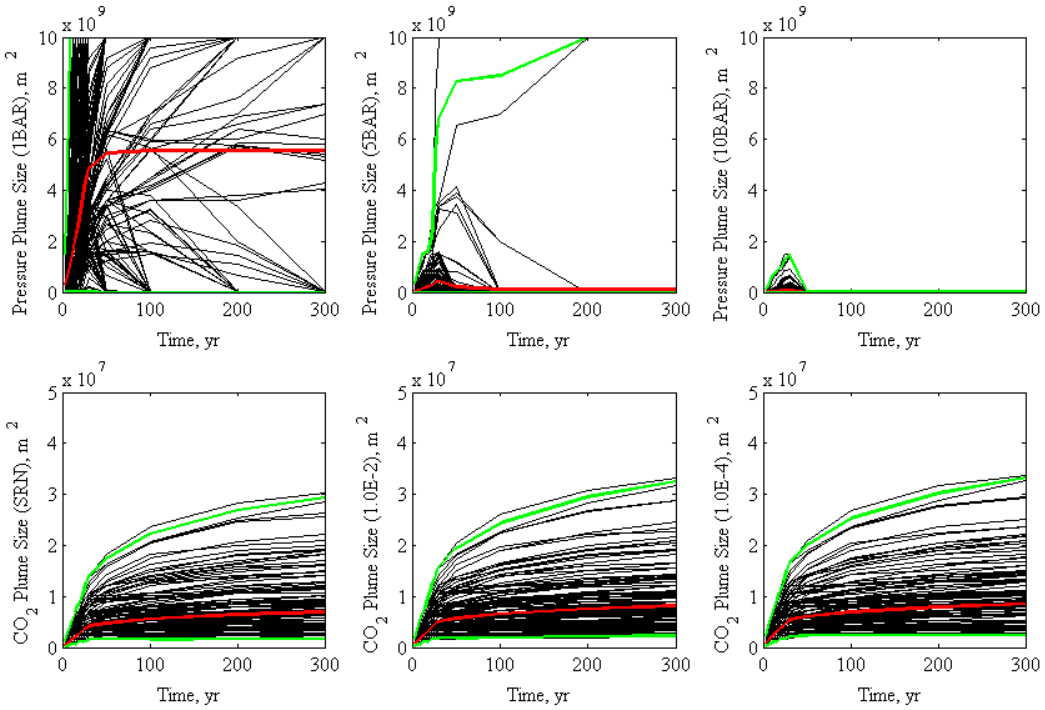

Figure A12: Monte Carlo simulations for a closed system, injection rate = 250 kt/yr, dip=0.

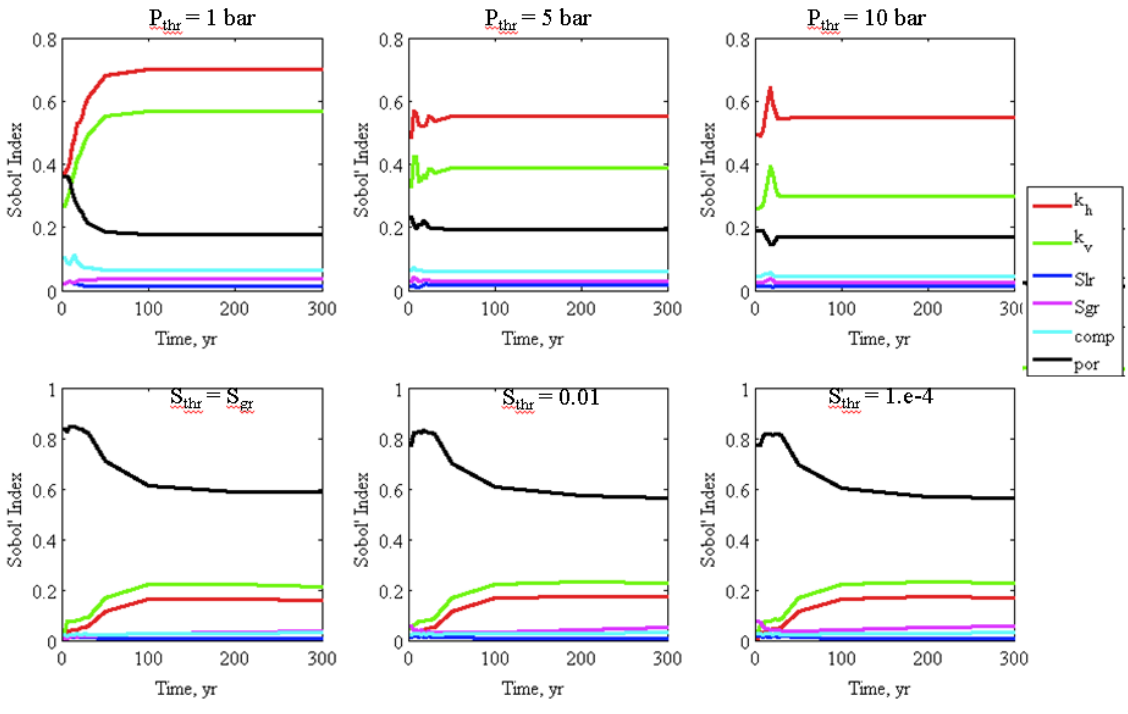

Figure A13: Sobol' index over time for injection rate = 250 kt/yr, dip=0, open system.

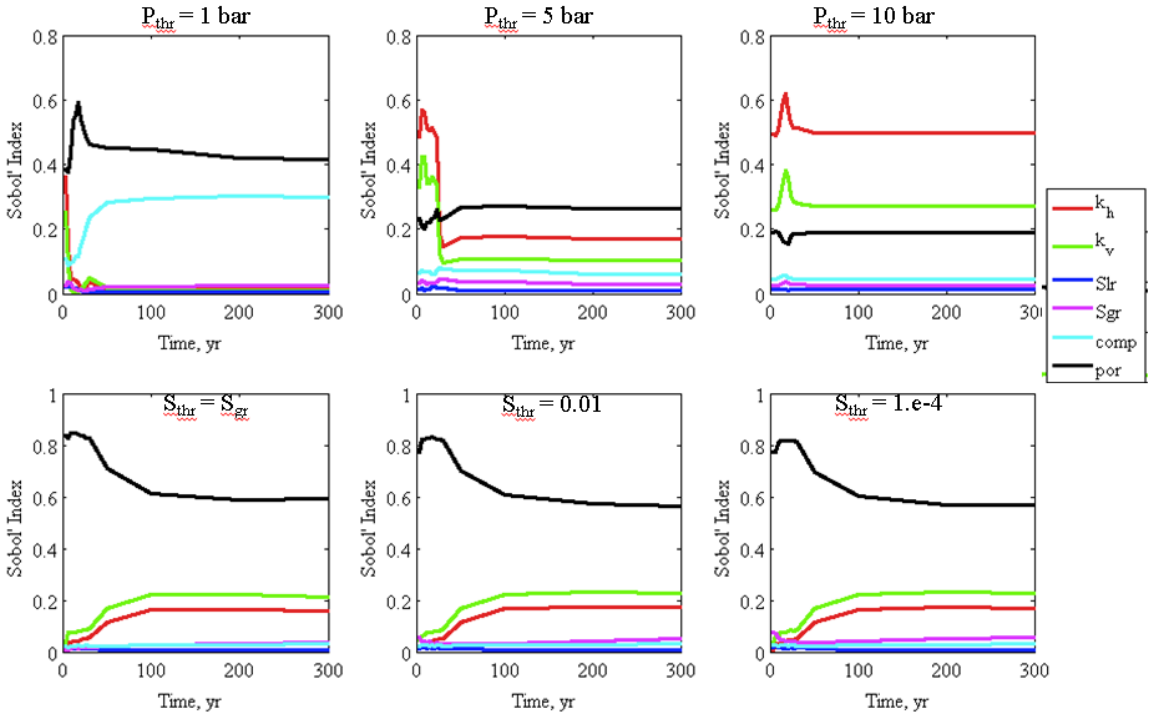

Figure A14: Sobol' index over time for injection rate = 250 kt/yr, dip=0, closed system.

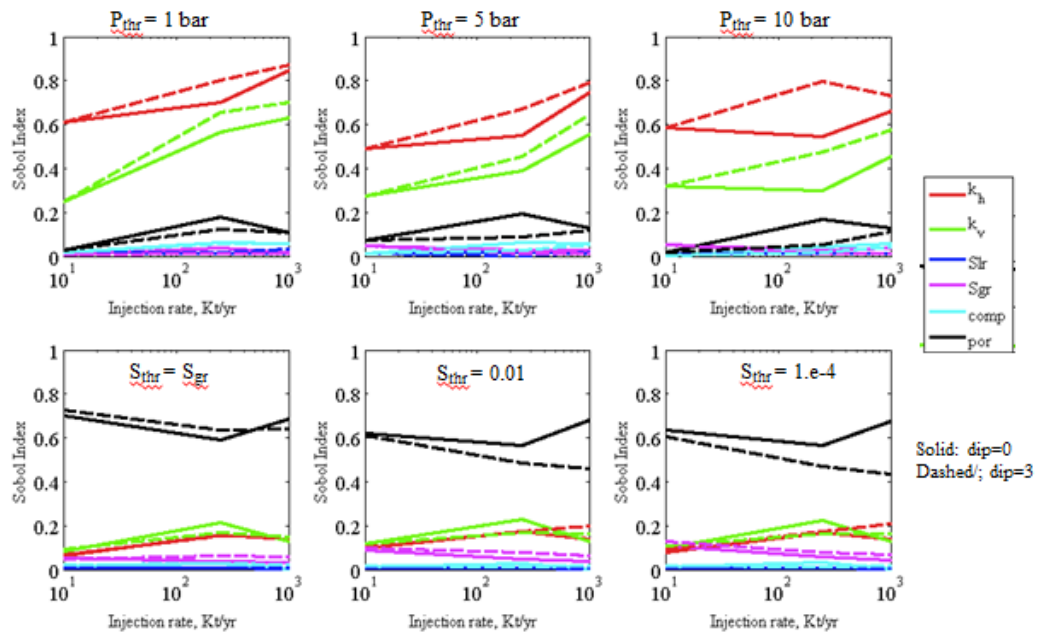

Figure A15: Sobol' index at the end of injection (300 years) for an open system.

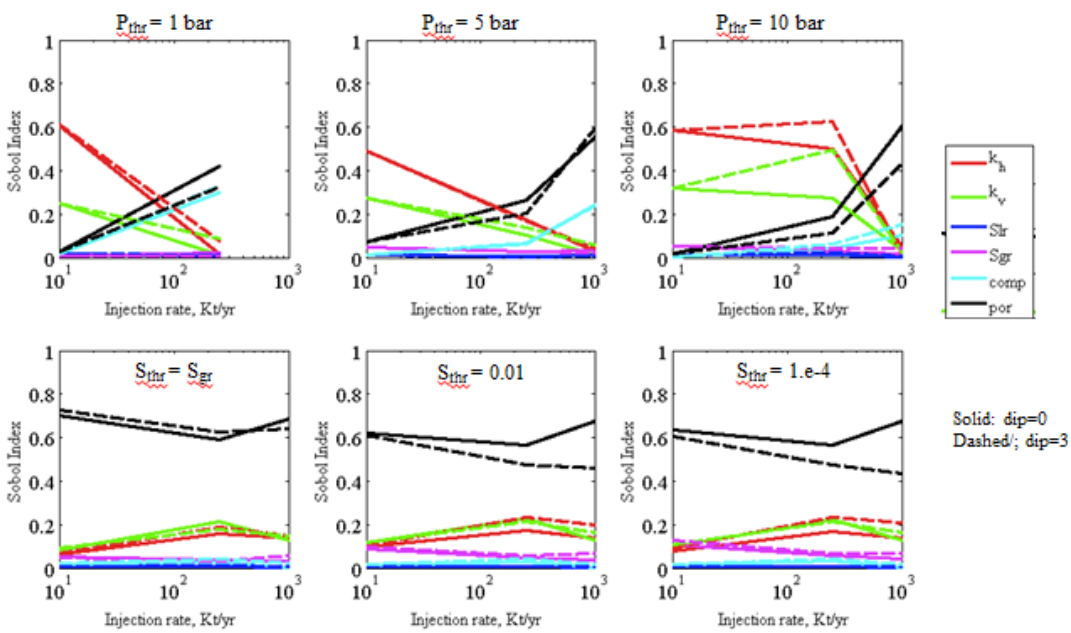

Figure A16: Sobol' index at the end of injection (300 years) for a closed system.

In general, the findings from the sensitivity analysis are consistent with the conclusion from the previous section, which investigated one factor at a time. The pressure plume size is affected by boundary conditions, threshold values and injection volumes. Permeability is the most important factor for determining pressure plume sizes if the pressure front has not reached boundary. Otherwise, porosity plays a more important role. For the CO_2 plume size, the porosity is always

the most important factor. The plume extent is not significantly affected by boundary conditions and threshold values.

Kimberlina Model

1. Model and scenario description

The reservoir-scale CO_2 migration model was developed based on a geological study in the Southern San Joaquin Basin, California, using geologic and hydrogeologic data obtained from many oil fields in that region. Although the detail model description is available in Zhou et al. (2011), Zhou and Birkholzer (2011), Birkholzer et al. (2012) and Wainwright et al. (2013), it is summarized here for completeness. The model domain includes twelve discontinuous or continuous (stacked) formations from the crystalline base rock to the top shallow aquifer, extending 84 km in the eastern direction and 112 km in the northern direction (Figure A17a). This study assumes that CO_2 injection is conducted in the center of the domain.

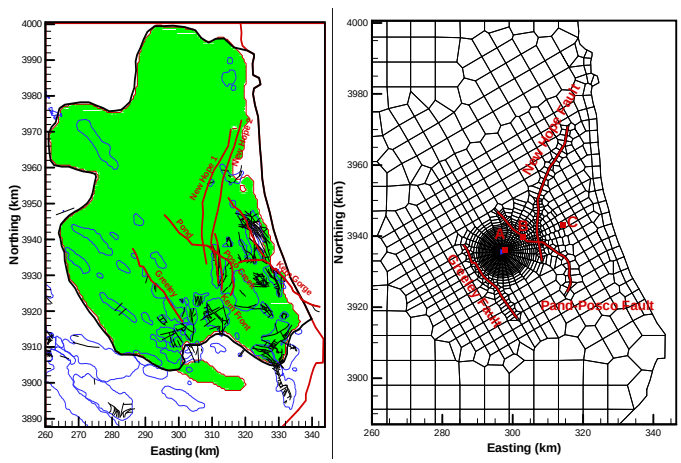

(a) (b)

Figure A17: Plan view of (a) the Vedder formation (green area) with faults (red lines), and (b) the model domain with numerical grid. In (a), blue polygons show hydrocarbon fields in the region with data used for the development of geologic model and spatial distribution of rock properties. In (b), the red lines delineate the faults that are explicitly represented in the model, the blue point is the injection location, and the red dots (Points A, B and C) are used for point-based performance measures.

The target reservoir is a deep saline sandstone formation, the Vedder formation, underlying low-permeable caprock, the Temblor-Freeman Shale. At the (assumed) injection site, the Vedder formation is about 400 m thick, and its top elevation is about 2,750 m below the ground surface. The caprock (TF Shale) is about 200 m thick. Based on well logs, one may distinguish six alternating sand/shale layers within the Vedder formation; these internal facies are considered laterally continuous in our study. The Vedder formation pinches out to the far south, west, and north of the injection site, and reaches the surface along the eastern boundary. Figure A17a also shows the outline of several faults in the area. Fault zone properties are quite uncertain; however, there are qualitative observations that most fault zones are less conductive than the adjacent sandstone formations (Birkholzer et al., 2011a). In this study, we assume a fault scenario representing partial compartmentalization where the lateral permeability of major faults is

reduced by a factor of 100 compared to the adjacent formation permeability. The faults are assumed non-conductive in shale formations.

As injection scenarios, we fixed the injection period as 50 years, and varied the constant injection rate ranging from 10 kt/yr to 5 Mt/yr. We defined the CO_2 plume size and the pressure plume size as the area of CO_2 saturation larger than the residual saturation of 0.25, and the area of pressure increase larger than 0.058 MPa at the reservoir-caprock interface, respectively. The threshold pressure value of 0.058 MPa is based on brine leakage studies related to Area of Review assessments of the California Central Valley, where this domain is located (Nicot et al., 2008).

2. Simulation tools

We used the massively parallel multiphase simulator TOUGH2-MP (Zhang et al., 2008) with the ECO2N module to simulate injection and migration of supercritical CO_2 in the brine reservoir. The ECO2N module describes the thermodynamics and thermophysical properties of H_2O-NaCl-CO_2 mixtures, including phase transitions and dissolutions (Pruess, 2005). The simulation time includes the injection period of 50 years, and a post-injection period of 150 years.

A 3-D mesh of 64,214 elements was generated representing the twelve formations. As mentioned before, the storage formation (the Vedder sandstone) was divided into three sand model layers and three alternating shale layers. The mesh design was such that we can accommodate a large number of simulations while accurately accounting for the CO_2 plume behavior in the storage formation. Figure A1b shows the plan view of the numerical mesh. Significant mesh refinement can be seen in the center of the domain, where multiphase processes and strong pressure buildup can be expected in response to CO_2 injection.

3. Selected results and key findings

Figure A18 shows the plume evolution and pressure buildup in the uppermost reservoir layer just below the caprock for the case with the injection rate of 1 Mt/yr. The pressure response to CO_2 injection is fast and eventually affects a large region close to all the boundaries. The semi-permeable faults clearly affect the pressure response by confining the pressure buildup to the region of injection between the faults. In the post-injection period, the pressure dissipates and returns back close to hydrostatic. CO_2 plume migration is generally a much slower process than pressure propagation. At the end of injection, the CO_2 plume remains within a 5.0 km radius from the injection point. After injection ends, the plume continues migrating eastward in the updip direction driven by buoyancy, until it arrives at the fault around 100 years and is stopped from further migration.

Figure A19 shows the temporal evolution of the pressure plume size (the area of pressure increase larger than 0.058 MPa) and CO_2 plume size (with saturation in the reservoir larger than the residual saturation) for different injection rates. In Figure A19a, for 1 Mt/yr and 5 Mt/yr cases, the pressure plume size increases strongly and in an almost linear trend up to around 20 years after injection start, after which the increase slows down considerably, with another distinct trend change after about 30 years. Such distinct changes in the overpressure-zone curve can be attributed to the pressure field reaching the lateral faults or arriving at the formation boundaries. The pressure plume size is zero for 10 and 50 kt/yr cases, because the injection does not create overpressurization beyond the threshold value. In Figure A19b, the CO_2 plume area increases gradually until approximately 80 years after injection and then remains constant. The

gradual increase occurs during the period of updip CO_2 migration, up to the point that the plume arrives and stopped at the fault.

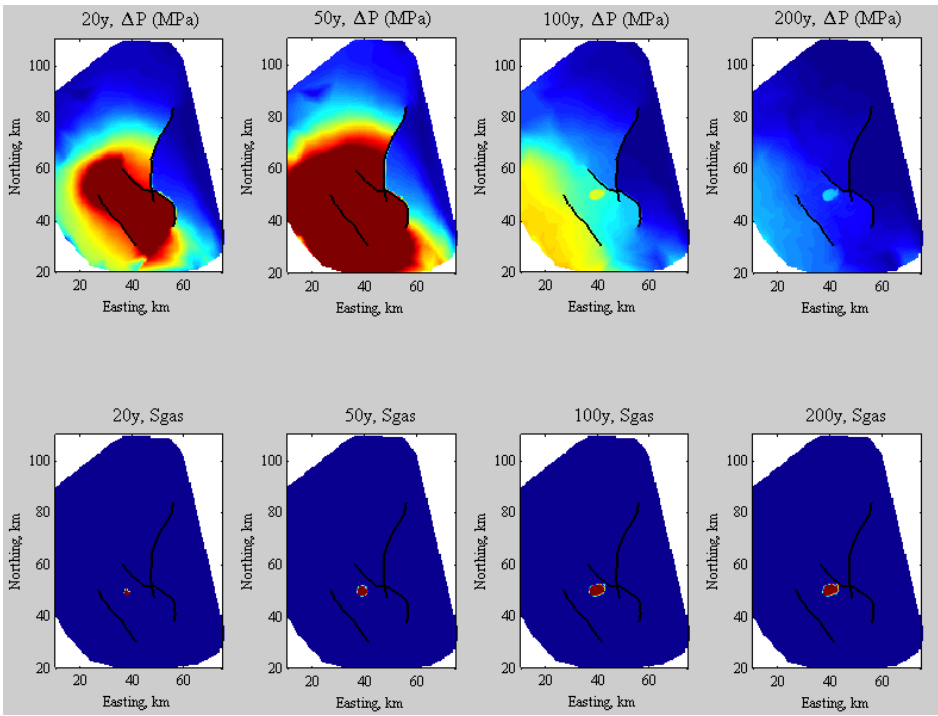

Figure A18: Pressure buildup and CO_2 plume size for injection rate of 1 Mt/yr.

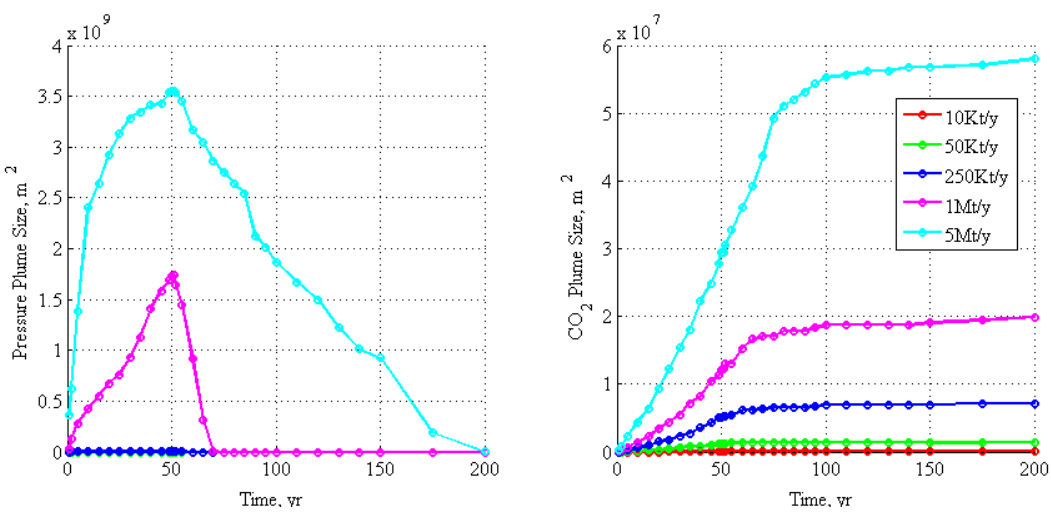

(a) (b)

Figure A19: Pressure plume size (P_{thr}=0.053 Mpa) and CO_2 plume size (S_{thr}=0.25) as a function of time for the five injection rates.

Figure A20 shows the pressure and CO_2 plume size as a function of the injection rates. In Figure A20a, the correlation between pressure plume size and injection rates is almost linear, when the injection rate is larger than 250 kt/yr. This figure also suggests that one may find a threshold

injection rate below which the injection can be achieved without creating any over-pressurized zone compared to the regulatory standard. In Figure A20b, the CO_2 plume sizes have an approximately log-linear relationship. The CO_2 plume size is significant smaller than the pressure plume size at the same injection rate except when the injection rates are small. These results may suggest that having a low injection rate could avoid over-pressurized zone and hence reduce the plume size in general.

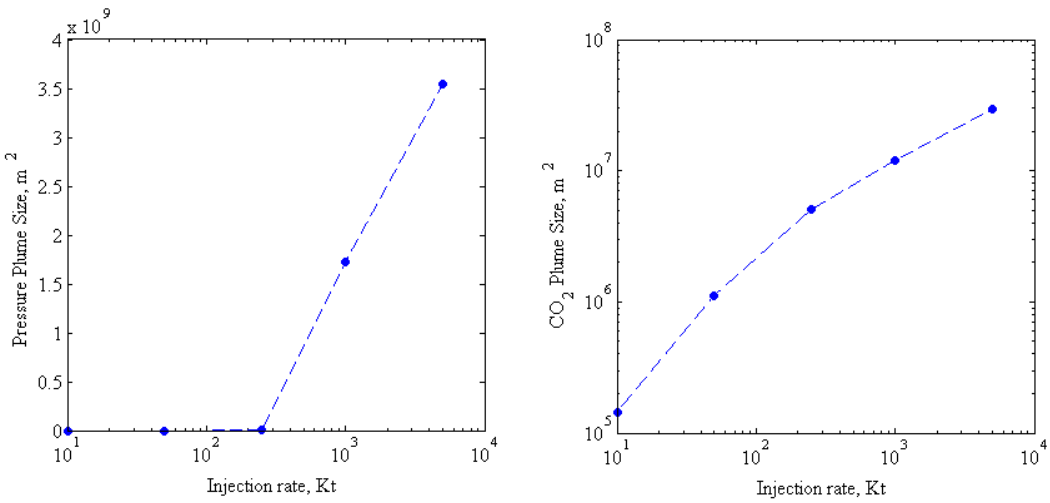

Figure A20: (a) Pressure plume size and (b) CO_2 plume size as a function of injection rates at 200 years.

References:

Bandilla, K. W.; Kraemer, S. R.; Birkholzer, J. T. Using semi-analytic solutions to approximate the area of potential impact for carbon dioxide injection, *International Journal of Greenhouse Gas Control* **2012,** *8*, 196–204. doi: 10.1016/j.ijggc.2012.02.009

Birkholzer, J. T.; Zhou, Q.; Cortis, A.; Finsterle, S. A sensitivity study on regional pressure buildup from large-scale CO_2 storage projects. *Energy Procedia* **2011,** *4*, 4371–4378.

Nicot, J.-P.; Oldenburg, C. M.; Bryant, S. L.; Hovorka, S. D. Pressure perturbations from geologic carbon sequestration: Area-of-review boundaries and borehole leakage driving forces. Presented at the 9th International Conference on Greenhouse Gas Control Technologies (GHGT-9), Washington, DC, Nov 16–20, 2008; GCCC Digital Publication Series #08-03h.

Nicot, J. -P.; Hovorka, S. D.; Knox, P. R.; Naing, T. Area of review: how large is large enough for carbon storage? In *Proceedings of the 2006 UIC Conference of the Groundwater Protection Council*, 2006; Abstract 17, GCCC Digital Publication Series #06-05.

Pruess, K. *ECO2N: A TOUGH2 fluid property module for mixtures of water, NaCl and CO_2*; Report LBNL-57952; Lawrence Berkeley National Laboratory, Berkeley, CA, 2005.

USEPA. Geologic Sequestration of Carbon Dioxide: Underground Injection Control (UIC) Class VI Well Area of Review Evaluation and Corrective Action Guidance for Owners and Operators; Office of Water, EPA 816-D-10-007, 2011.

Wainwright, H. M.; Finsterle, S.; Zhou, Q.; Birkholzer, J. T. Modeling the performance of large-scale CO_2 storage systems: A comparison of different sensitivity analysis methods. *International Journal of Greenhouse Gas Control* **2013,** *17*, 189–205.

Wainwright, H. M.; Finsterle, S.; Jung, Y.; Zhou, Q.; Birkholzer, J. T. Making sense of global sensitivity analyses. *Computers & Geosciences* **2014,** *65*, 84–94.

Zhang, K.; Wu, Y. S.; Pruess, K. *User's Guide for TOUGH2-MP – A massively parallel version of the TOUGH2 Code*; Report LBNL-315E; Lawrence Berkeley National Laboratory, Berkeley, CA, 2008.

Zhou, Q.; Birkholzer, J. T.; Tsang, C.; Rutqvist, J. A method for quick assessment of CO_2 storage capacity in closed and semi-closed saline aquifers, *International Journal of Greenhouse Gas Control* **2008,** 626–639. doi:10.1016/j.ijggc.2008.02.004

Zhou, Q.; Birkholzer, J. T.; Wagoner, J. L. Modeling the potential impact of geologic carbon sequestration in the southern San Joaquin basin, California. The Ninth Annual Carbon Capture & Sequestration, Pittsburgh, PA, 2011.

Zhou, Q.; Birkholzer, J.T. On scale and magnitude of pressure build-up induced by large-scale geologic storage of CO_2. *Greenhouse Gases. Sci. Technol.* **2011,** *1*, 11–20.

APPENDIX B: DETAILS OF SIMULATIONS OF CITRONELLE-LIKE FIELD

Primary considerations in subsurface sequestration of anthropogenic carbon dioxide (CO_2) are the knowledge of the capacity of a geological formation to store CO_2, the size of pressure plumes and CO_2 plumes during and after injection, and impact of maximum pressure on seismic activity, and the ability to monitor and mitigate any deviations from expected performance. At a glance, a formation with a reasonable pore volume would appear to be a good candidate for the purpose. However, not all high-porosity formations are suitable for permanent storage of the gas. Some of them lack a suitable storage environment that will foster physical mechanism(s) of gas trapping. In the absence of a trapping mechanism, a free gas cap is artificially created in the formation, which may not warrant long-term storage of the injected gas. Saline aquifers, for example, could be considered among the acceptable target locations, allow aqueous-phase precipitation reactions as well as absorption by the formation water. The dissolved gas promotes density-driven natural convection of water and the related hydrodynamic instabilities, consequently, the injected gas could be transported and dispersed over large distances depending on the boundary conditions of the aquifer.

At the West Virginia University we performed systematic series of reservoir modeling studies of anthropogenic CO_2 sequestration in Citronelle dome, Alabama, where all relevant scenarios and conditions to address the questions of the plume size and pressure differences were considered. The *objective* was to systematically simulate CO_2 sequestration, i.e., saturation dynamics, and pressure behavior over a range of operational and geological conditions and to derive conclusions about the factors influencing plume size and pressure behavior during and after injection. Latin hypercube sampling (LHS), i.e., statistical method for generating a sample of plausible collections of parameter values from a multidimensional distribution, was used to generate performance metrics as a function of the size of injection, time following injection, injection operations, and geologic environment. Pressure and saturation plume sizes were then plotted against a dimensionless number and clear straight-line trends were obtained in log-log plots. Further studies have been performed to assess the various parameters impacting plume size area using the "Plackett–Burman" experimental design technique. The importance of each parameter on saturation and pressure plume sizes and their correlations are quantified.

Reservoir Models:

The Paluxy formation, a saline reservoir located in Citronelle Dome was selected for this study. This geologic structure is a broad, gently dipping anticline with no sign of faulting. The Paluxy formation is located at the depth of 2,865–3,200 m (9,400 to 10,500 ft), and is an inter-bedded sandstone that includes 17 sand layers separated by two extensive shale layers at the top and bottom. This reservoir has extremely low groundwater velocity and is considered to have satisfactory petrophysical properties for CO_2 sequestration (Haghighat et al., 2014; Koperna et al., 2012).

The main structure of this formation is based on the interpretation of petrophysical logs and core data from 16 well logs in three cross sections. Well number D-9-7 that has been used as reference well in three cross sections was selected as a hypothetical injection well to simulate CO_2 injection. Two different reservoir models built in CMG software were used in this study.

The first reservoir model, termed the "history matched model", is based on Cartesian grids with total of 796,875 grid blocks, i.e., 125*125*51 grids in i ,j and k directions, and covers 25 square kilometers (Figure B1). To account for heterogeneity of the formation seventeen porosity and

permeability maps were generated from 40 well logs, Figure B1. Field measurements of CO_2 injection rates and high frequency, real-time pressure data from two down-hole pressure gauges are history matched by Haghighat et al. (2013).

The second model is an upscaled reservoir model that uses similar site characteristics but was built to have more comparable results with other groups in the National Risk Assessment Partnership (NRAP). The upscaled model is also built based on Cartesian grids with total of 1,437,500 grid blocks, i.e., 250*250*23 grids in i ,j and k directions, and covers 100 square kilometers. In upscaled model, structure and isopach maps were also upscaled.

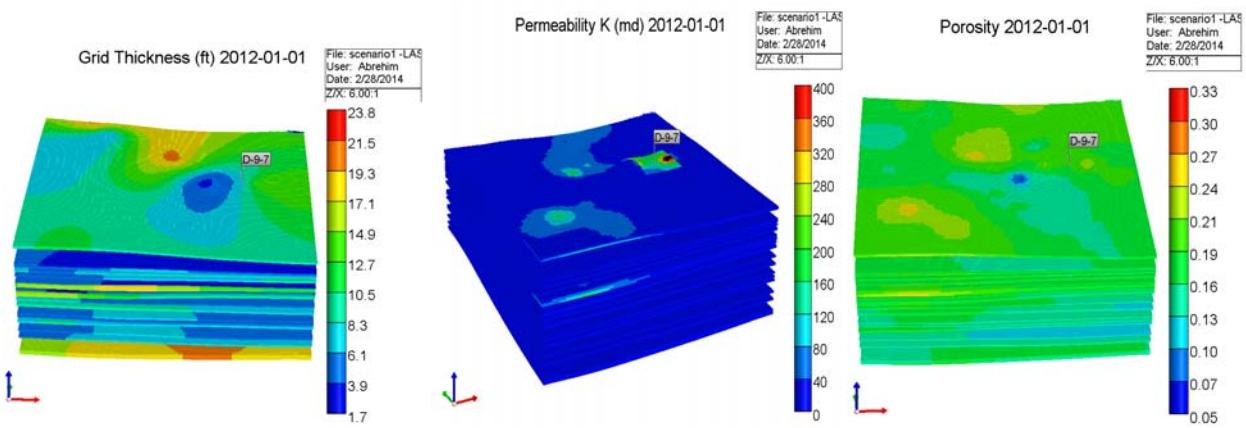

Figure B1: Reservoir grid thickness (left), permeability (mid), and porosity distribution (right).

Reservoir Simulation:

CO_2 injection and propagation of pressure and plumes in the formation was performed using a compositional simulator CMG-GEM capable of simulating multiphase, multi-component fluid flow and injection. The main operational constraint is that the maximum bottom-hole pressure was set to 43.437 MPa (13.572 MPa/km at approximately 3,200 m).

Systematic simulations were conducted over a range of operation and geological conditions and CO_2 plume expansion and pressure buildup was calculated, including saturation and pressure plume size. The following properties/conditions were varied in the simulation study of the upscaled model: injection duration (3 and 30 years), post injection duration (30 and 300 years), injection rates (50, 250, 1000, and 5,000 kt/yr), thickness of storage (large 200 m, medium 100 m, and small 50 m), geologic closure (semi-open vs. closed), heterogeneity (permeability, porosity, anisotropy, compressibility variations), salinity levels (for critical pressure buildup), fluid-rock interactions (relative permeability curves, residual gas and liquid saturations), and caprock and sub layer permeability. Different distributions were selected for parameters such as formation permeability, porosity, anisotropy, compressibility, salinity and cap rock and sub layer permeability. LHS was used to generate 200 realizations and aggregated to build the performance metrics in Table B1. For each realization the pressure plume size and CO_2 plume size was calculated based on three pressure thresholds: 1, 5 and 10 bar; and two saturation threshold values: 0.01 and 0.2. Figures B2 and B3 show samples of saturation and pressure

distributions at the end of 3 years of CO_2 injection using the history matched and upscaled models respectively.

Table B1: Performance metrics

	A	B	C	D	E	F	G	H	I	J	K
1	#	inj length (yrs)	kt/yr really injected	res_perm	res_anis	por	thick (m)	compr(1/psi)	salinity (ppm)	cap_perm (md)	subl_perm (md)
2	1	30	50.04	756.72	0.31	0.18	50	9.403E-06	110.97	0.000791301	0.000656654
3	3	30	540.75	171.45	0.45	0.25	50	2.927E-06	175.22	0.003181402	0.000249067
4	4	30	250.01	112.65	0.02	0.15	100	1.882E-06	45.43	0.000472601	0.000142739
5	5	30	655.47	235.87	0.05	0.27	50	4.787E-06	200.39	0.000140317	0.007254522
6	6	30	49.73	42.30	0.07	0.28	50	7.389E-06	185.86	0.000112221	0.000672853
7	7	30	416.94	470.57	0.13	0.05	50	4.067E-06	70.37	0.000644787	0.000302974
8	8	30	59.85	12.80	0.02	0.21	100	3.742E-06	205.20	0.000222065	0.001338744
9	9	30	276.10	29.47	0.04	0.35	200	1.783E-06	98.36	0.005426987	0.002043787
10	10	30	93.01	20.12	0.01	0.31	100	1.137E-06	60.31	0.000182914	0.000702715
11	11	30	1000.72	857.51	0.34	0.1	200	2.895E-06	25.96	0.002339068	0.000172451
12	13	30	250.15	379.73	0.01	0.34	50	2.648E-06	132.23	0.000155284	0.006641716
13	15	30	50.02	70.21	0.88	0.21	50	3.5E-06	210.72	0.001838777	0.00085147
14	16	30	49.32	11.02	0.02	0.23	200	9.674E-06	186.25	0.000125254	0.003295114
15	17	30	50.04	39.20	0.52	0.3	200	6.75E-06	124.10	0.001495979	0.001304823
16	18	30	608.86	520.24	0.02	0.15	50	1.361E-06	128.39	0.002225391	0.000610544
17	19	30	50.04	317.45	0.17	0.16	200	2.554E-06	153.80	0.00012638	0.004667032
18	21	30	136.14	25.75	0.24	0.23	100	1.427E-06	151.73	0.00350812	0.002646346
19	22	30	1538.83	943.04	0.03	0.2	100	3.351E-06	120.07	0.000192027	0.00036838
20	23	30	50.04	434.28	0.02	0.26	200	6.286E-06	54.06	0.000209572	0.000542067
21	24	30	999.94	361.79	0.04	0.23	100	5.799E-06	37.77	0.001061593	0.009286373
22	25	30	77.97	14.96	0.05	0.14	100	8.838E-06	135.55	0.000441078	0.000810613
23	26	30	250.17	333.24	0.10	0.22	100	4.199E-06	133.93	0.000288803	0.005936614
24	27	30	517.61	193.36	0.03	0.31	50	4.401E-06	196.40	0.002786857	0.000742324
25	28	30	98.26	15.68	0.84	0.05	100	1.081E-06	191.23	0.000312884	0.00146594
26	29	30	250.15	92.60	0.47	0.07	200	6.595E-06	226.60	0.000536414	0.000957346
27	30	30	250.17	569.83	0.19	0.27	50	2.775E-06	111.91	0.001403453	0.000102201
28	31	30	73.94	28.43	0.04	0.32	50	1.012E-05	22.42	0.003096676	0.00348293
29	32	30	1000.71	411.52	0.08	0.12	200	2.01E-06	166.73	0.000264128	0.008276463
30	33	30	156.11	17.41	0.69	0.32	200	1.264E-06	130.96	0.005571118	0.001254895
31	35	30	50.04	217.98	0.55	0.16	50	5.051E-06	29.17	0.000148693	0.003991354
32	36	30	99.41	10.19	0.09	0.12	200	5.892E-06	64.32	0.000686566	0.001895419
33	37	30	86.84	15.90	0.25	0.12	100	1.606E-06	221.84	0.008141297	0.00114872
34	38	30	706.86	283.83	0.01	0.12	100	3.95E-06	214.05	0.000100075	0.000486528
35	39	30	1470.91	977.22	0.58	0.24	50	2.134E-06	216.07	0.001996493	0.000427637
36	40	30	1000.72	581.16	0.28	0.1	200	2.274E-06	183.18	0.004264975	0.003637678
37	41	30	50.04	161.78	0.07	0.13	50	5.628E-06	53.49	0.001362306	0.000190938
38	42	30	250.17	299.29	0.06	0.06	100	2.518E-06	203.15	0.00025621	0.000598076
39	43	30	250.17	619.92	0.04	0.21	200	4.431E-06	126.13	0.006342083	0.000409137
40	45	30	50.04	536.69	0.01	0.06	50	3.518E-06	170.88	0.00028463	0.005170405
41	47	30	202.67	21.40	0.75	0.31	200	1.281E-06	208.72	0.008416908	0.000110305
42	48	30	49.95	95.90	0.11	0.28	50	1.195E-06	118.69	0.000994524	0.000333305
43	51	30	49.95	117.28	0.02	0.07	100	1.439E-06	217.77	0.000345635	0.000180297
44	52	30	192.57	68.81	0.18	0.07	50	1.306E-06	74.11	0.000613798	0.009950373
45	56	30	49.95	44.66	0.12	0.25	200	7.258E-06	41.71	0.001157724	0.00026458
46	57	30	249.77	89.57	0.02	0.08	100	3.276E-06	148.65	0.006198384	0.000397983
47	58	30	49.95	40.61	0.15	0.22	100	8.237E-06	94.91	0.002142625	0.000187887
48	61	30	63.68	14.22	0.01	0.29	100	2.227E-06	142.22	0.005004741	0.000135138
49	62	30	238.33	24.33	0.23	0.15	200	6.092E-06	145.41	0.00016113	0.002126824
50	63	30	49.95	58.05	0.71	0.15	100	4.871E-06	83.76	0.000756955	0.000512719
51	66	30	249.77	120.88	0.01	0.09	200	5.261E-06	20.49	0.001712159	0.00100362
52	67	30	49.95	75.40	0.03	0.09	200	5.455E-06	11.37	0.005207427	0.000282852
53	70	30	49.95	108.92	0.01	0.18	50	9.153E-06	207.42	0.000481302	0.000209171
54	72	30	38.89	11.56	0.99	0.08	50	4.265E-06	103.12	0.001114616	0.001694952
55	74	30	49.95	83.25	0.13	0.19	100	1.949E-06	49.09	0.00576268	0.001437578
56	75	30	249.77	274.87	0.62	0.23	50	1.684E-06	34.58	0.002728687	0.000351286
57	76	30	249.77	135.12	0.76	0.34	200	3.073E-06	139.81	0.00042151	0.002778193
58	83	30	46.92	10.61	0.16	0.25	100	1.469E-06	138.86	0.00948109	0.002913846
59	85	30	50.04	55.92	0.03	0.11	200	3.267E-06	146.85	0.001990656	0.001978445
60	86	30	250.11	245.49	0.03	0.17	50	1.751E-06	159.83	0.001246474	0.003386937
61	90	30	50.04	684.98	0.40	0.19	200	1.055E-06	91.14	0.000571376	0.0002196
62	91	30	50.04	302.36	0.08	0.27	100	2.051E-06	13.95	0.004003571	0.001816141
63	93	30	250.17	148.21	0.20	0.1	200	1.564E-06	101.51	0.00016943	0.003115713
64	94	30	50.04	204.84	0.05	0.33	100	5.341E-06	72.22	0.00258025	0.002405819
65	95	30	250.17	451.90	0.35	0.19	50	3.182E-06	97.24	0.000830965	0.000203507
66	96	30	250.17	224.13	0.41	0.34	200	2.427E-06	177.23	0.000932545	0.000115806
67	97	30	50.04	641.15	0.94	0.17	100	2.661E-06	69.04	0.00031677	0.007077424
68	99	30	127.42	46.19	0.03	0.33	50	7.722E-06	56.31	0.006687582	0.001516843

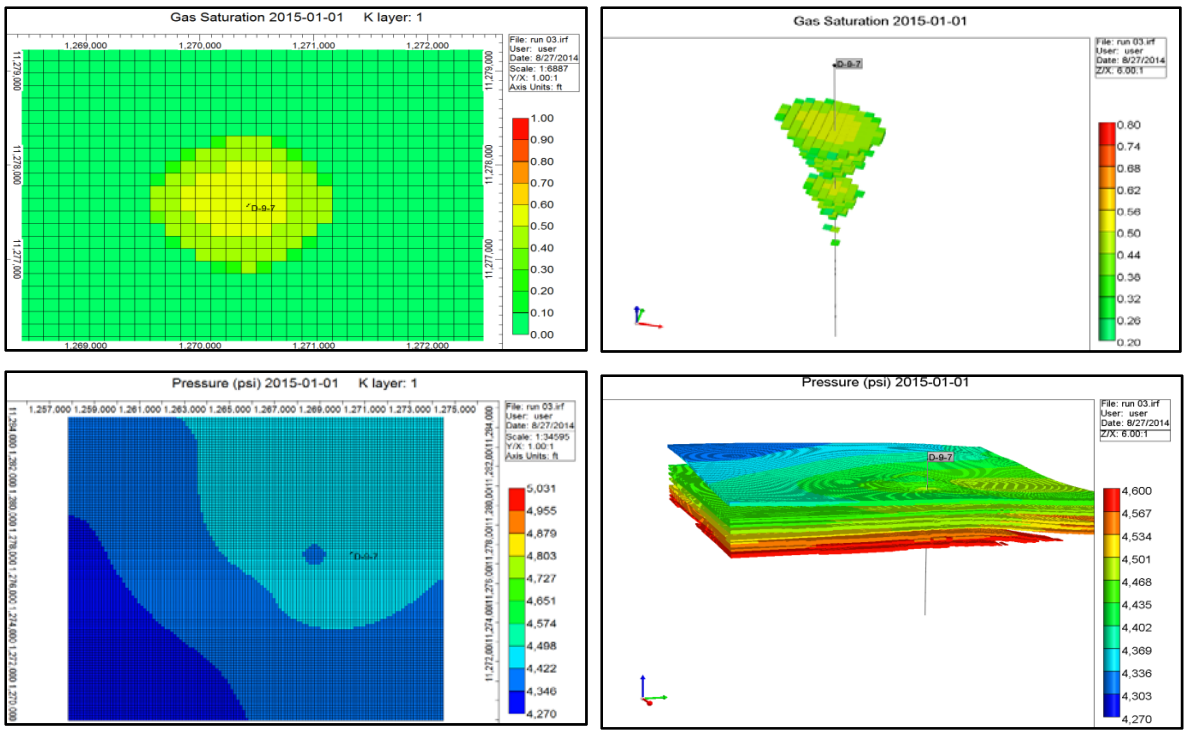

Figure B2: CO_2 saturation distribution (top) and pressure distribution (bottom) at the end of 3 years injection in the history matched model.

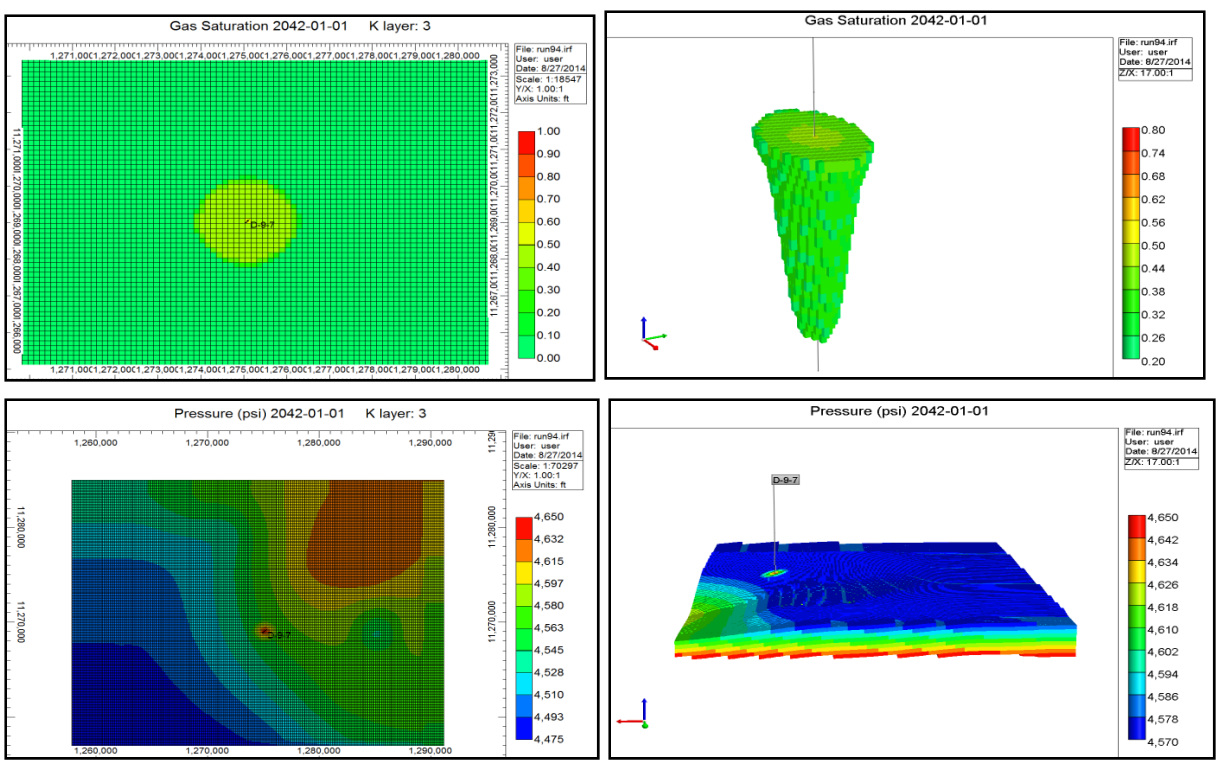

Figure B3: CO_2 saturation distribution (top) and pressure distribution (bottom) at the end of 30 years injection in the upscaled model.

Plume Size Trends:

The 200 realizations were generated using LHS from typical distributions assigned to different operational and geological parameters and the impact on saturation and pressure plume sizes was analyzed. Due to the cross correlations between different parameters impacting plume size, a dimensionless number was defined that includes the expected important parameters, i.e., injection rate, injection time, porosity, permeability and thickness, and was used to study the plume size behavior. Figure B4 clearly shows a linear relationship between saturation plume size and this dimensionless number, where increasing the dimensionless number leads to higher saturation plume size. This linear trend is preserved at different saturation thresholds, i.e., 0.01 and 0.2. Including more parameters such as anisotropy, normalized compressibility and salinity in the dimensionless number preserved this general trend, but with larger variability. Figure B5 shows a similar linear trend between pressure plume size and this dimensionless number at 5 and 10 bar pressure thresholds. After a critical value of this dimensionless number the pressure wave reaches the boundary of the closed reservoir. A similar trend but with more variability can be observed when 1bar is used as the pressure threshold. Figure B6 shows the pressure wave reaches the boundary of the reservoir much faster when 1 bar is the threshold, than when 5 and 10 bar pressure thresholds apply.

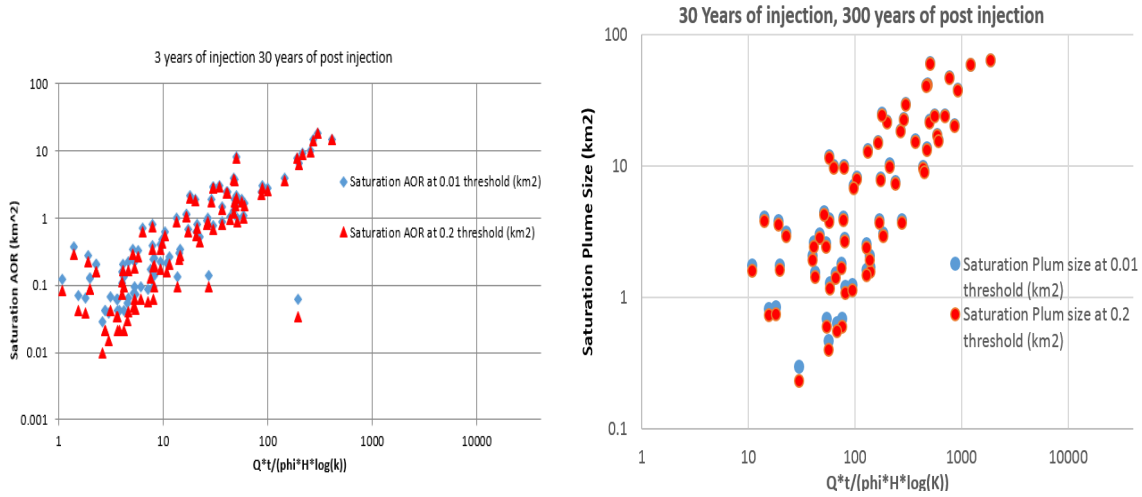

a)

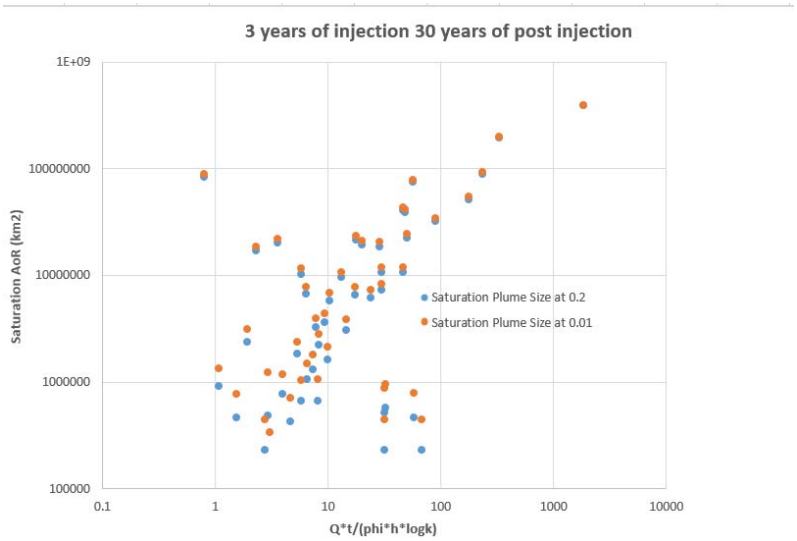

b)

Figure B4: a) Saturation Plume Size vs. Dimensionless number using the upscaled model for a closed system; b) Saturation Plume Size vs. Dimensionless number using the upscaled model for a semi-open system.

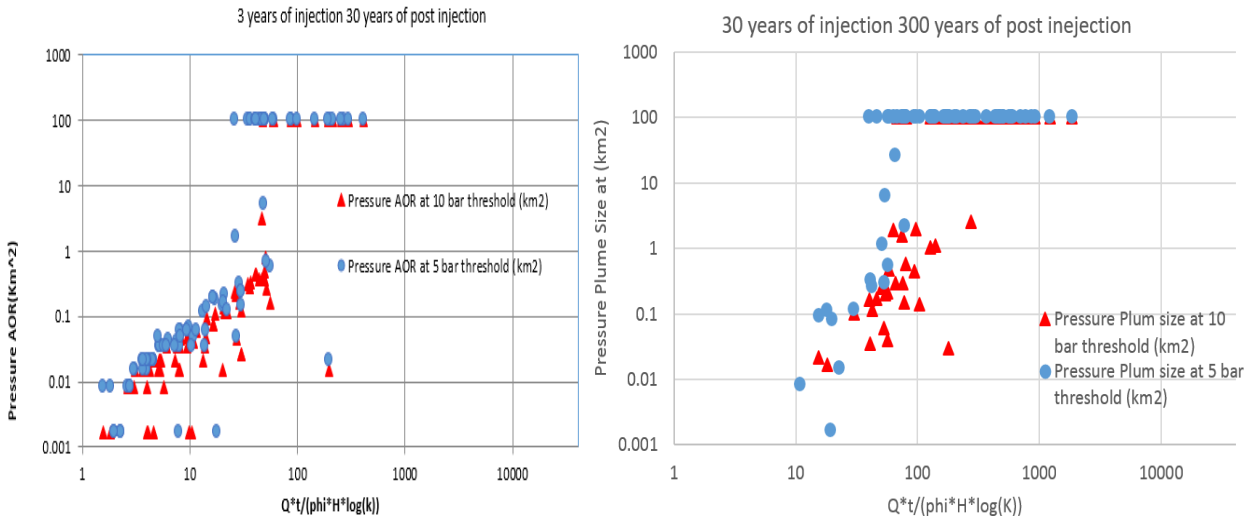

Figure B5: Pressure Plume Size vs. Dimensionless number using the upscaled model.

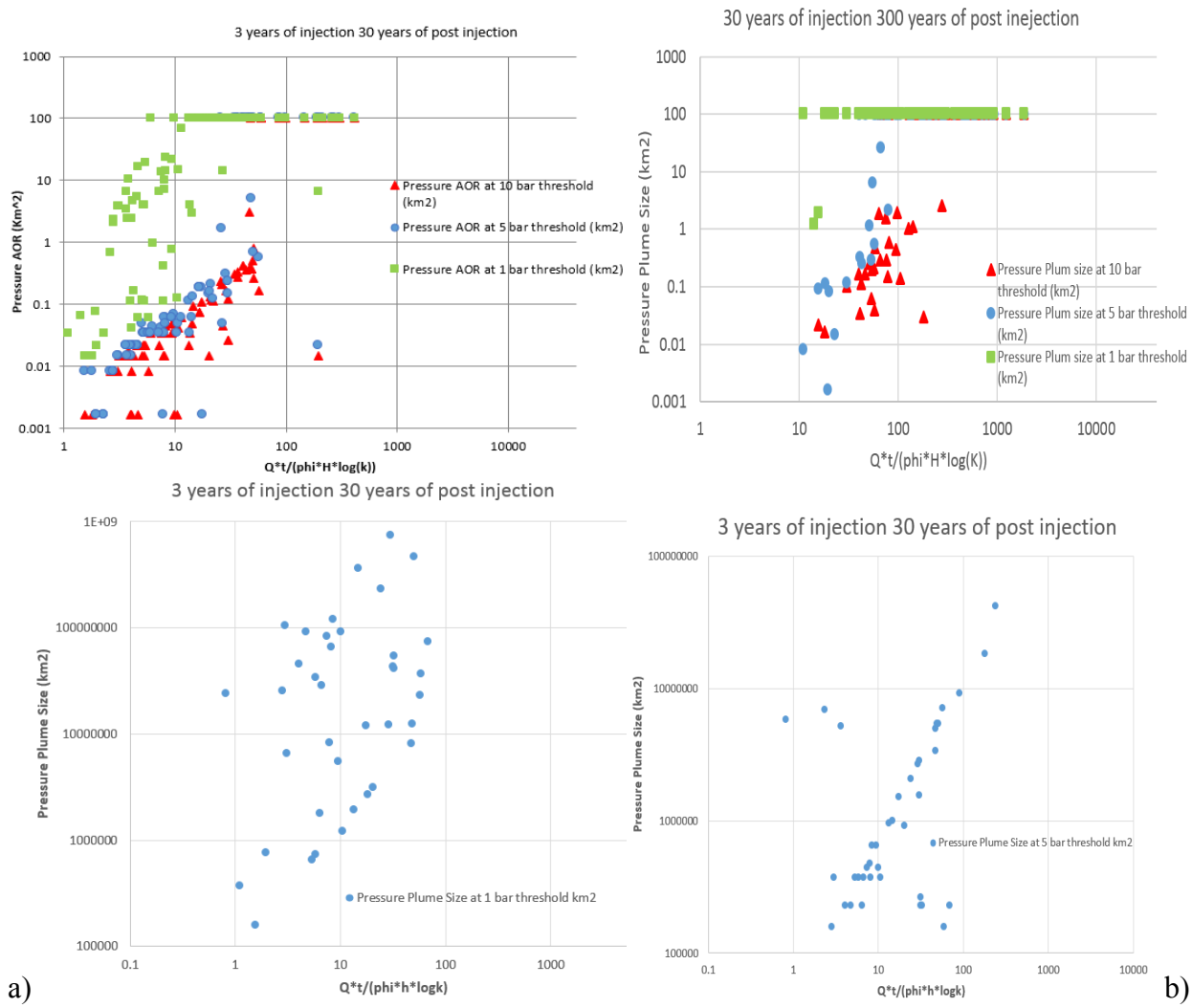

Figure B6: a) Pressure Plume Size vs. Dimensionless number using upscaled model for closed system; b) Pressure Plume Size vs. Dimensionless number using upscaled model for semi-open system.

Point studies were performed to provide more detailed information on how pressure is changing in different locations of the reservoir. Figure B7 (left) depicts the pressure buildup with time at 1, 2, and 3 kilometers away from the injection point in a scenario with 3 years of injection and 50 years post-injection. During the injection time the pressure builds up rapidly at different locations and declines fast after shut-in of the injection. For the case where 50 kt/year of CO_2 is injected it reaches an equilibrium pressure almost 20 years after injection stops. Figure B7 (right) compares all different scenarios with close to 50 kt/year CO_2 injection and confirms the general trend of pressure buildup and decline as previously observed in Figure B7 (left). Injecting larger amount of CO_2 into the closed boundary formation causes the pressure to build up rapidly. However, due to boundary effects we do not see the same fast pressure decline as in the case of an open boundary reservoir (see Figure B8).

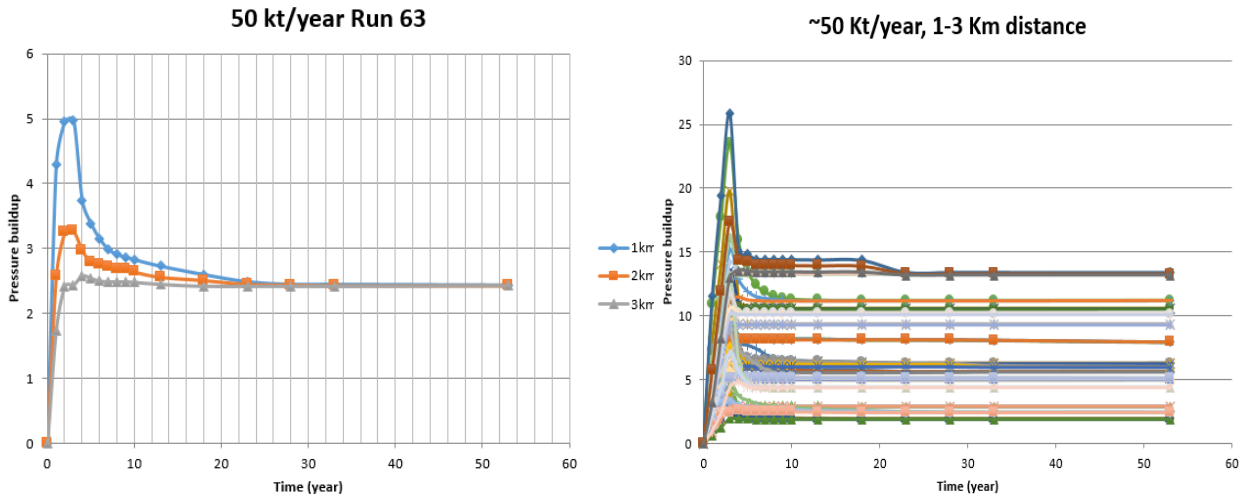

Figure B7: Pressure buildup vs time at 1, 2, and 3 km away from injection point.

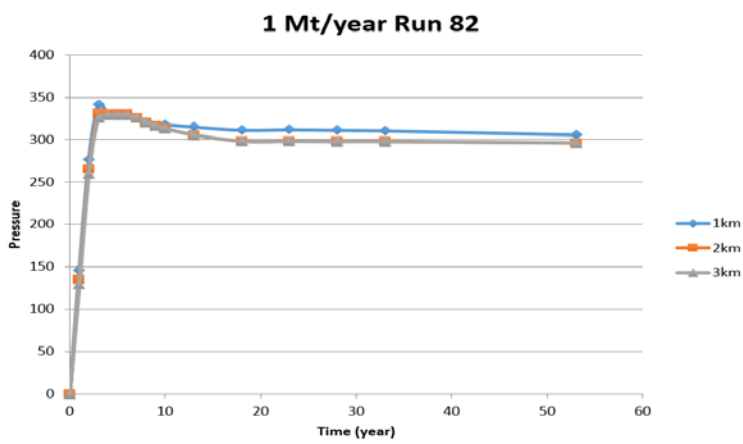

Figure B8: Pressure vs time behavior at closed boundary condition

Uncertainty Analysis Using Design of Experiments

A systematic approach was used to find the most important parameters impacting the saturation and pressure plume size for both reservoir models (history matched and upscaled). This included determining the parameters of interest, performing a screening analysis to find those parameters with the largest impact, and performing a comprehensive analysis to understand the main effects with two-factor interactions using Plackett-Burman analysis. Minitab statistical software was used to perform the analysis. The Plackett-Burman (PB) design used here is the most compact two-level design that requires (n+1) runs where n is the number of factors. In PB design all the columns in the design matrix are orthogonal to each other, and thus can analyze all the main effects. In order to perform the significance test we use a design matrix with 12 runs instead of 8 runs for both models. Table B2 shows the terminology of the two-level design matrix for history matched and upscaled models where the highest value for the factors are represented with (+1), and the low values with (-1). Table B3 shows the design matrix used here. In this study pressure and saturation plume sizes with different thresholds are considered as the simulation response.

Table B2: Parameter setting of PB design

Parameter	-1	+1	Unit
A: Permeability	10.19	977.224	md
B: kv/kh	0.010654	0.994728	NA
C: Porosity	0.05017	0.34789	%
D: Thickness	50	200	m
E: Compressibility	1.06E-06	1.01E-05	1/psi
F: Salinity	11.37096	228.1210	Ppm
G: Inj rate	20	4274	Kt/yr

Table B3: PB matrix for 7 variables, -1=low value, +1=high value

	Factor 1	Factor 2	Factor 3	Factor 4	Factor 5	Factor 6	Factor 7
RUN	A: Permeability	B: kv/kh	C: Porosity	D: Thickness	E: Compressibility	F: Salinity	G: Inj rate
	md	NA	%	m	1/psi	ppm	Kt/yr
1	-1	1	1	-1	1	-1	-1
2	-1	-1	1	1	1	-1	1
3	-1	1	1	1	-1	1	1
4	1	-1	-1	-1	1	1	1
5	1	1	-1	1	-1	-1	-1
6	-1	-1	-1	-1	-1	-1	-1
7	1	1	1	-1	1	1	-1
8	1	-1	1	-1	-1	-1	1
9	-1	1	-1	-1	-1	1	1
10	1	1	-1	1	1	-1	1
11	1	-1	1	1	-1	1	-1
12	-1	-1	-1	1	1	1	-1

The Pareto charts and normal plots of standardized effects have been used to study the simulation response for different cases. The Pareto chart displays the relative size of the effect of each parameter on the simulation response. Dimensionless statistics were used to scale the effects in terms of standard deviations. On the other hand a Normal plot can quantify the effect polarity of each variable on simulation response. Figure B8 shows the Pareto charts and Normal plots analyzed using the PB matrix design, where saturation plume size is used as the simulation response. Pareto charts for both 0.01 and 0.2 saturation thresholds show that main parameters impacting the size of a CO_2 saturation plume are reservoir permeability (highest impact), injection rate, porosity and compressibility, whereas salinity anisotropy and thickness show no significant impact on CO_2 plume size. Normal plots also show that reservoir permeability, injection rate and compressibility have a positive correlation with saturation plume size, whereas porosity has a negative correlation. Figure B9 shows the Pareto charts and Normal plots of PB matrix design analysis where pressure plume size is used as the simulation response. Based on Pareto charts for 5 and 10 bar pressure thresholds, the main parameters impacting pressure plume size include the injection rate (highest impact) and reservoir permeability, whereas other parameters show much less impact on pressure plume size. The Pareto chart for the 1 bar pressure threshold also identifies the injection rate as the most important parameter; however, in this case of reservoir permeability, reservoir thickness and porosity show significant impacts on Plume Size Area. Figure B11 shows the summary of this qualitative assessment of operational and geological parameters on pressure and saturation plume size.

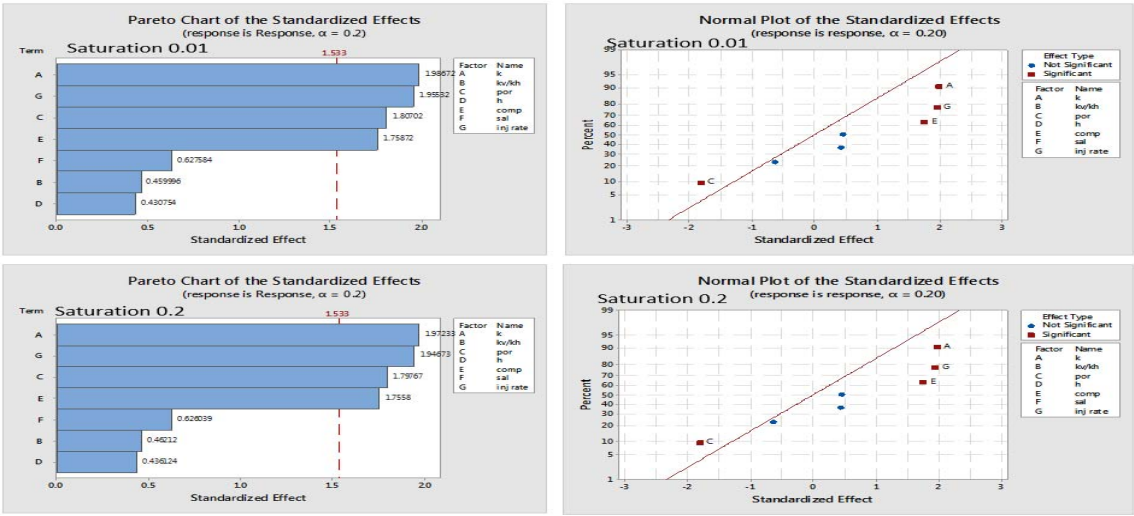

Figure B9: PB design analysis of upscaled model using saturation plume size for closed system.

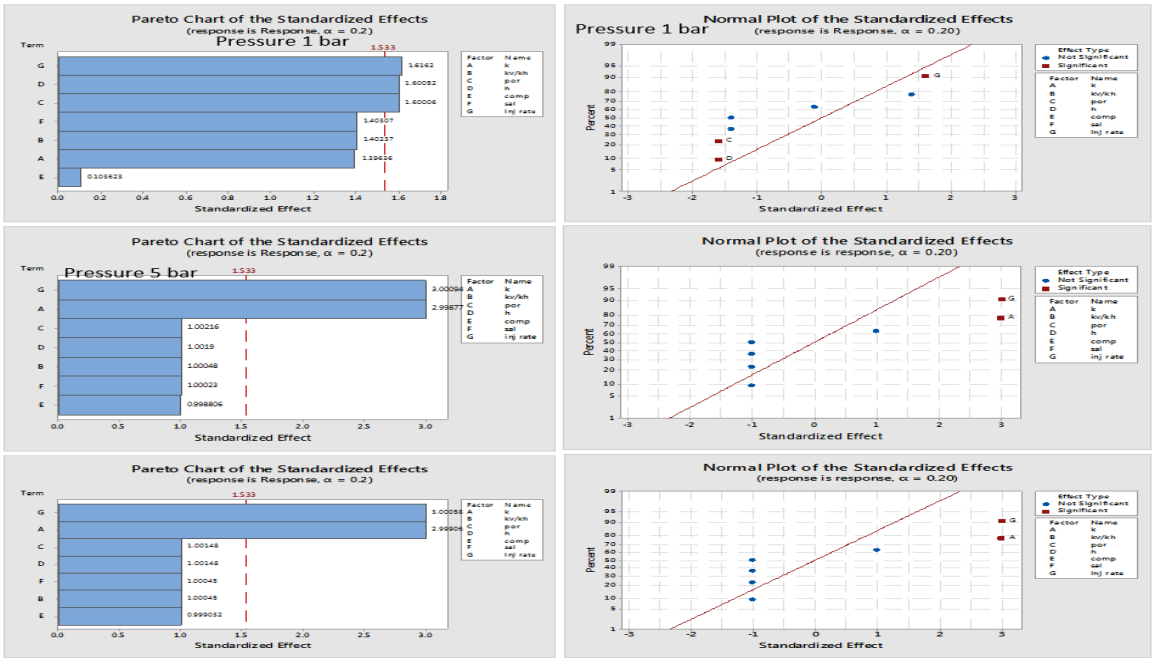

Figure B10: PB design analysis of upscaled model using pressure plume size for closed system.

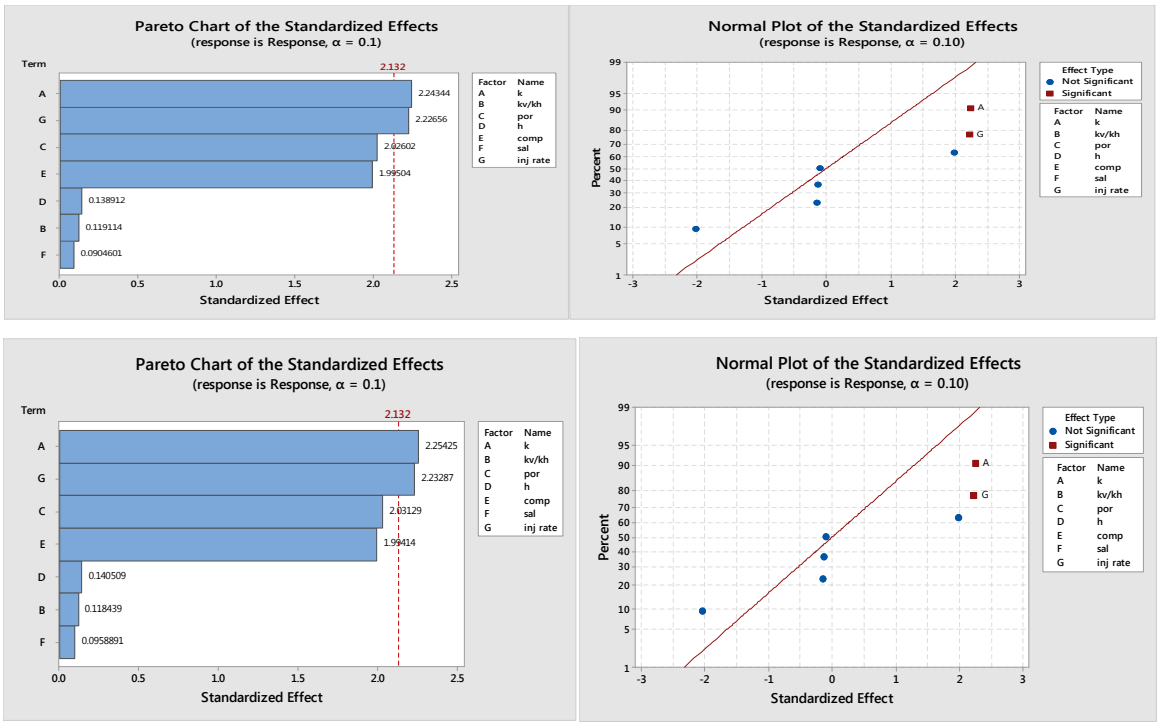

Figure B11: PB design analysis of upscaled model using saturation plume size for semi-open system using 0.2 and 0.01 of threshold respectively.

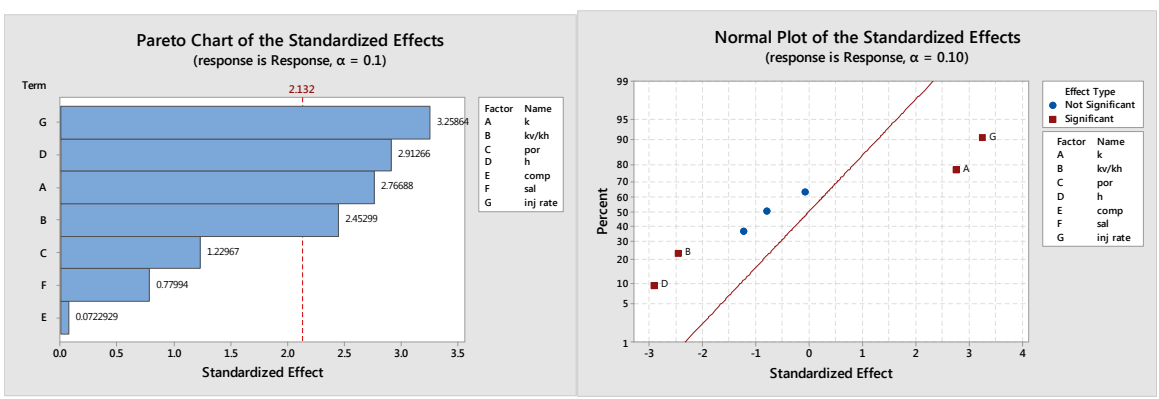

Figure B12: PB design analysis of upscaled model using pressure plume size for semi-open system using 1 bar of threshold.

References:

Haghighat, S. A.; Mohaghegh, S. D.; Gholami, V.; Shahkarami, A. Pressure History Matching for CO2 Storage in Saline Aquifers: Case Study for Citronelle Dome. 2013 Carbon Management Technology Conference Alexandria, VA, 2013; Manuscript #P306522.

Koperna, G. J.; Kuuskraa, V. A.; Reistenberg, D. E.; Rhudy, R.; Trautz, R.; Hill, G.; Esposito, R. A. The SECARB Anthropogenic Test: The First US Integrated Capture, Transportation, and Storage Test. 2012 Carbon Management Technology Conference, Orlando, FL, 2012.

APPENDIX C: DETAILS OF SIMULATIONS OF ROCK SPRINGS UPLIFT (RSU) AND RELATED FIELDS

C.1 WORK SUMMARY

As a part of U.S. Department of Energy's (DOE) National Risk Assessment Partnership (NRAP), Los Alamos National Laboratory (LANL) has performed a series of calculations of the evolution of pressure and CO_2 plumes based on reservoir simulation of CO_2 injection for a variety of parameter ranges of interest. Single-well CO_2 injection at rates from 0.1 to 15 Mt yr^{-1} was considered for time periods ranging from one to 15 years, and with post-site monitoring up to 90 years post-injection. Subsurface permeability is one of the most important parameters controlling plume evolution, but it is generally highly heterogeneous and difficult to constrain. To provide realistic uncertainty bounds for predicted CO_2 and pressure plumes, simulations for each parameter set are performed for multiple, equally-likely realizations of heterogeneous permeability.

C.2 RESERVOIR SIMULATION

AoR calculations presented in this report are based on reservoir simulation of CO_2 injection scenarios. We use the multi-phase, multi-fluid subsurface flow, transport and geomechanics code FEHM developed at LANL for diverse applications such as CO_2 sequestration, oil and Gas production, geothermal energy extraction, environmental remediation, and nuclear repository performance (Zyvoloski, 2007; Kelkar et al., 2014). We consider a scenario of CO_2 injection for a period of time, t_{inj}, at a depth z_{inj} = –2.5 km, injection at a specified fixed rate, Q, followed by a monitoring period, t_{pisc}, during which there is no injection. The reservoir model is based on a potential CO_2 sequestration site at the Rock Springs Uplift (RSU) in Wyoming (Deng et al., 2012). At RSU storage would occur within the Weber sandstone and Madison limestone with structural trapping provided by the overlying Phosphoria and Chugwater formations, all of which dip at 4°. Site-specific geologic data, including wellbore density and neutron porosity logs, are used to develop a geologic model for the site. Each of the four main geological units is further subdivided into high, medium, and low permeability sub-regions, with the permeability values for each derived from core analysis. An indicator geostatistics approach with transitition probabilities is then applied to generate 29 statistically-identical realizations of the spatial distribution of these discrete sub-units. A cut-away view of one such realization is provided in Figure C1(A). Each CO_2 injection simulation is repeated for all 29 permeability realizations. Table C1 summarizes parameter sets for the CO_2 injection scenarios discussed in this report. Linear relative permeablity properties are assumed with a residual brine saturation of 0.1, zero capillary pressure, and aquifer compressibility 10^{-4} MPa^{-1}. Two grids were used to investigate boundary effects: a 16x16 km^2 and 100x100 km^2 comprising 525 k and 669 k nodes, respectively. Fixed pressure hydrostatic boundary conditions were applied on all boundaries, with a hydrostatic initial condition, 35 °C/km geothermal gradient, and surface temperature of 29 °C.

C.3 CALCULATION OF AREA OF REVIEW

The sizes of two types of plumes, CO_2 and pressure, are investigated in this work. The CO_2 and pressure plumes are defined as the areas enclosed by threshold values for CO_2 saturation (S_{thr}) and for increases in reservoir pressure (ΔP_{thr}). In defining the CO_2 plume, it is common to take

S_{thr}= 0. In many of the plots presented in this report, ΔP_{thr}= 1 MPa, although sensitivity of the size of a pressure plume to this parameter is investigated.

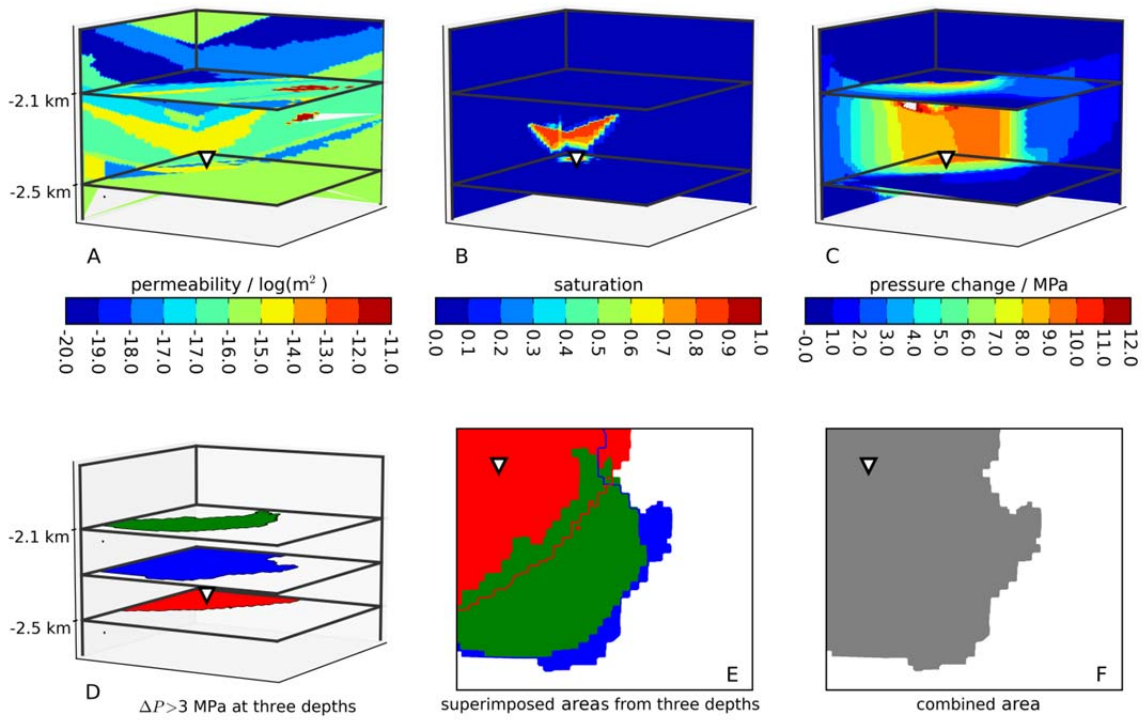

Figure C1: Demonstration of the determination of the area of pressure plume for stacked plumes. (Determination of the area of the stacked CO_2 plumes follows similar steps.) (A) Cutaway view of heterogeneous permeability structure for one model realization. Dip of the modeled formations is evident. (B) Cutaway view of CO_2 plume after 10 years injection. (C) Cutaway view of pressure plume. (D) Extent of pressure plume (AoR_P) at three depths with front defined by 3 MPa overpressure contour. (E) In 2-D, pressure plumes for each depth stacked on one another. (F) Combined area of the pressure plume as the superposition of plumes from all depths. In all subplots, the position of the injector is indicated by the white triangle.

Both the CO_2 and pressure plumes in the reservoir are defined as 3-D volumes, yet the area to be output is a 2-D area; thus, it is necessary to project the 3-D plume onto a 2-D horizontal plane. Figure C1 demonstrates how this is achieved. Horizontal slices are taken of the 3-D pressure plume at different depths—3 in the demonstration below but typically 20 in practice—each of which defines an area (for a given ΔP_{thr}) for its depth. The cumulative area at the surface is the area covered by one or more of these depth-specific areas.

C.4 TRENDS OF PLUME AREAS

Figure C2 presents areas of pressure and CO_2 plumes for three simulation sets (each set comprising 29 permeability realizations) of CO_2 injection for a 3-year period at rates of 0.1, 1, and 5 Mt yr^{-1}. For the two higher injection rates, the pressure plume grows linearly with time during the injection phase and continues to grow after injection has ceased (Figure C2(A)). A maximum is reached 1 to 5 years after the end of injection after which time the size of the pressure plume declines. Permeability heterogeneity is responsible for scatter around the

ensemble mean, particularly at later times; nevertheless, the broad time behavior is consistent for all profiles.

Table C1: CO_2 injection scenario parameters. Each parameter set is simulated using 29 different permeability realizations, for a total of 493 simulations.

Set #	Injection rate, Q, (Mt yr^{-1})	Injection time, t_{inj}, (yr)	Post-site monitor, t_{pisc}, (yr)	Volume injected CO_2 (Mt)	Grid dimensions (km)
1	0.1	3.0	27.0	0.3	16x16
2	1.0	3.0	27.0	3.0	16x16
3	5.0	3.0	27.0	15.0	16x16
4	0.1	10.0	90.0	1.0	16x16
5	1.0	10.0	90.0	10.0	16x16
6	5.0	10.0	90.0	50.0	16x16
7	0.1	3.0	27.0	0.3	100x100
8	1.0	3.0	27.0	3.0	100x100
9	5.0	3.0	27.0	15.0	100x100
10	0.1	10.0	90.0	1.0	100x100
11	1.0	10.0	90.0	10.0	100x100
12	5.0	10.0	90.0	50.0	100x100
13	1.0	15.0	15.0	15.0	100x100
14	2.0	7.5	22.5	15.0	100x100
15	3.0	5.0	25.0	15.0	100x100
16	7.5	2.0	28.0	15.0	100x100
17	15.0	1.0	29.0	15.0	100x100

The size of pressure plume clearly depends on the value of ΔP_{thr} used to define it (Figure C2(B)), with lower thresholds enclosing much larger areas. At a given time, area of the pressure plume is larger for higher injection rates.

Figure C2(C) shows the evolution of CO_2 plume area with time. At all injection rates, the CO_2 plume is smaller than pressure plume for the corresponding time, although the decline in AoR_P with ongoing dissipation of the pressure plume (Figure C2(A)) suggests this may not always be the case. The result of a pressure plume that is larger than the CO_2 plume is consistent with the findings of Birkholzer and Zhou (2009) and Bandilla et al. (2012).

Unlike for pressure, the CO_2 plume does not diminish in size at the end of the injection. Figure C2(C) shows that the CO_2 plume is mostly stable or slowly increasing in the post-injection period. Permeability heterogeneity contributes uncertainty in the stable size of the CO_2 plume by as much as ±33%.

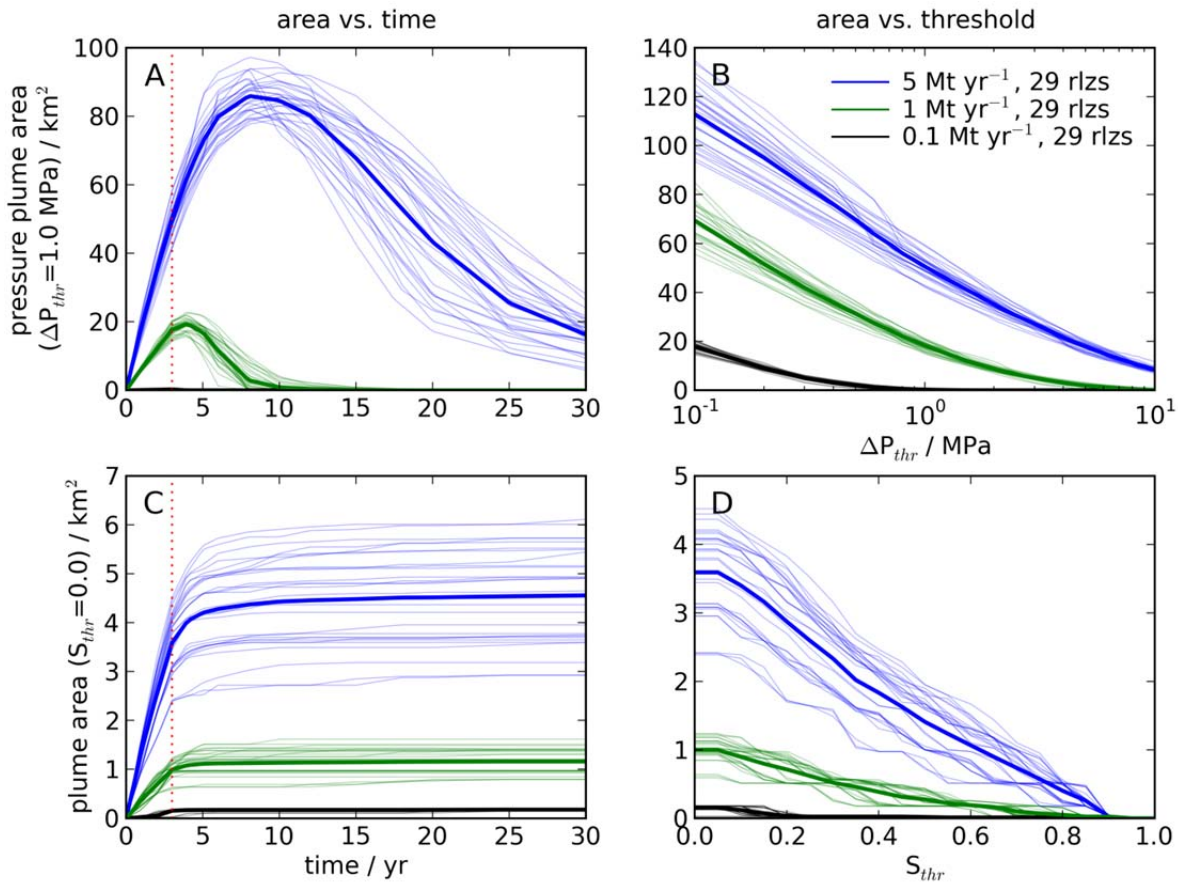

Figure C2: Summary of plume-area calculations for 3 year injection simulations at three different injection rates: 0.1 (black), 1 (green) and 5 Mt yr^{-1} (blue). Individual realizations are lightly colored while the ensemble average is bolded. (A) pressure plume area for ΔP_{thr}=1 MPa as a function of time. The end of injection is indicated by a red dotted line. (B) AoR_P at the end of injection for different ΔP_{thr} (C) Area of CO_2 plume for S_{thr}=0 as a function of time. (D) Area of CO_2 plume at the end of injection for different S_{thr} .

Calculations of the areas of the pressure and CO_2 plume for the 10 year CO_2 injection scenarios (sets 10, 11 and 12 in Table C1) are broadly consistent with those presented in Figure C2, except that areas are generally larger, consistent with the higher volume injection. Variability around the ensemble mean is also consistent with the 3 year injection case, with the largest uncertainty associated with the size of the CO_2 plume (Figure C3(C)).

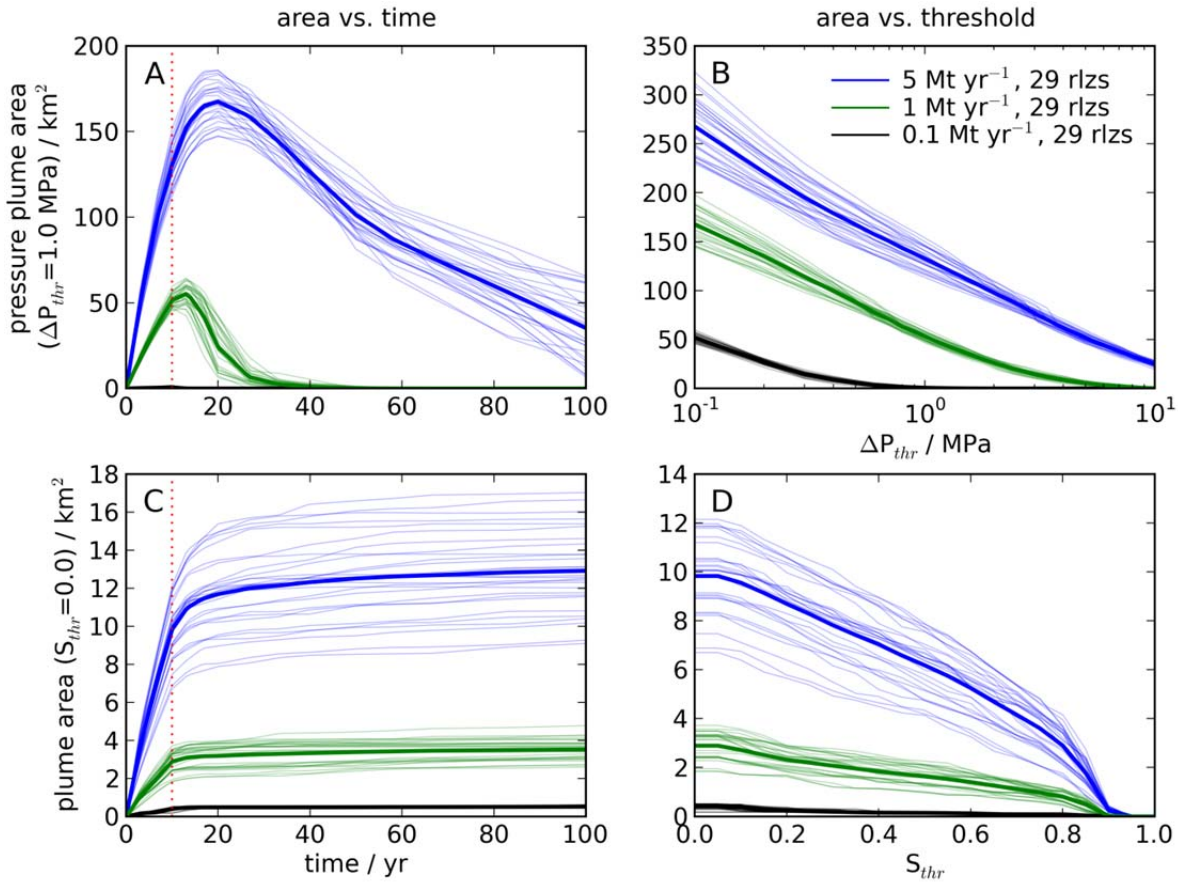

Figure C3: As for Figure C2, summary of calculations of plume areas for 10 year injection simulations at three different injection rates: 0.1 (black), 1 (green) and 5 Mt yr^{-1} (blue). Individual realizations are lightly colored while the ensemble average is bolded. (A) AoR$_P$ forΔP_{thr}=1 MPa as a function of time. The end of injection is indicated by a red dotted line. (B) Area of pressure plume at the end of injection for different ΔP_{thr}. (C) Area of CO_2 plume for S_{thr}=0 as a function of time. (D) Area of CO_2 plume at the end of injection for different S_{thr}.

C4.1 AoR Threshold

The ensemble average profiles presented in Figures C2 and C3 are either for specific threshold values (ΔP_{thr} or S_{thr}) or at specific times (the end of injection). It is illustrative of the underlying processes to investigate how these profiles change with modification of the threshold or observation time (Figure C4).

For the CO_2 injection at 5 Mt yr^{-1} for a period of 10 years, Figure C4(A) plots the evolving pressure-plume area with decreasing values of ΔP_{thr} selected from the range suggested by Bandilla et al. (2012). As expected, pressure-plume area increases as lower values of ΔP_{thr} are considered, with a maximum pressure-plume area of 600 km^2 recorded 30 years after the end of injection for a value of 0.1 MPa. Furthermore, the maximum pressure-plume area occurs at an increasingly later time post injection as smaller values of ΔP_{thr} are considered. This reflects the relative time-scales over which large vs. small overpressure perturbations are dissipated in underground formations.

The coincidence of profiles at later time (25 to 100 years) in Figure C4(D) shows the CO_2 plume has largely stabilized 15 years after the end of injection. Over the same time period, the pressure-plume area vs. ΔP_{thr} curves in Figure C4(B) are decreasing, indicating slow dissipation of the pressure plume over decadal time scales.

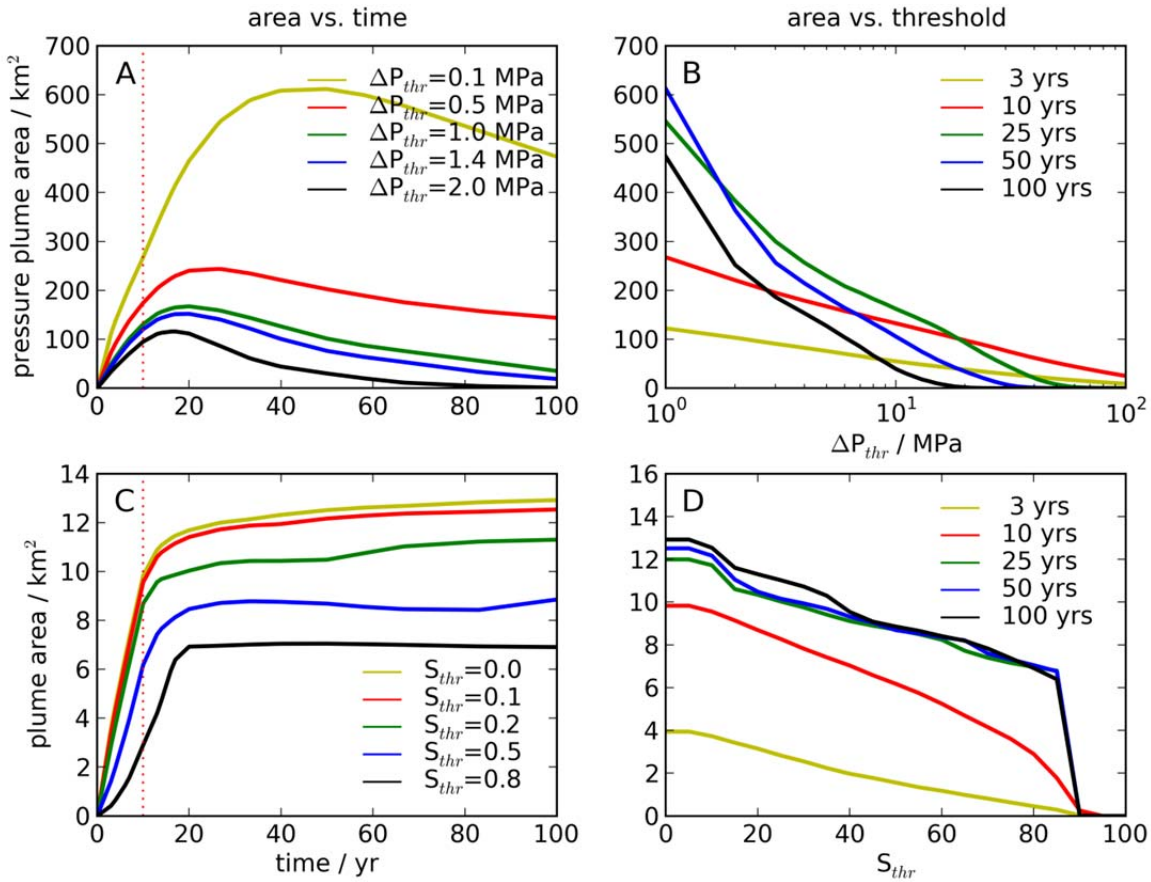

Figure C4: As for Figure C3, but applying different threshold values in the calculation of plume area. (A) Ensemble pressure-plume area with time for different values of ΔP_{thr}. (B) Pressure-plume area as a function of ΔP_{crit} at different times during the simulation. (C) CO_2 plume area with time for different values of S_{thr}. (D) CO_2 plume area as a function of S_{thr} at different times during the simulation.

C4.2 Grid Size

Use of a smaller-than-optimal grid imposes a boundary effect on pressure evolution during the injection simulation. Simulations presented here make use of constant pressure or "open" boundaries conditions on all sides of the model. This implicitly assumes that, physically, the model domain is smaller than the size of the storage formation; closing these boundaries to fluid flow would artificially reduce the size of the modeled storage formation. Closed boundaries also lead to more rapid build-up of pressure in the reservoir as the brine is less able to migrate away from the displacing CO_2 plume.

By definition, imposing a fixed pressure at one of the model's lateral boundaries forces the pressure increase at that location to be zero. However, on a larger grid, and in the absence of a

pressure constraint at that same location, the pressure rise could be non-zero. This is the first mechanism by which grid size and boundary effects can artificially modify estimation of pressure-plume area, in this case, underestimating its extent. This grid effect introduces a larger error as smaller values of ΔP_{thr} are used to constrain pressure-plume area because these contours extend further from the injection well and are more likely to approach and be influenced by the boundary.

The second mechanism is time-dependent. When pressure at a boundary is fixed to a value lower than it would assume on larger grid, pressure gradients in the model are also modified (typically, they will be sharper near the boundary). Pressure gradients control the rate of flow and sharper gradients near the boundary will tend to increase the rate of CO_2 and brine transport away from the injector, as well as lowering pressures in the model interior. Thus, for smaller grids, CO_2 will flow more rapidly from the injector and CO_2-plume area will tend to be overestimated.

Any discrepancies in simulations performed on different grids are numerical in nature; nevertheless, these effects are important to explore so as to provide confidence in simulation results. Figure C5 plots ensemble average plume-area profiles for the 10 year injection simulations at the three different injection rates: 0.1, 1, and 5 Mt yr^{-1}. Solid profiles denote simulations performed on a large 100x100 km^2 mesh and the same as those in Figure C3. Dashed profiles are for the same simulations performed on a 16x16 km^2 mesh.

In Figure C5(A), the time evolution of the pressure-plume area is the same on the large and small grids when injecting at a rate of 1 Mt yr^{-1}; however, the small grid underestimates maximum pressure-plume area by ~15% for simulated injection of 5 Mt yr^{-1}. For the larger injection rate (and injection volume), the correspondingly larger pressure-plume area is more susceptible to a boundary effect that underestimates its size. This is further illustrated in Figure C5(B), which shows an increasing underestimate by the small versus the large grid at lower values of ΔP_{thr} and larger pressure-plume areas.

Figure C5(C) shows that the spatial extent of the CO_2 plume tends to be overestimated by ~10% at later time when the smaller grid is used. As suggested earlier, this overestimate is derived from a boundary effect that artificially increases flow rates away from the injector.

If the small, 16x16 km grid introduces significant error to estimate of plume area, what guarantees are there that similar errors—albeit smaller, at lower values for ΔP_{thr} or for larger injection volumes—are not introduced by the larger, 100x100 km grid? The upper limit of plume area modeled on the small grid is 256 km^2, corresponding to the horizontal span of the model domain. While it is clear that the area of the CO_2 plume at all injection rates is well below this limit (Figure C5(C)), area of the pressure plume does appear to be nearing—and indeed turning away from at low values for ΔP_{thr}—this ceiling. In contrast, the maximum plume area that can be modeled on the larger grid is 10,000 km^2, which is much larger than the maximum value of ~260 km^2 in Figure C5(B), and ~600 km^2 in Figure C4. Thus we are confident that plume-area calculations quoted for the larger grid are not adversely impacted by boundary effects.

Clearly, it is important to investigate and rule out such grid effects in these calculations, particularly where large injection volumes or low values of ΔP_{thr} could lead to very large estimates of plume area.

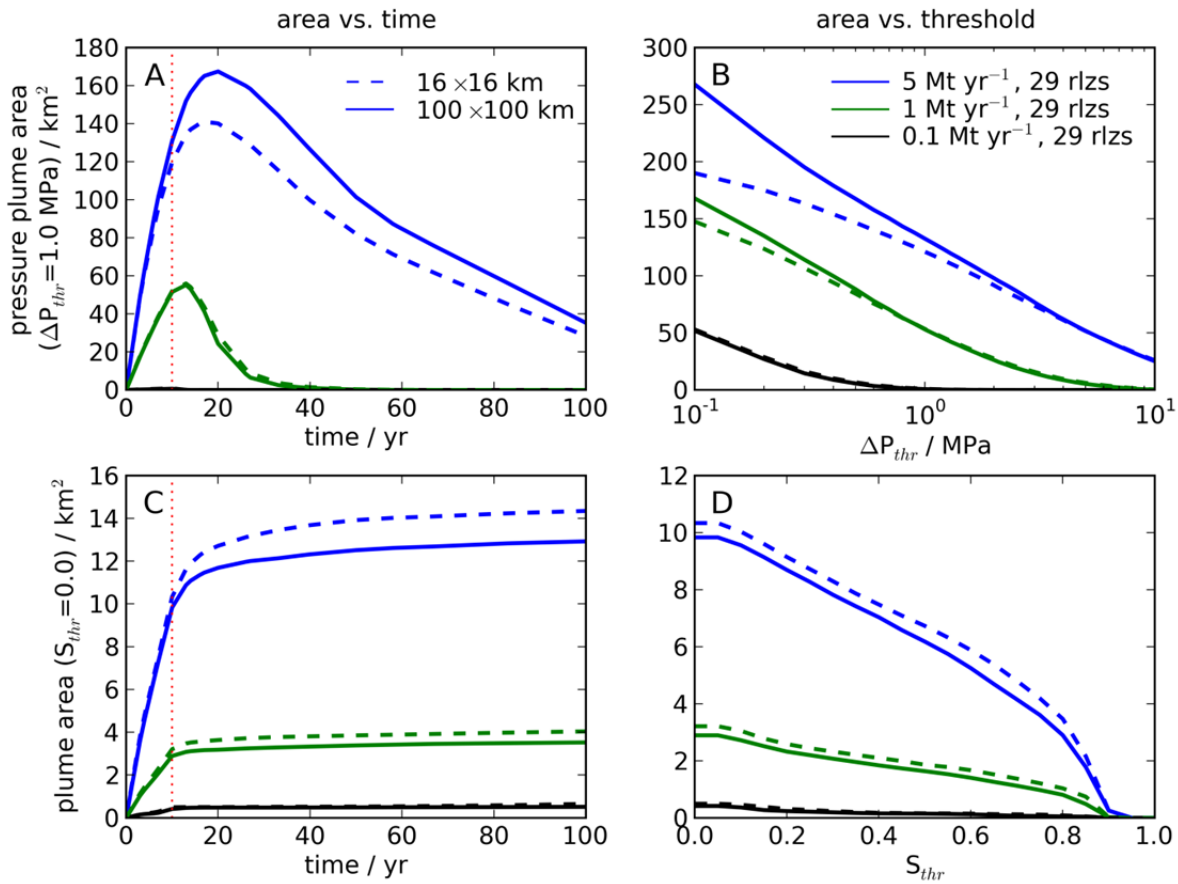

Figure C5: As for Figure C3, but comparing ensemble AoR results for a 16x16 km^2 mesh (dashed) against a 100x100 km^2 mesh (solid) for three different injection rates: 0.1 (black), 1 (green), and 5 Mt yr^{-1} (blue).

C4.3 Injection Rate

Supposing that a given volume of CO_2 is required to be injected, is there any significant effect on the size of the plume area due to the rate at which that CO_2 is emplaced? While injection of a fixed volume at a higher rate will likely lead to a larger overpressure in the vicinity of the injection well—and this may be limited by safe operating overpressures where induced seismicity is concerned—it is not clear how injection rate will affect the propagation of ΔP_{thr} contours away from the injector.

Figure C6 plots the evolution of the areas of the pressure and CO_2 plumes with time for 15 Mt of CO_2 that has been injected at five different rates, from 1 to 7.5 Mt yr^{-1}, and thus over five different time spans (from 15 to 2 years). To facilitate the comparison, the time axis for each injection has been translated so that the origin in each case corresponds to the end of the injection period; thus injection appears to start earlier for some profiles than others.

During the injection phase, pressure-plume area increases more rapidly at higher injection rate, although AoR_P tends to be smaller when injection stops. Nevertheless, pressure diffusion in the post-injection period tends to aid convergence of the profiles, with similar maximum AoR_Ps recorded between 3 and 6 years after the injection has ceased and similar rates of decline

occurring thereafter. The profiles of the CO_2 plume area (Figure C6(B)) show similar behavior, with convergence occurring rapidly after the end of injection at a similar stable plume size of 4 to 4.5 km^2.

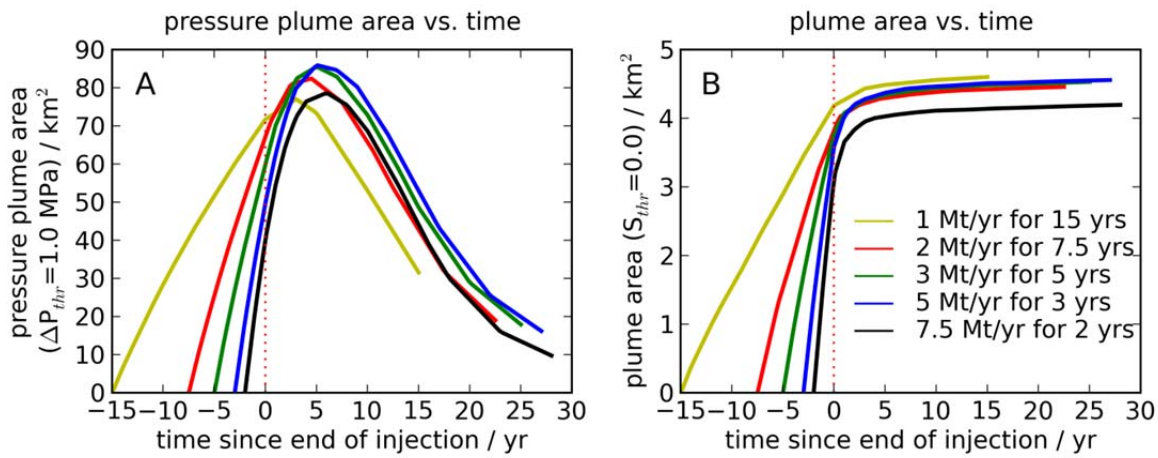

Figure C6: Comparison of plume-area evolution when injecting the same volume of CO_2 (15 Mt) at different rates: 1 (yellow), 2 (red), 3 (green), 5 (blue) and 7.5 Mt yr^{-1} (black). Because t_{inj} is different for each simulation, the time axes for each profile have been shifted so that the end of the injection for each simulation is at time 0.

C4.3 Injection Volume

Figure C7 shows the relationship between total injected volume of CO_2 and the maximum recorded plume area. Data are available for six injection volumes, corresponding to the three simulated injection rates (0.1, 1, and 5 Mt yr^{-1}) and two simulated injection times (3 and 10 years). Profiles of pressure-plume for different values of ΔP_{thr} show reasonably linear trends on the log-log axes. This would indicate a power-law dependence of AoR_P on injected volume V, i.e., pressure-plume area $(\Delta P_{thr}) \propto V^n$ where the exponent n ranges between 0.65 (for ΔP_{thr}=0.1 MPa) and 0.8 (for ΔP_{thr}=2.0 MPa). The vertical offset of profiles for decreasing values of ΔP_{thr} is indicative of the significant increase in the size of the pressure plume as lower overpressure thresholds are used to define it.

The CO_2 plume exhibits a similar linear relationship when plotted on log-log axes. Profiles of CO_2-plume areas for different values of S_{thr} more closely overlap and have gradients ranging between 0.83 and 0.9.

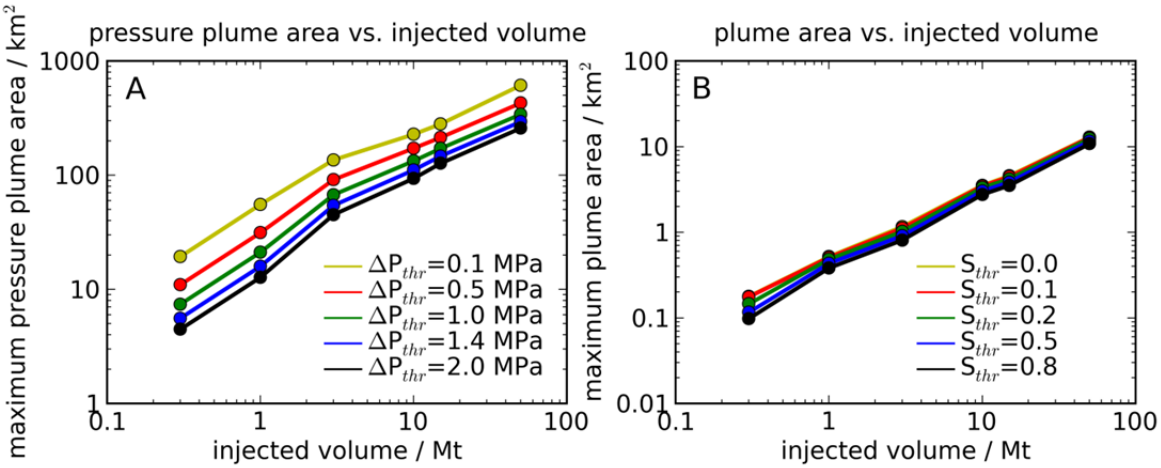

Figure C7: Maximum plume area for different injected volumes and critical thresholds: (A) ΔP_{thr} and (B) S_{thr}.

C.4 REFERENCES

Bandilla, K. W.; Kraemer, S. R.; Birkholzer, J. T. Using semi-analytic solutions to approximate the area of potential impact for carbon dioxide injection. *Int J Greenh Gas Cont* **2012,** *8*, 196–204.

Birkholzer, J. T.; Zhou, Q. Basin-scale hydrogeologic impacts of CO_2 storage: Capacity and regulatory implications. *Int J Greenh Gas Cont* **2009,** *3*, 745–756.

Deng, H.; Stauffer, P. H.; Dai, Z.; Jiao, Z.; Surdam, R. C. Simulation of industrial-scale CO_2 storage: Multi-scale heterogeneity and its impacts on storage capacity, injectivity and leakage. *Int J Greenh Gas Cont* **2012,** *10*, 397–418.

Kelkar, S.; Lewis, K.; Karra, S.; Zyvoloski, G.; Rapaka, S.; Viswanathan, H.; Mishra, P. K.; Chu, S.; Coblentz, D.; Pawar, R. A simulator for modeling coupled thermo-hydro-mechanical processes in subsurface geological media. *Int J Rock Mech Min Sci* **2014,** *70*, 569–580.

Zyvoloski, G. A. *FEHM: A control volume finite element code for simulating subsurface multi-phase multi-fluid heat and mass transfer*; LA-UR-07-3359; Los Alamos National Laboratory Report, Los Alamos, NM, 2007.

NRAP is an initiative within DOE's Office of Fossil Energy and is led by the National Energy Technology Laboratory (NETL). It is a multi-national-lab effort that leverages broad technical capabilities across the DOE complex to develop an integrated science base that can be applied to risk assessment for long-term storage of carbon dioxide (CO_2). NRAP involves five DOE national laboratories: NETL, Lawrence Berkeley National Laboratory (LBNL), Lawrence Livermore National Laboratory (LLNL), Los Alamos National Laboratory (LANL), and Pacific Northwest National Laboratory (PNNL).

Technical Leadership Team

Diana Bacon
Lead, Groundwater Protection Working Group
Pacific Northwest National Laboratory
Richmond, WA

Jens Birkholzer
LBNL Technical Coordinator
Lawrence Berkeley National Laboratory
Berkeley, CA

Grant Bromhal
Technical Director, NRAP
Lead, Reservoir Performance Working Group
Office of Research and Development
National Energy Technology Laboratory
Morgantown, WV

Chris Brown
PNNL Technical Coordinator
Pacific Northwest National Laboratory
Richmond, WA

Susan Carroll
LLNL Technical Coordinator
Lawrence Livermore National Laboratory
Livermore, CA

Tom Daley
Lead, Strategic Monitoring Working Group
Lawrence Berkeley National Laboratory
Berkeley, CA

Robert Dilmore
NETL Technical Coordinator
Office of Research and Development
National Energy Technology Laboratory
Pittsburgh, PA

Nik Huerta
Lead, Migration Pathways Working Group
Office of Research and Development
National Energy Technology Laboratory
Albany, OR

Rajesh Pawar
LANL Technical Coordinator
Lead, Systems/Risk Modeling Working Group
Los Alamos National Laboratory
Los Alamos, NM

Tom Richard
Deputy Technical Director, NRAP
The Pennsylvania State University
NETL-Regional University Alliance
State College, PA

Josh White
Lead, Induced Seismicity Working Group
Lawrence Livermore National Laboratory
Livermore, CA

Sean Plasynski
Director
Strategic Center for Coal
National Energy Technology Laboratory
U.S. Department of Energy

John Wimer
Director
Office of Coal and Power R&D
National Energy Technology Laboratory
U.S. Department of Energy

Susan Maley
Technology Manager
Crosscutting Research
National Energy Technology Laboratory
U.S. Department of Energy

Mark Ackiewicz
Director
Division of Carbon Capture and Storage
Office of Fossil Energy
U.S. Department of Energy

NRAP Executive Committee

Cynthia Powell
Director
Office of Research and Development
National Energy Technology Laboratory
U.S. Department of Energy

Alain Bonneville
Laboratory Fellow
Pacific Northwest National Laboratory

Donald DePaolo
Chair, NRAP Executive Committee
Associate Laboratory Director
Energy and Environmental Sciences
Lawrence Berkeley National Laboratory

Melissa Fox
Program Manager
Applied Energy Programs
Los Alamos National Laboratory

Roger Aines
Chief Energy Technologist
Lawrence Livermore National
Laboratory

Grant Bromhal
Technical Director, NRAP
Office of Research and Development
National Energy Technology Laboratory